STUDY OF THE IMPACT OF ATMOSPHERIC VARIABILITY ON SUBSURFACE METHANE EMISSIONS: APPLICATION TO LEAK DETECTION AND QUANTIFICATION FOR UNDERGROUND NATURAL GAS PIPELINE LEAKS

By

Shanru Tian

DISSERTATION

Submitted in partial fulfillment of the requirements
for the degree of Doctor of Philosophy at
The University of Texas at Arlington
December 2022

Arlington, Texas

Supervising Committee:

Kathleen M. Smits, Supervising Professor
Luca Maddalena
Melanie L. Sattler
Nick Fang
Stuart N. Riddick

Abstract

Study of the Impact of Atmospheric Variability on Subsurface Methane Emissions: Application to Leak Detection and Quantification for Underground Natural Gas Pipeline Leaks

Shanru Tian, Ph.D.

The University of Texas at Arlington, 2022

Supervising Professor: Kathleen M. Smits

Natural gas (NG), taken as a bridging fuel for achieving a low-carbon future, has rapidly grown to be a significant component of the global energy system and requires extensive pipeline infrastructures, most of them buried underground. Fugitive methane (CH_4) emissions from NG pipeline leaks pose environmental, safety, and economic threats to the public. An effective leak detection and quantification (LDAQ) survey method is critical to identifying a leak and assessing the size when it has occurred, thus initiating appropriate response actions to repair it and accounting for the environmental risks accurately. However, gaps exist between LDAQ survey methods, and the effectiveness remains unclear. This doctoral study focuses on bridging such gaps that currently exist within the scientific, industrial, and policy-making communities by investigating 1) how atmospheric variability affects subsurface NG emissions and 2) how we can account for this understanding in LDAQ survey methods. Specifically, three phases are defined. First, this study systematically analyzed the influences of atmospheric variability and survey parameters on the detection probability (DP) of LDAQ surveys. A validated DP model was developed that incorporates the leak rate, survey distance, survey speed, atmospheric stability, wind speed, and air temperature. Results demonstrate that DP is highly impacted by survey speed,

atmospheric stability, and wind speed. The options of favorable weather conditions to have a high DP (e.g., >50%) decrease rapidly with the increase in survey speed. Next, the atmospheric dispersion inverse modeling method was used to investigate the subsurface CH_4 emissions and quantify the emission estimate accuracy against the known controlled NG release rates. Results show the large temporal variability of CH_4 emissions from NG pipeline leaks. At least 6 h of data is needed to have an emission estimate accuracy within $\pm$ 27% of the controlled release rate on average. With 1 h of data, the probability that the emission estimate is within ±50% of the controlled release rate ($P_{\pm 50\%}$) is 50%, but it approaches 100% when 3–4 h of data is collected. Finally, atmospheric CH_4 plume shape and size were characterized to provide a physical base for designing or using the survey parameters. Results demonstrate that survey parameters (i.e., survey speed, and height) are significantly affected by atmospheric stability, wind speed, and air humidity driving the plume variability. The maximum survey speed is about 25 mph in Pasquill–Gifford (PG) stability A (Extremely unstable conditions), but it reduces to 16 mph in PG G (Extremely stable conditions). Leak survey typically has a large range of survey speed options (0–25 mph) at 5 m above the ground under unstable (PG A to B/C), calm to medium speed (0–3 m s^{-1}), and high to very high (50–80%) humidity conditions. Overall, this dissertation provides a foundation to advance the efficiency of LDAQ survey methods by adopting scientific findings into engineering practices. Results benefit emission mitigation efforts at a variety of scales and applications from local pipeline safety and maintenance to large-scale environmental risk assessment.

Acknowledgement

Life runs like a marathon. When I look back on my journey of pursuing a doctoral degree, I want to thank the world, the people I met, and the opportunities I got.

First, I would like to thank my advisor, Dr. Kathleen M. Smits, for her full support, guidance, and encouragement during my Ph.D. study. It is fortunate to work with her. She always stands by the students and puts them, students, as the priority of her plan. I appreciate the opportunities she gave me to present my work across various platforms such as industry practitioners, her cooperators, and national conference, and much invaluable advice for my career development. These training opportunities and advice guide me to grow faster and more professionally. I also want to thank my dissertation committee, Dr. Luca Maddalena, Dr. Melanie L. Sattler, Dr. Nick Fang, and Dr. Stuart N. Riddick for all their time and inspiration. I gratefully acknowledge the funding supports from the U.S. Department of Transportation Pipeline and Hazardous Materials Safety Administration under Grant Nos. 693JK31810013 and 693JK32010011; Colorado Oil and Gas Conservation Commission (COGCC) Mark Martinez & Joey Irwin Memorial Public Projects Fund; Trent R. Dames and William W. Moore Fellowship, American Society of Civil Engineers (2021); Dissertation Fellowship, the University of Texas at Arlington (2022); STEM GTA fellowship, Department of Civil Engineering, the University of Texas at Arlington (2022 Fall).

I want to express my deep appreciation to Director Daniel J. Zimmerle, Dr. Stuart N. Riddick, Dr. Younki Cho, Dr. Clay S. Bell, Dr. Timothy Vaughn, and Dr. Kristine Bennett from Colorado State University. Drs. Riddick and Cho provided me with many insightful ideas and constructive comments for my research and papers and trained me to think critically. I would also appreciate assistance from Aidan Duggan, Fancy Cheptonui, Mercy Mbua, and Wendy Hartzell. Also, I would like to thank all the fellow members of Dr. Smits's research group, past and present; Navodi

Jayarathne, Richie Kolodziej, Jui-Hsiang Lo, Michelle Schwartz, Nathaniel Steadman, José Velásquez, Bo Gao, Zhen Li. You all helped me with this academic Marathon run. I still remember the beautiful garden scenery along the I70 interstate at Salina City, Kansas, when Navodi and I drove nearly 950 miles from Arlington, Texas, to Fort Collins, Colorado, in 2021 Fall, and those four-month stays at Fort Collins.

Finally, I would like to thank my family and my love Min in China. With your support and efforts behind me over these years, I can have the chance to focus on my Ph.D. study in Texas, the Pacific Ocean apart, 7500 miles from China. I am proud of your support forever and endeavor to make a difference in the world as my top life goal.

Dedication

To where I am from and where I am going.

Table of Contents

Abstract ii

Acknowledgement iv

Dedication vi

Table of Contents vii

List of Figures xi

List of Tables xv

List of Abbreviations xvii

Chapter 1 Introduction 1

1.1 Motivation and Problems 1

1.2 Research Goals, Questions, and Hypotheses 3

1.3 Dissertation Structure 6

Chapter 2 Background and Literature Review 8

2.1 Significance of Mitigating Methane Emissions from Underground Natural Gas Pipeline Leaks 8

2.1.1 Climate and Air Quality 8

2.1.2 Public Safety 9

2.2 Leak Detection and Quantification Survey Challenges for Underground Natural Gas Pipeline Leaks 10

2.2.1 The Knowledge Gap in Understanding the Efficiency of Leak Detection and Quantification Survey Methods 10

2.2.2 Environmental Factors Affecting the Efficiency of Leak Detection and Quantification Survey Methods 13

Chapter 3 Investigating Detection Probability of Mobile Survey Solutions for Natural Gas Pipeline Leaks Under Different Atmospheric Conditions 17

3.1 Abstract 18

3.2 Introduction 19

3.3 Material and Methods 22

3.3.1 Experiment and Measurement Approaches 22

3.3.2 Methodology 25

3.4 Results 28

3.4.1 Empirical Detection Probability with Different Survey Speeds 28

3.4.2 Empirical Detection Probability with Different Atmospheric Stability Conditions 29

3.4.3 Validation of the Detection Probability Model 31

3.4.4 Modeled Detection Probability for Walking and Driving Surveys 34

3.5 Conclusions 39

3.5.1 Leak Detection 39

3.5.2 Implications for Leak Detection Solutions 39

Chapter 4 Estimating Methane Emissions from Underground Natural Gas Pipelines Using an Atmospheric Dispersion-Based Method 41

4.1 Abstract 42

4.2 Introduction 43

4.3 Materials and Methods 47
4.3.1 Experimental Testbed/Setup 47
4.3.2 Experiment Procedure 50
4.3.3 Model Setup 51
4.4 Results 53
4.4.1 Impact of Atmospheric Stability on CH_4 Mole Fraction 53
4.4.2 Methane Emissions Calculated by WindTrax 54
4.4.3 Effect of Atmospheric Stability on CH_4 Emission Estimates 56
4.4.4 Effect of Time Averaging on CH_4 Emission Estimates 58
4.5 Discussion 59
4.6 Conclusions 61
Chapter 5 Improving the Efficacy of Leak Detection and Quantification Survey Methods Using 3D Plume Measurements 63
5.1 Abstract 64
5.2 Introduction 65
5.3 Materials and Methods 69
5.3.1 Experiment and Measurement Approaches 69
5.3.2 Plume Width 70
5.4 Results 73
5.4.1 Diurnal Variability in Plume Width 73

5.4.2 Variability in Plume Width Due to Different Atmospheric Stability Conditions 74

5.4.3 Variability in Plume Width with the Change in Air Humidity, Wind Speed, and Air Temperature 75

5.5 Discussion 78

5.6 Conclusions 79

Chapter 6 Conclusions, Discussions and Future Research 81

6.1 Conclusions 81

6.2 Discussions 84

6.3 Recommendations for Future Research 85

Appendix A Field Experiments* 88

Appendix B Supplemental Materials for Chapter 4 91

Appendix C Numerical Modeling of Atmospheric Methane Plume 99

Appendix D Copyright Permission 103

Appendix E Coauthor Release Forms 104

References 113

List of Figures

Figure 1.1 Framework of the doctoral research 5

Figure 3.1 Empirical detection probability as a function of distance with the mobile survey speed ranging from 2 to 34 mph for the five controlled experiments (Exp1–5), respectively. 29

Figure 3.2 Empirical detection probability as a function of the Pasquill-Gifford (PG) stability class with the mobile survey speed of 2–34 mph for the five controlled experiments (Exp1–5), respectively. PG stability class A denotes the extremely unstable condition, PG stability class B/C denotes the unstable condition, PG stability class D denotes the neutral condition, PG stability class E/F denotes the stable condition, and PG stability class G denotes the extremely stable condition. No observation data is available for PG stability class E/F in Exp1–2, and PG stability class D for Exp 3–5. 30

Figure 3.3 Empirical detection probability as a function of the binned wind speed with the mobile survey speed of 2–34 mph for the five controlled experiments (Exp1–5), respectively. The binned wind speed interval is 0–1, 1–3, 3–5, and 5–10 m s^{-1}, representing the the calm, low, medium, and large wind conditions, respectively, according to the measured wind speed range during the experiments. 31

Figure 3.4 Modeled DP vs Empirical DP. The empirical DP is from the test data. The red dashed line is the 1:1 line. The blue line is the fitted equation between Modeled DP and Empirical DP where y is Modeled DP, and x is Empirical DP. The coefficient of determination (R^2) between Modeled DP and Empirical DP is 0.76. 33

Figure 3.5 Sensitivity analysis of each variable in the model on modeled DP. a)–f) shows the effect of changing leak rate, survey distance, survey speed, air temperature, wind speed, and 1/L input, respectively, while keeping other variables the same as the base case. In the base case, the leak rate is 0.5 g min^{-1}, survey speed is 2 mph, survey distance is 1 m, air temperature is 15 $°C$, wind speed is 0.1 m s^{-1}, and 1/L is -0.2 m^{-1}. The value of each variable in the base case is the lower limit of the data used for developing the DP model. The maximum value of each variable in a)–f) is the upper limit of the data used for developing the DP model. 34

Figure 3.6 Modeled DP as a function of survey speed under different PG stability classes and wind speed conditions. a)–e) is the modeled DP for a small leak (q: 0.5 g min^{-1}). f)–j) is the modeled DP for a large leak (q: 8 g min^{-1}). The survey distance is 5 m, air temperature is 25 $°C$ (average temperature during the experiments). The calm wind is 0–1 m s^{-1}, the low wind is 1–3 m s^{-1}, the medium wind is 3–5 m s^{-1}, and the high wind is 5–10 m s^{-1} according to the measured wind speed range during the experiments. The value of 1/L is -0.2, -0.05, 0.001, 0.05 and 0.2 m^{-1} for PG stability class A, B/C, D, E/F and G, respectively. The error bar is ±1 standard deviation. Note, calm, small, and medium winds typically occur during unstable or stable conditions (PG A, B/C, E/F, G). Medium and large winds generally occur during neutral conditions (PG D) (Pasquill, 1961). 36

Figure 3.7 Weighed DP for walking and driving surveys under different PG stability and wind speed conditions. The survey distance is 5 m, air temperature is 25 °C (the average temperature during the experiments). The emission rate is from three publicly available emission rate datasets (Table 3.2). The calm wind is 0–1 m s^{-1}, the low wind is 1–3 m s^{-1}, the medium wind is 3–5 m s^{-1}, and the high wind is 5–10 m s^{-1} according to the measured wind speed range during the experiments. The value of 1/L is -0.2, -0.05, 0.001, 0.05, and 0.2 m^{-1} for PG stability class A, B/C, D, E/F, and G, respectively. The assumed driving survey speeds are 11 and 22, 34 mph, representing the field survey's low, medium, and high driving speeds, respectively (Table 3.3). The error bar is ±1 standard deviation. Note, calm, small, and medium winds typically occur during unstable or stable conditions (PG A, B/C, E/F, G). Medium and large winds generally occur during neutral conditions (PG D) (Pasquill, 1961) 38

Figure 4.1 Plan views of the above ground and surface measurement locations relative to the NG leak location. a) The above ground sensor to measure the atmospheric CH_4 was located at T1 for the first three experiments and T2 for the fourth experiment, due to a change in the predominant wind direction. b) The gridded layout represents the surface CH_4 measurement locations. In each direction, each point is 0.5 m apart with direction spaced by 45°. 49

Figure 4.2 Mean normalized CH_4 mole fraction grouped by the Pasquill-Gifford (PG) stability class for the four experiments (Exp1–4). C_b is the background CH_4 mole fraction (ppm), C_{obs} is the measured CH_4 mole fraction (ppm), Q_{ctr} is the release rate (kg hr^{-1}). The error bar represents $\pm 1\sigma$(σ: standard error). The total number of data points is 70, 10, 22, and 47 for PG stability classes A, B-C, E-F, and G. Note, PG stability class D was not included due to limited data points (6). The averaging interval for each data point is 10 minutes. 54

Figure 4.3 a) Box and whisker plots of estimated surface CH_4 emissions (Q, kg hr^{-1}) compared with the controlled release rate (Qctr, kg hr^{-1}) for the four controlled release experiments (Exp1–4); Boxes and whiskers in a) show the median (orange), 25^{th} and 75^{th} percentile (blue), and minimum and maximum values (black). The mean is depicted by the hollow red diamond. The black circles represent the outliers, and the green cross-mark is the controlled release rate (Q_{ctr}). b) The average ratio of estimated surface CH_4 emissions (Q, kg hr^{-1}) to the controlled release rate (Q_{ctr}, kg hr^{-1}) grouped by the Pasquill-Gifford (PG) stability classes. Data are from the experimental base case. The total number of data points in b) is 70, 10, 22, and 47 for PG stability classes A, B-C, E-F, and G. Note, PG stability class D was not included due to limited data points (6). 56

Figure 4.4 a) The average ratio of estimated surface CH_4 emissions (Q, kg hr^{-1}) to the controlled release rate (Qctr, kg hr^{-1}) grouped by the Pasquill-Gifford (PG) stability classes. b) The average dispersion coefficients (σu: along-wind direction; σv: crosswind direction; σw: vertical direction) grouped by the Pasquill-Gifford (PG) stability class. The unit of dispersion coefficient is m s^{-1}. The data in a) and b) are from the sensitivity cases, as shown in Table 4.2. The error bars in a) and b) represent $\pm 1\sigma$(σ: standard error). The total number of data points is 326, 91, 58, 191, and 355 for PG stability class A, B–C, D, E–F, and G, respectively. 57

Figure 4.5 Probability ($P_{\pm 50\%}$) that the calculated mean CH_4 emissions (Q, kg hr^{-1}) are within ± 50% of the controlled release rate (Q_{ctr}, kg hr^{-1}) with the rolling mean time ranging from 0.33 to 9.33

hours. The data were individual surface CH_4 emission points from the base case (Baserun). The probability was calculated by dividing the number of emission estimates within ± 50% of the controlled release rate by the total sample size in each rolling time interval. 59

Figure 5.1 Elevated CH_4 mixing ratio ($C\text{-}C_0$) as a function of crosswind distance from the plume center (y=0). The red cross is the measurement point. The red line is the Gaussian fit curve (R^2: 0.76). The black dashed line is the defined detectable threshold (i.e., CH_4 mixing ratio enhancements of 0.1 ppm above the background value) for calculating plume width ($ymax - ymin$). C is the binned CH_4 mixing ratio. $C0$ is the background CH_4 mixing ratio (2.0 ppm). The sample data used here is the binned average of the 5-minute measurements at 5.0 m above the ground from the experiment..... 72

Figure 5.2 The plume width and survey speed at heights between 0.5 and 7 m above the ground during the day (07:00–17:00) and at night (00:00–07:00, 17:00–24:00). The error bar is ±1 standard error. 74

Figure 5.3 The plume width and survey speed at heights between 0.5 and 7 m above the ground under different stability conditions ranging from PG stability class A to G. The error bar is ±1 standard error. 75

Figure 5.4 a)-b) the plume width and survey speed at heights between 0.5 and 7 m above the ground under different humidity conditions; c) the average relative humidity (RH), temperature (T), and wind speed (WS) in each humidity condition. The categorized relative humidity interval is 0–50%, 50–80%, and 80–100% for the low, high, and very high humidity conditions, respectively (Ku-Mahamud and Khor, 2009). The error bar is ± 1 standard error. The unit of WS is converted to km hr^{-1} for visualization purposes. 76

Figure 5.5 Plume width and survey speed at heights between 0.5 and 7 m above the ground under different wind speed, and air temperature conditions. The categorized wind speed interval is 0–1, 1–3, and 3–12 m s^{-1} for the calm, low, medium, and medium to high wind conditions, respectively (Tian et al., 2022). The temperature bin interval is according to the measured temperature range during the experiments. The error bar is ± 1 standard error..... 78

Figure A.1 Methane Emission Technology Evaluation Center (METEC) site at Colorado State University (CSU). 88

Figure A.2 Top view of sensor layout in the METEC pipeline testbed..... 89

Figure A.3 Left: installments of the 3D sonic anemometer and weather sensors; Right: walking survey CH_4 measurements. 89

Figure A.4 Left: laboratory experiments to test the multiplexer system; Right: field 3D plume experiments using the multiplexer system. 90

Figure B.1 Time series of solar radiation, air temperature, wind direction, and wind speed at 1 m (blue line) and 6 m (red line) above the ground, and Obukhov length (L) from June 1st to June 5th,

2020. The Obukhov length was calculated using 1 min 3D sonic data (YOUNG Model 81000 Ultrasonic Anemometer) at 6 m height. Data were averaged every 10 minutes. The time is MDT (Mountain Daylight Time). The meteorological sensor ATMOS 41 was in an adjustment period before June 1st, 9:00 AM, 2020. Thus, meteorological data from ATMOS 41 showed abnormal values before this time. 94

Figure B.2 The surface CH_4 mole fraction plots for the four experiments (Exp1–4). The red contour is 100 ppm CH_4 mole fraction. The release rate is 0.08, 0.18, 0.27, 0.52 kg hr-1 of CH_4 for Exp1-4 (Figure B.2a to 2d), respectively..... 96

Figure B.3 Cumulative distribution frequency (CDF) of 10-min averaged CH4 mole fraction at 1 m above ground for all experiments (Exp1–4). 97

Figure B.4 The normalized CH_4 mole fraction ($(C_{obs}-C_b)/Q_{ctr}$) and crosswind distance (Y) in the Pasquill-Gifford (PG) stability class A (extremely unstable) and E–F (stable), respectively. C_b is the background CH_4 mole fraction (ppm), C_{obs} is the measured CH_4 mole fraction (ppm), Q_{ctr} is the release rate (kg hr^{-1}). 98

Figure C.1 Model domain (L: 100 m, W: 50 m, H: 50 m) for the CFD modeling. The red shaded circle at the bottom is the leak surface area. The crossline (red, green) shows the center of the model domain..... 101

Figure C.2 The modeled CH_4 mole fraction profiles at two stability conditions (unstable: red dot; slightly unstable: green dot) with the same surface emission rate. Top left: vertical profile at the center of the model domain. Top right: along with the distance at the height of 2 m. Bottom center: along with the crosswind distance at the height of 2 m. 102

List of Tables

Table 3.1 General information of the five controlled belowground NG release experiments at the METEC site from June 21st to July 4th, 2021. The release rate ranged from 0.5 to 8.5 g min^{-1}. The total number of passing was 3,472 for the five experiments. 23

Table 3.2 General information of three publicly available CH_4 emission rate datasets from NG distribution pipelines. Emission rates in these three datasets were measured directly using surface flux chambers, where all datasets show a right-skewed distribution characteristic. The total sample size used is 443. Three super large emission points were removed to be consistent with the range of controlled NG release rates in the DP model. 27

Table 3.3 Survey distance and speed for walking and driving surveys. The assumed driving survey speed is 11, 22, and 34 mph, which represents the low, medium, and high speeds of the field driving survey, respectively. The survey distance was assumed as 5 m downwind of the pipeline based on general field survey practices..... 28

Table 3.4 Estimated mean regression coefficients and the respective p values in the fitted model. μ is the mean value, σ is the standard error (SE). μ and σ were calculated by bootstrapping the training data 1000 times..... 32

Table 4.1 Background CH_4 mole fraction (1 m above ground, 10 m from the leak source) and surface expression area for Exp1–4. Standard deviations from the background CH_4 mole fraction are noted in parentheses. 52

Table 4.2 General information about the stability sensitivity and base case in WindTrax. L in the base case (Baserun) was calculated using Equations 4.1–4.2. The Obukhov length for the seven sensitivity cases (Srun1–7) were -75 to 100% of L, respectively ($L \neq 0$ in Wind WindTrax (Flesch et al., 2004)), other input model parameters were the same as the Baserun. 53

Table 5.1 General information of the fourteen controlled belowground NG release experiments at the METEC site between March 2nd and April 29th, 2022. The release rate was 0.44 kg hr^{-1} of CH_4. The measurement distance is 7 m downwind of the pipeline, and the height ranges from 0.5 to 7 m. The variables considered here include different Pasquill-Gifford (PG) stability classes ranging from PG A to G, calm to high wind speed, low to very high humidity, and freezing to nonfreezing air temperature. The categorized wind speed interval is 0–1, 1–3, and 3–12 m s^{-1} for the calm, low, and medium to high wind conditions, respectively (Tian et al., 2022). The categorized relative humidity interval is 0–50%, 50–80%, and 80–100% for the low, high, and very high humidity conditions, respectively (Ku-Mahamud and Khor, 2009). 70

Table 5.2 Pearson correlation coefficients (r) and the respective p values between air temperature (T, degC), relative humidity (RH, %), and wind speed (WS, m s^{-1})..... 77

Table C.1 The design schemes for uncoupled numerical dispersion experiments. It includes the modeling under different atmospheric stabilities from the most unstable (PG A) to the most stable (PG F) with constant surface CH_4 emission conditions. 101

List of Abbreviations

NG	Natural Gas
CH_4	Methane
LDAQ	Leak Detection and Quantification
DP	Detection Probability
UAV	Unmanned Aerial Vehicle
U.S. EPA	U.S. Environmental Protection Agency
ABL	Atmospheric Boundary Layer
PG	Pasquill–Gifford stability class
L	Monin-Obukhov length
METEC	Methane Emission Technology Evaluation Center, Colorado State University
CFD	Computational fluid dynamics model
UNEP&CCAC	United Nations Environment Programme and Climate and Clean Air Coalition

Chapter 1 Introduction

1.1 Motivation and Problems

The consumption of natural gas (NG), taken as a short-term bridging fuel to a low-carbon renewable future, has surged globally as it produces fewer undesirable by-products such as CO_2, NO_x, SO_2, and particulates per unit of energy than coal or petroleum (Liang et al., 2012; The National Academy of Sciences, 2022). Global NG consumption is expected to increase by more than 40% between 2018 and 2050 (~1.2% annual growth) (U.S. Energy Information Administration, 2020). NG pipeline systems deliver energy to consumers and have a vast distribution network of over 3 million miles throughout the continental United States (U.S. Energy Information Administration, 2021a). Leak detection and quantitation (LDAQ) surveys for NG pipeline systems have historically been driven to reduce pipeline leaks resulting in safety incidents and, more recently, a relatively achievable approach to help mitigate climate change and fulfill the goals of the Paris agreement by reducing CH_4 emissions from NG pipeline leaks (Nisbet et al., 2020).

Recently, many LDAQ surveys, including walking surveys, driving surveys, UAV (unmanned aerial vehicle) surveys, and aircraft surveys, have improved the understanding of the number of leaks and CH_4 emissions from the NG pipeline systems (Kligman, 2011; Phillips et al., 2013; Gallagher et al., 2015; Vaughn et al., 2017; Zimmerle et al., 2017; Weller et al., 2018; Cho et al., 2020; Li et al., 2020; Riddick et al., 2021; FlyARH, 2021; LASEN, 2021; Heliops, 2022). However, the efficiency of LDAQ surveys is poorly characterized as the parameters of survey protocols (i.e., survey distance, height, speed, and atmospheric conditions during the survey) are selected subjectively by the surveyors. In addition, no controlled belowground NG releases experiments have been conducted to justify the selected parameters of the survey protocols, creating a challenge

in understanding the representativeness of these surveys for detecting the number of actual NG pipeline leaks and associated emission estimates.

There is a significant disparity in CH_4 emission estimates in the U.S. from NG pipeline leaks based on different LDAQ survey methods (Brandt et al., 2014; Lamb et al., 2015; Weller et al., 2020; U.S. EPA, 2022). For CH_4 emissions from the U.S. NG distribution pipeline leaks, the driving survey-based estimate in the U.S. is approximately five times larger than the walking survey-based estimate (Lamb et al., 2015; Weller et al., 2020; U.S. EPA, 2022). Such a disparity is mainly caused by the difference in activity factors (leak per mile) and emission factors (emission per leak), where both factors depend on the LADQ survey method. However, none of the LDAQ survey methods to date have been assessed quantitatively using the ground-truth data from the subsurface NG pipeline leaks. It thus poses a challenge to evaluate which method has an emission estimate representing the actual CH_4 emissions from the NG pipeline leaks. The leak detection density was 50% more at night than during the day when using a vehicle to survey the same area (Gallagher et al., 2015). In an above-ground site-by-site comparison campaign, the driving survey-based quantification method generally has a larger emission estimate than the walking survey-based method, with a difference of up to 13 times on average (Weller et al., 2018). Therefore, without assessing the efficiency of various LDAQ survey methods using controlled underground NG release experiments, many questions exist about the performance of current LDAQ surveys on mitigating CH_4 emissions from NG pipeline leaks.

Given the problems discussed above, this doctoral research is devoted to filling the knowledge gaps that exist between different LDAQ surveys for detecting and quantifying CH_4 emissions from NG pipeline leaks using sets of controlled release experiments under different atmospheric conditions, with the purpose of advancing the physical base to understand the accuracies of these

methods across a range of audiences such as industry practitioners, the scientific community, and policymakers.

1.2 Research Goals, Questions, and Hypotheses

The overarching goal of this Ph.D. work is to advance our understanding of atmospheric variability on NG emissions from subsurface leakage and how operators and solution providers can account for this information in decision-making. This work will advance the understanding of the efficiency of various LDAQ survey methods under a wide range of atmospheric conditions using a combination of controlled field experiments, data analytics, and mathematical modeling (Figure 1.1). This study focuses on bridging the gap that currently exists within the scientific, industrial, and policy-making communities on the capabilities of both leak detection and quantification methods. This dissertation aims to address the following first-order research questions:

(1) What environmental and procedural factors have the most significant impact on the probability of detection for underground NG pipeline leaks, and how can this be accounted for in practice?

    Currently, most research in DP for NG leakage is applied to aboveground infrastructure. In addition, LDAQ survey methods have not been tested against controlled experiments, resulting in a complete lack of understanding of DP for pipeline scenarios. My hypothesis is that LDAQ methods vary significantly in their ability to accurately detect pipeline leaks, mainly driven by variability in atmospheric conditions and the speed of detection (e.g., how fast the survey method is conducted). The objectives of this research, described specifically in chapter 3, are to systematically investigate how atmospheric variability and survey

parameters affect the DP of a subsurface NG emission, and to provide a validated DP model for cross-domain communities to quantify the efficiency of mobile leak survey methods by incorporating these statistically significant factors, including the leak rate, survey distance, survey speed, and atmospheric stability, wind speed, and air temperature.

(2) How much data (and what kind) is needed to estimate emissions from NG pipeline leaks accurately?

Current quantification approaches for subsurface CH_4 emissions only rely to the instantaneous CH_4 measurements, hypothesizing that the CH_4 mole fraction magnitude can infer the leak size alone. The environmental conditions are therefore not fully considered in the leak estimate. Furthermore, considerable controversy exists on the CH_4 emission estimates among these quantification methods, and none of them have been verified using controlled underground releases. Thus, it remains unknown about the representativeness of these estimates on the actual subsurface CH_4 emissions. My hypothesis is that the CH_4 more fraction magnitude cannot infer the leak size alone, and the atmospheric variability significantly impacts the surface CH_4 emissions. Therefore, the objectives of this research, described specifically in chapter 4, are to use the atmospheric inverse modeling method to investigate the subsurface emissions, test the accuracy by comparing estimates directly against known, controlled underground leak rates, and provide a measure for having an estimate representative of the actual subsurface leak by considering the impacts of atmospheric variability.

(3) What atmospheric factors significantly impact CH_4 plume shape and size from subsurface NG pipeline leaks? How does the 3D gas plume characterization contribute to optimizing LDAQ survey protocol methodology?

The LDAQ survey protocol methodology depends on the operators, and there is a lack of a physical base for the design and use of the survey protocol methodology among these methods. The efficiency of these survey protocol methodology is poorly understood. Currently, no work was found to understand the plume behavior from underground NG pipeline leaks and link this understanding with the design or use of survey protocol methodology. My hypothesis is that the success of detecting a leak highly depends on the ability to observe the elevated CH_4 mixing ratio within the aboveground plume, and understanding plume evolution is an essential factor for the design or use of survey protocol methodology. The objectives of this research, described specifically in chapter 5, are to characterize near-field 3D gas plume behaviors in a range of atmospheric conditions, reveal the significant atmospheric factors shaping the plume variability, and use these physical findings to inform the survey protocol methodology.

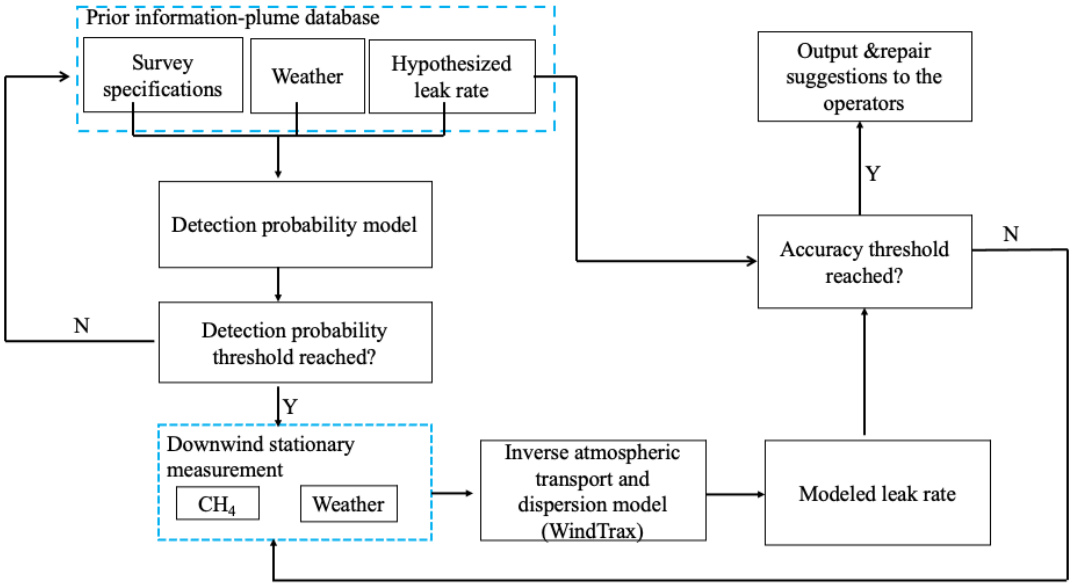

Figure 1.1 Framework of the doctoral research

1.3 Dissertation Structure

This dissertation consists of six chapters and five appendices. Chapter 1 introduces the general motivation, problems, research goals, questions, and objectives. Chapter 2 provides the literature review information on the topics related to this dissertation. The subsequent three chapters are modified from three manuscripts on the following topics: investigating the detection probability of mobile survey solutions for natural gas pipeline leaks under different atmospheric conditions (Chapter 3), estimating methane emissions from underground natural gas pipelines using an atmospheric dispersion-based method (Chapter 4), and improving the efficacy of leak detection and quantification survey methods using 3D plume measurements (Chapter 5).

Chapter 3 investigates the detection probability of mobile survey methods for underground NG pipeline leaks in a comprehensive approach and presents a validated DP model for mobile survey methods providers to optimize the survey protocols. The results highlighted the dependence of the detection efficiency of the leak survey methods on survey speed, atmospheric stability, and wind speed. This chapter is based on the paper that has been published in Environmental Pollution entitled “Investigating detection probability of mobile survey solutions for natural gas pipeline leaks under different atmospheric conditions” by Shanru Tian (Primary researcher and author), Stuart N. Riddick (Research scientist, Colorado State University), Younki Cho (Research scientist, Colorado State University), Clay S. Bell (Research scientist, Colorado State University), Daniel J. Zimmerle (Senior research associate, Methane Emissions Technology Evaluation Center, Colorado State University), Kathleen M. Smits (Professor, Southern Methodist University). Approval for the republication of the manuscript was confirmed by Environmental Pollution Journal and all co-authors.

Chapter 4 focuses on CH_4 emission estimate accuracy compared to controlled known leak rates from underground NG pipeline leaks under realistic conditions. The results show that the surface CH_4 emissions have a large temporal variability due to the change in atmospheric stability, and a certain amount of data is required to have a representative estimate of the real below-ground NG leak rate. This chapter is based on the paper published in Elementa: Science of the Anthropocene entitled "Estimating methane emissions from underground natural gas pipelines using an atmospheric dispersion-based method" by Shanru Tian (Primary researcher and author), Kathleen M. Smits (Professor, Southern Methodist University), Younki Cho (Research scientist, Colorado State University), Stuart N. Riddick (Research scientist, Colorado State University), Daniel J. Zimmerle (Senior research associate, Colorado State University), Aidan Duggan (Research scientist, Colorado State University). Approval for the republication of the manuscript was confirmed by Elementa: Science of the Anthropocene Journal and all co-authors.

Chapter 5 focuses on the characterization of leaked 3D CH_4 plume behaviors under a range of atmospheric conditions and uses the findings to provide a physical base for designing or using survey protocols for NG pipeline leak survey activities. This chapter is based on a research article in review.

Chapter 6 presents conclusions and recommendations for future research.

Chapter 2 Background and Literature Review

2.1 Significance of Mitigating Methane Emissions from Underground Natural Gas Pipeline Leaks

2.1.1 Climate and Air Quality

With the population and economic growth, the newly released international energy outlook by the U.S. Energy Information Administration (EIA) projects that global consumption of natural gas (NG) is expected to increase by 31% between 2020 and 2050 (~1% annual growth) (U.S. Energy Information Administration, 2021b). The use of NG (60–98% CH_4) is considered a short-term bridging fuel to a low-carbon renewable future as it emits 29–44% less CO_2, 79–80% less NOx, 92–99.7% fewer particulates, and 99.9% less SO_2 than other fossil fuels (coal and petroleum) (Liang et al., 2012). In the United States, NG provides 29% of the total energy consumption, heats about half of the homes, and generates 33% of the total electricity (The National Academy of Sciences, 2022). On the other hand, NG is the fast-growing fossil energy in China, and the share of NG in the whole energy mix is expected to increase by 9% between 2016 and 2030 (~0.6% annual growth) to fulfill the carbon-neutral target (National Development and Reform Commission of China, 2016).

However, some studies (Howarth, 2014; Zhang et al., 2016; Alvarez et al., 2018) showed that natural gas leakages might erode the climate benefit of natural gas use as methane (CH_4) has a relatively short lifetime (CH_4: ~12 years; CO_2: 300–1000 years), and a global warming potential 86 times greater than that of CO_2 over a 20-year horizon (IPCC, 2014). Anthropogenic methane emissions contribute to about 60% of global methane emissions, mainly from fossil fuel (35%), agriculture (40%), and waste (20%) (UNEP&CCAC, 2021). Due to the short lifetime of methane and its powerful global warming potential, reducing anthropogenic methane emissions is a practical approach to rapidly reducing near-term warming rates (UNEP&CCAC, 2021; Nisbet et

al., 2020). By 2030, global methane emissions need to reduce by 40-45% to prevent temperature rise to the 1.5 ℃ targets (UNEP&CCAC, 2021). The fossil fuel and waste sectors are expected to have the most significant potential for achieving methane emission mitigation targets (UNEP&CCAC, 2021; Nisbet et al., 2020). Besides, methane oxidation is a primary process for producing tropospheric ozone (a primary air pollutant to human health) (Fiore et al., 2008; Jackson et al., 2021). Thus, reducing methane emissions will improve air quality by reducing the tropospheric ozone concentrations and reducing ozone exposure to health risks, such as premature mortality and cardiovascular diseases (Shindell et al., 2012; Malley et al., 2017).

2.1.2 Public Safety

As a critical infrastructure across the production and delivery lifecycle, the natural gas pipeline expands significantly because of the rapid growth of NG consumption around the world (Global Energy Monitor, 2022). There are about 3 million miles of pipeline networks throughout the continental United States (U.S. Energy Information Administration, 2021a). Unlike other infrastructures in the NG supply chain, the pipelines are mostly buried belowground, and some of them, such as distribution pipelines, travel across the business and residential areas. Over the past 20 years (2002–2021), U.S. natural gas leaks and explosions resulted in 227 fatalities, 1,030 injuries, and an estimated total cost of $6.22 billion (PHMSA., 2022). Common causes of pipeline leakage include corrosion, incorrect operation, excavation or similar ground disturbances, natural force damage caused by ground shifts or above-ground loads, and equipment failure (PHMSA, 2018). Given the vast mileage and spatial distribution of NG pipelines, effective leak detection and quantification (LDAQ) survey methods are critical to identifying a leak promptly when it has occurred, thus initiating appropriate responses to repair the pipeline quickly. Fixing the leaks

timely can prevent accidents, reduce public safety and property risk, lower economic costs, and reduce CH_4 emissions to meet the global greenhouse gas emission-reduction goals.

2.2 Leak Detection and Quantification Survey Challenges for Underground Natural Gas Pipeline Leaks

2.2.1 The Knowledge Gap in Understanding the Efficiency of Leak Detection and Quantification Survey Methods

Currently, a variety of leak detection and quantification survey methods are in use to mitigate CH_4 emissions from underground NG pipeline leaks, including walking survey (PHMSA., 2017; GPTC, 2018; Chen et al., 2020; Cho et al., 2020; Riddick et al., 2021), driving survey (Phillips et al., 2013; Gallagher et al., 2015; Von Fischer et al., 2017; Zimmerle et al., 2017; Weller et al., 2018; Keyes et al., 2020), unmanned-aerial-vehicle (UAV) survey (Golston et al., 2018; Yang et al., 2018; Barchyn et al., 2019; Fox et al., 2019; Li et al., 2020), and aircraft survey (Kligman, 2011; Vaughn et al., 2017; FlyARH, 2021; LASEN, 2021; Heliops, 2022). Surveyors in a walking survey walk at a distance of up to 30 m from the pipelines to detect enhanced CH_4 mole fractions between 0 and 1 m above the ground, using a hand-held analyzer such as Heath Inc. Remote Methane Leak Detector (RMLD; range: 0–99,999 ppm-m; sensitivity: 5−10 ppm-m; frequency: 3 Hz) or a Bascom-Turner Gas-Rover (GR; range: 5–10,000 ppm; accuracy: 2% ± 10 ppm; frequency: 1–2 Hz) (Zimmerle et al., 2017; Weller et al., 2018; Cho et al., 2020; Riddick et al., 2021). Surveyors in a driving survey, drive a vehicle at a speed of 4–15 m s^{-1} (9–34 mph) at a distance of up to 200 m from the source to detect enhanced CH_4 mole fractions between 0.3 and 4.5 m above the ground using a tracer gas analyzer, such as Picarro GasScouter (range: 0–20 ppm; precision: < 0.5 ppb) or an ABB micro-portable greenhouse gas analyzer (MGGA; range: 0.01–

100 ppm; precision: < 2 ppb) (Phillips et al., 2013; Jackson et al., 2014; Gallagher et al., 2015; Rella et al., 2015; Von Fischer et al., 2017; Caulton et al., 2018; Weller et al., 2020). The UAV survey flies at a speed of 2–30 m s^{-1} (4–67 mph) at a distance of up to 1,000 m from the source to detect enhanced CH_4 mole fractions or path-integrated CH_4 mole fractions with a flight height of up to 122 m, equipped with a point gas analyzer such as (e.g., ABB MGGA) or path-integrated gas analyzer (e.g., Heath Inc., RMLD) (Golston et al., 2018; Yang et al., 2018; Barchyn et al., 2019; Fox et al., 2019; Li et al., 2020). The aircraft survey flies at a survey speed of 11–51m s^{-1} (25–114 mph) at a distance of 900–1500 m from the source to detect enhanced CH_4 mole fractions or path-integrated CH_4 mole fractions with a flight height of 60–580 m, usually equipped with remote sensing infrared imaging spectrometer such as Kairos Aerospace's hyperspectral CH_4 imaging system (resolution: 3 m) (Kligman, 2011; Vaughn et al., 2017; Sherwin et al., 2021; FlyARH, 2021; LASEN, 2021; Heliops, 2022). Although these survey methods have been increasingly applied to detect and quantify NG pipeline leaks, the effectiveness remains unclear, creating a challenge in interpreting the disparity in reported leak densities and emission rates based on different survey methods.

A recent field driving survey campaign in 2018 reported hundreds of leak indications from the urban distribution pipeline in the service areas of two local distribution Companies (LDC) (Weller et al., 2018). However, a subsequent walking survey by LDC field crews failed to find more than 80% of leaks detected by the driving survey. The driving surveyors then visited 30 random driving-based leak indication locations yet not discovered by the walking surveyors and confirmed that this disparity was due to the large false negative rate of the walking surveyors. However, due to the unavailability of detailed survey parameters for both surveys, such as survey time, weather conditions, survey heights, and distances, it is difficult to justify the disparity of both methods in

detection efficiency reported in this study. The Pacific Gas & Electric (PG&E) conducted two side-by-side studies (Sacramento gas service area: 4,256 miles of NG distribution pipeline; Diablo gas service area: 3,593 miles of NG distribution pipelines) to compare the detection efficiency of the walking survey and driving survey (Clark et al., 2012; Kerans et al., 2012). In both studies, the driving survey was followed by approximately five weeks of the competition of the walking survey. Both surveys covered almost the same pipeline mileage and areas. The results showed that both methods detected a different subset of leaks, and the percentage of overlapped detection was only 5% and 12%, respectively. Given the time lag between two surveys in these two PG&E studies, the low percentage of overlapped detection in both methods is probably due to the difference in environmental conditions and survey parameters. Also, the results of the field driving survey campaigns in Durham, NC, following the same route at different times, showed that leak detection density was 50% higher at night (0.33 leaks per mile) compared to daytime conditions (0.22 leaks per mile) when (Gallagher et al., 2015).

On the other hand, great controversy exists on actual CH_4 emissions from the NG supply chain system. Generally, the national estimate of CH_4 emissions for each NG source category is compiled as the products of the emission factor (emission per leak) and the activity factors (leaks per length of each material). The newly released U.S. Environmental Protection Agency's current greenhouse gas inventory shows that the NG supply chain system in the U.S emitted 6.6 Tg of CH_4 emissions in 2020 and is the second largest source of CH_4 emissions, responsible for 25% of the total CH_4 emission (U.S. EPA, 2022). The assessment report also demonstrates that CH_4 emissions from the NG supply chain decreased by 16% between 1990 and 2020 (0.5% annual decrease). This decreasing trend is consistent with a previous study that measured CH_4 emissions from 13 urban distribution systems across the U.S. and found decreasing CH_4 emissions from NG

distribution systems (Lamb et al., 2015). However, some studies pointed out that the U.S. EPA inventory underestimates CH_4 emissions from the NG supply chain (Brandt et al., 2014; Brandt et al., 2016; Alvarez et al., 2018; Plant et al., 2019; Weller et al., 2020). The estimated national CH_4 emission in U.S. distribution mains from the driving survey campaigns is approximately five times greater than the U.S. EPA 2017 CH_4 emission estimate from the NG pipeline mains (Weller et al., 2020). Such a disparity mainly attributes to emission and activity factors' variability (Plant et al., 2019; Weller et al., 2020). The U.S. EPA approach generally estimate the emissions by extrapolating a certain amount of direct surface dynamic chamber measurements into the national scale with a 85% detection probability assumed (Campbell, 1996; Lamb et al., 2015; U.S. EPA, 2022). For the driving survey approach, the emission factors are developed using a statistically fitted linear model that relates the maximum CH_4 mole fraction, the total plume peak area, and the ratio of maximum CH_4 mole fraction to peak area (Weller et al., 2018; Weller et al., 2020). And the activity factors are estimated as a function of pipe age and materials by fitting the leak indication data from the survey to the pipeline information (i.e., age and materials) (Weller et al., 2020). None of the above approaches have verified their accuracy against the controlled belowground NG release rates. Therefore, assessing the efficiency of LDAQ survey methods is the first step to understanding these disparities in national CH_4 emissions from NG pipeline leaks and estimating the actual NG pipeline emissions accurately, which eventually benefits the CH_4 reduction climate efforts to achieve a sustainable future.

2.2.2 Environmental Factors Affecting the Efficiency of Leak Detection and Quantification Survey Methods

Detecting and quantifying subsurface NG pipeline leaks is quite challenging as the leaked CH_4 plume shape and size change with the change in the soil and atmospheric conditions (Forde et al., 2019; Ulrich et al., 2019; NARUC, 2019; Cho et al., 2020; Gao et al., 2021; Riddick et al., 2021). The leaked subsurface CH_4 could migrate up to 6 m from the pipeline depending on the leak size and soil conditions, such as soil properties and moisture (Ulrich et al., 2019; Cho et al., 2020). The primary mechanisms for CH_4 plume transport in the subsurface are advection and diffusion, with advection dominating close to the leak point, whereas diffusion dominates as the plume moves away from the leakage source (Okamoto and Gomi, 2011; Mitton, 2018; Gao et al., 2021). Subsurface conditions such as soil heterogeneity, soil moisture, temperature, and pressure gradients (due to high pipeline pressure) take primary control of the fate and transport of CH_4 plumes in the soil (Poulsen Tjalfe G. et al., 2003; Ho, Clifford K., 2006; Chamindu Deepagoda et al., 2016; Smith et al., 2018). Moreover, atmosphere pressure-induced barotropic pumping also affects the subsurface transport and emission of gas into the atmosphere (Auer et al., 1996; Forde et al., 2019).

After the fugitive CH_4 enters the atmosphere, the shape and size of the leaked CH_4 plume are mainly governed by atmospheric conditions such as atmospheric stability, wind speed, air temperature, and air humidity (Carpenter et al., 1971; Arya, 2001; Stull, 2012; Leelőssy et al., 2014; Thorpe et al., 2016; Ulrich et al., 2019; Riddick et al., 2021; Cho et al., 2022). The atmosphere in the atmospheric boundary layer (ABL) has a typical daily cycle. The atmosphere tends to be unstable, with larger wind, higher air temperature, and lower humidity during the day, but it is usually stable with lower wind, lower air temperature, and higher humidity at night (Arya, 2001; Stull, 2012). The gas plume generally becomes narrower and more concentrated as the atmospheric conditions changes from the unstable to stable (Arya, 2001; Riddle et al., 2004; Stull,

2012; Leelőssy et al., 2014). The plume shape tends to be longer and narrower during high wind speed conditions but shorter and wider during low wind conditions (Carpenter et al., 1971; Thorpe et al., 2016). For a large subsurface NG leak (0.44 kg h^{-1} of CH_4), the atmospheric CH_4 mixing ratio within 0.1 m above the ground drops below 100 ppm (0.01 vol %) under moderate wind conditions (average wind speed: > 2 m s^{-1}), while the subsurface CH_4 mixing ratio exceeds 80 vol % below 0.2 m of the ground (Ulrich et al., 2019). However, there has been no work to systematically understand the atmospheric CH_4 plume behaviors from subsurface emissions over a range of atmospheric conditions, and explicitly link these findings with LDAQ survey methods, with a goal of advancing the efficiency of LDAQ survey methods.

Some aboveground emission studies for NG aboveground infrastructures have demonstrated that LDAQ survey efficiency is a function of survey protocol parameters and environmental conditions (Rella et al., 2015; Thorpe et al., 2016; Caulton et al., 2018; Ravikumar et al., 2018; Barchyn et al., 2019; Bell et al., 2020; Zimmerle et al., 2020; Sherwin et al., 2021). The controlled single-blind detection tests found a power-law relationship between leak detection probability and detection distance between 1.5 and 15 m of the leak source for the walking survey equipped with an optical gas imaging (OGI) camera (Ravikumar et al., 2018). By adjusting the survey speed, the highly experienced OGI surveyors can detect 1.7 (1.5–1.8) times more aboveground leaks than less experienced surveyors (Zimmerle et al., 2020). The UAV and airplane survey experiments for aboveground controlled release showed that detection probability (DP) is the highest under moderate wind speed conditions (2–2.5 m s^{-1}) (Barchyn et al., 2019; Sherwin et al., 2021). However, another walking survey experiment found no relationship between the DP and wind speed (Ravikumar et al., 2018). Like the wind speed, some aboveground release experiments have shown that DP is positively related to the leak size (Rella et al., 2015; Ravikumar et al., 2018; Bell

et al., 2020), such a relationship yet does not exist in other studies (Barchyn et al., 2019; Ravikumar et al., 2019). The current driving survey-based quantification methods have reported a large uncertainty between –50% and 350% for aboveground NG infrastructure emission estimates due to large atmospheric variability (Lan et al., 2015; Rella et al., 2015; Yacovitch et al., 2015). At least ten repeat driving survey transects are needed to reduce uncertainty due to the atmospheric variability, and the uncertainty is estimated at 0.05–6.5 times the emission rate for single-transect sites and 0.5–2.7 times the emission rate for sites with more than ten transects (Caulton et al., 2018).

Chapter 3 Investigating Detection Probability of Mobile Survey Solutions for Natural Gas Pipeline Leaks Under Different Atmospheric Conditions

Tian, S., Riddick, S.N., Cho, Y., Bell, C.S., Zimmerle, D.J. and Smits, K.M., 2022. Investigating detection probability of mobile survey solutions for natural gas pipeline leaks under different atmospheric conditions. Environmental Pollution, p.120027. DOI: https://doi.org/10.1016/j.envpol.2022.120027

3.1 Abstract

The 2015 Paris agreement aims to cut greenhouse gas emissions and keep global temperature rise below 2 °C above pre-industrial levels. Reducing CH_4 emissions from leaking pipelines presents a relatively achievable objective. While walking and driving surveys are commonly used to detect leaks, the detection probability (DP) is poorly characterized. This study aims to investigate how leak rates, survey distance and speed, and atmospheric conditions affect the DP in controlled belowground conditions with release rates of 0.5–8.5 g min^{-1}. Results show that DP is highly influenced by survey speed, atmospheric stability, and wind speed. The average DP in Pasquill–Gifford stability (PG) class A is 85% at a low survey speed (2–11 mph) and decreases to 68%, 63%, 65%, and 60% in PG B/C, D, E/F, and G respectively. It is generally less than 25% at a high survey speed (22–34 mph), regardless of stability conditions and leak rates. Using the measurement data, a validated DP model was further constructed and showed good performance (R^2: 0.76). The options of modeled favorable weather conditions (i.e., PG stability class and wind speed) to have a high DP (e.g., >50%) are rapidly decreased with the increase in survey speed. Walking survey is applicable over a wider range of weather conditions, including PG stability class A to E/F and calm to medium winds (0–5 m s^{-1}). A driving survey at a low speed (11 mph) can only be conducted under calm to low wind speed conditions (0–3 m s^{-1}) to have an equivalent DP to a walking survey. Only calm wind conditions in PG A (0–1 m s^{-1}) are appropriate for a high driving speed (34 mph). These findings showed that driving survey providers need to optimize the survey schemes to achieve a DP equivalence to the traditional walking survey.

3.2 Introduction

Natural gas (NG), composed of 60–98% methane (CH_4), is considered a cleaner energy source than other fossil fuels, such as coal. NG has been promoted as a transition fuel until renewable technologies can prove greenhouse gas (GHG) emission free energy (Alvarez et al., 2012; Levi, 2013; Zhang et al., 2016; Zou et al., 2018; Zhang et al., 2022). Its use has grown rapidly and is now a significant component of the global energy resource (Heath et al., 2015; Schivley et al., 2018; Zhang et al., 2022). For example, NG provides 30% of the energy consumption in the U.S. and requires an extensive infrastructure including three million miles of NG pipeline (U.S. Energy Information Administration, 2021a; National Academies of Sciences, 2022). Leak detection for pipeline systems has historically been driven primarily by concerns of public safety to reduce fatal and non-fatal incidents caused by pipeline leaks. However, more recently reducing CH_4 emissions from NG systems, including pipelines, has been identified as a way to help mitigate climate change and meet the goals of the Paris agreement (Nisbet et al., 2020).

From 2002 to 2021, the Pipeline and Hazardous Materials Safety Administration (PHMSA) reported 2,986 NG pipeline incidents (153 from gathering lines, 1,439 from transmission lines, and 1,394 from distribution lines), resulting in 227 fatalities (38 and 189 from transmission and distribution lines, respectively) and 1,030 injuries (6, 157 and 867 from gathering, transmission and distribution lines, respectively) (PHMSA., 2022). Recent studies suggest that the NG supply chain system in the U.S. was responsible for 6.6 Tg of CH_4 emissions in 2020, corresponding to 0.79% of the 111.2 billion cubic feet per day (bcf day^{-1}) of NG produced (~833.45 Tg NG yr^{-1}) (U.S. Energy Information Administration, 2022; U.S. EPA, 2022). CH_4 has a global warming potential 86 times greater than that of CO_2 over a 20-year horizon (IPCC, 2014), and the environmental benefits of using NG as a near-term bridging fuel would be offset if the NG supply

chain emits CH_4 more than 3.2% of the total NG production (Alvarez et al., 2012; UNFCCC, 2022). Reducing CH_4 emissions from the NG supply chain presents a relatively straightforward objective for GHG mitigation while improving public safety.

Currently, walking and driving surveys are commonly used to detect NG leaks from pipelines (Phillips et al., 2013; Gallagher et al., 2015; Zimmerle et al., 2017; Weller et al., 2018; Cho et al., 2020; Li et al., 2020; Riddick et al., 2021). In a walking survey, surveyors walk along the pipelines and detect enhanced CH_4 mole fractions using a handheld instrument, such as a Bascom-Turner Gas-Rover (GR; range: 5–10,000 ppm; accuracy: 2% ± 10 ppm; frequency: 1–2 Hz) or Heath Inc. Remote Methane Leak Detector (RMLD; range: 0–99,999 ppm-m; sensitivity: 5–10 ppm-m, frequency: 3 Hz) (Zimmerle et al., 2017; Weller et al., 2018; Cho et al., 2020; Riddick et al., 2021). GR measures the surface CH_4 mole fraction by drawing air from the surface onto a dual catalytic combustion sensor (for measuring between 0 to 2 vol % CH_4) or a thermal conductivity sensor (2 to 100 vol % CH_4) (Cho et al., 2020; Riddick et al., 2021). RMLD uses laser technology (Tunable Diode Laser Absorption Spectroscopy) to measure the path-integrated CH_4 mole fraction (reported as ppm-m) remotely within a 30 m distance of the pipeline (Heath Consultants, 2009). A driving survey measures the CH_4 mole fraction in the air at a distance of up to 200 m from the source using a trace gas CH_4 analyzer, such as an ABB micro-portable greenhouse gas analyzer (MGGA; range: 0.01–100 ppm; precision: < 2 ppb) or Picarro GasScouter (range: 0–20 ppm; precision: < 0.5 ppb) (Phillips et al., 2013; Jackson et al., 2014; Gallagher et al., 2015; Von Fischer et al., 2017; Zimmerle et al., 2017; Weller et al., 2018; Keyes et al., 2020). The height of the sensor mounted on the vehicle varies between 0.3 and 4.5 m depending on the driving survey method, and survey speeds range between 4 and 15 m s^{-1} (9–34 mph) (Phillips et al., 2013; Jackson et al., 2014; Gallagher et al., 2015; Zimmerle et al., 2017; Weller et al., 2018). Even though there is a lot of

interest in these survey methods, there is not a clear understanding of best practices, specifically how survey distance, survey height, survey speed, and atmospheric conditions could affect the probability of leak detection. While prior studies have used walking and driving surveys to detect subsurface NG leaks (Phillips et al., 2013; Gallagher et al., 2015; Von Fischer et al., 2017; Weller et al., 2018; Cho et al., 2020; Keyes et al., 2020), the survey detection probability (DP) was not characterized.

Currently, there is no quantitative relationship between subsurface leak rate and DP for controlled belowground leak conditions. Some aboveground emission studies have shown that DP increases with the emission rate (Rella et al., 2015; Ravikumar et al., 2018; Bell et al., 2020). Others suggested that the relationship does not always exist (Ravikumar et al., 2019). One recent study, using a drone with a survey speed of 15–20 m s^{-1} (34–45 mph), showed no relationship between leak rate and DP (Barchyn et al., 2019). Other aboveground studies have found a strong relationship between downwind distance and the DP, where controlled single-blind detection tests using an optical gas imaging (OGI) camera found a power-law relationship between leak size and detection distance between 1.5 and 15 m of the leak source (Ravikumar et al., 2018). Zimmerle et al. (2020) indicated that the experience of OGI surveyors significantly impacted the DP, and highly experienced surveyors detected 1.7 (1.5−1.8) times more aboveground leaks than less experienced surveyors, primarily by adjusting the survey speed.

In addition to leak rate and survey protocols, prior studies have explored how atmospheric conditions, mostly wind speed, affect the DP (Thorpe et al., 2016; Ravikumar et al., 2018; Barchyn et al., 2019; Bell et al., 2020). Similar to the leak rate, the effect of wind speed on DP is unclear. Thorpe et al. (2016) did not find any significant relationship between wind speed and DP using an airborne visible/infrared imaging spectrometer (AVIRIS-NG) during the controlled release

experiments. This finding was also consistent with Ravikumar et al. (2018). In contrast, two aboveground controlled release experiments showed that the drone and airplane surveys have the highest DP in moderate wind speeds (2–2.5 m s^{-1}) (Barchyn et al., 2019; Sherwin et al., 2021). A belowground controlled release experiment from Riddick et al. (2021) showed that surface CH_4 mole fractions are mostly affected by atmospheric stability and suggested avoiding walking surveys during strong winds or strong solar irradiance conditions. A recent study (Tian et al., 2022) pointed out that subsurface leaks can be quantified using time-averaged downwind CH_4 concentration measurements. The authors know of no peer-reviewed studies that systematically investigate how leak rate sizes, survey protocols, and atmospheric conditions affect the DP of subsurface NG emissions. Thus, this study aims 1) to investigate how the leak rate, survey distance and speed, and atmospheric conditions affect the DP of a subsurface NG emission; 2) to develop a validated DP model for practitioners that incorporates the leak rate, survey distance, survey speed, and weather conditions including atmospheric stability, wind speed, and air temperature; 3) to model the weighted DP for walking and driving surveys using three published and publicly available emission rate datasets from NG distribution pipeline leaks. To our knowledge, this is the first time that a validated DP model has been developed, considering all critical parameters of the leak survey measured from belowground emission experiments.

3.3 Material and Methods

3.3.1 Experiment and Measurement Approaches

Five controlled NG release (87±2 vol % CH_4) experiments were conducted from June 21st to July 4th, 2021, with the release rate ranging from 0.5 to 8.5 g min^{-1}(Table 3.1) at Colorado State University's Methane Emission Technology Evaluation Center (METEC) in Fort Collins, CO, U.S.

The release rates were chosen to represent the range of leaks from the underground NG pipelines observed in the field (Lamb et al., 2015; Von Fischer et al., 2017). The testbed used here is a rural testbed with short surface vegetation (average height: 0.05 m). The pipeline was buried at 0.9 m below the ground surface along the east-west direction of the site and backfilled with the native soil (sandy loam, U.S. Department of Agriculture Soil Texture Classification). Gas was injected through stainless-steel tubing (0.635 cm, model SS-T4-S-035-20, Swagelok, USA) into the testbed from an aboveground 145-liter compressed natural gas (CNG) tank. The gas flow rate was controlled by pressure regulators, solenoid valves, and choked flow orifices. It was measured by a thermal mass flow meter (range: 0–11 g min^{-1}, accuracy: ±1%, Omega FMA1700 series). A detailed description of this testbed can be found in prior publications (Mitton, 2018; Ulrich et al., 2019; Cho et al., 2020).

Table 3.1 General information of the five controlled belowground NG release experiments at the METEC site from June 21st to July 4th, 2021. The release rate ranged from 0.5 to 8.5 g min^{-1}. The total number of passing was 3,472 for the five experiments.

Exp	Date	Release rate (g min^{-1})	Total number of passings
1	June 21 to June 26, 2021	0.5	1282
2	June 30 to July 01, 2021	0.8	434
3	June 28 to June 29, 2021	1.6	318
4	July 01 to July 02, 2021	3.5	730
5	July 02 to July 04, 2021	8.5	708

During each experiment, CH_4 mole fraction and GPS coordinate data were collected while walking at distances (1, 5, 10, and 20 m) downwind of the emission point and perpendicular to the wind direction. CH_4 mole fractions were measured using a high-precision gas analyzer (GasScouter™ G4301, Picarro, Inc.), with 0.1 ppb measurement precision at a 1 Hz measurement interval. GPS data were collected using a Picarro A0946 unit with a position accuracy of < 1 m and 1 Hz update frequency. At each distance downwind of the emission point, transects were measured at three heights (0.05, 0.25, and 0.5 m), which typically simulate both walking and

driving surveys (Phillips et al., 2013; Zimmerle et al., 2017; Cho et al., 2020; Riddick et al., 2021). The survey speed was 1 m s^{-1} (~2 mph) on average, and the transect length was 80 m. Here, one complete measurement per distance per height is defined as "one passing", and the total number of passings was 3,472 for the five experiments (Table 3.1). In order to show how survey speed affects detection probability, the measured CH_4 mole fraction data in each walking passing were extended to produce a series of data simulating increased survey speed from 2 to 15 m s^{-1} (4–34 mph) using a down-sampling method as follows: 1) The walking survey speed is 1 m s^{-1}, and the gas analyzer measures the CH_4 mole fraction at 1 Hz. Thus, the walking survey data represent approximately 1 m intervals along the transect in each pass (i.e., 1 m interval in every two adjacent samples); 2) When the survey speed increases to 2 m s^{-1}, every other sample is selected to simulate a 2 m interval in each passing; 3) The down-sampling was repeated for other speeds from 3 to 15 m s^{-1} by selecting every 3 to 15 m in each passing, respectively. This approach assumes that the instrument has a fast response time (e.g., 1–10 Hz) and, therefore able to detect the CH_4 emissions from the belowground pipeline leaks. Instruments with response times in the 1–10 Hz range are increasingly available in recent years, such as the Li-Cor LI-7700 open path CH_4 analyzer (frequency: 10 Hz, precision: < 5 ppb) or the ABB's LGR-ICOS™ ultrasensitive gas analyzer (frequency: 10 Hz; precision < 1ppb). This down-sampling approach based on a 1–10 Hz frequency instrument may not work well in some situations. For example, if the plume width is less than the sampling interval linked to a fast-driving speed. We also acknowledge that this assumption did not consider the influence of the vehicle on the plume in a real driving survey situation and not always driving downwind of the emission source. The 3D wind fields, and air temperature were measured at 8 Hz using an RM Young 81000 Ultrasonic Anemometer installed 6 m above the ground at the METEC site. Previous studies (Bosveld and Beljaars, 2001; Bardal et

al., 2018) have shown that the 3D sonic anemometer measurements with varying sampling intervals between 1 to 10 Hz do not influence the average vertical flux estimate. However, the uncertainty in the flux estimate increases with a decrease in the sampling interval. Therefore, the 8 Hz sampling interval used in this study will generally satisfy sampling rate requirements to estimate the average vertical flux and stability parameter (i.e., Monin-Obukhov length) accurately.

3.3.2 Methodology

In this work, the subsurface leak was defined as either detection or non-detection for each pass along the pipeline. A pass was considered a detection if a 0.2 ppm CH_4 mole fraction enhancement was observed over the 2.0 ppm background (10% change) at the METEC site. The background CH_4 mole fraction was calculated by averaging the measurements 10 m upwind of the subsurface leaks. This threshold is consistent with a previous study that used the driving survey to conduct pipeline leak detection in 15 metro areas (Luetschwager et al., 2021). The empirical DP was calculated as the number of detected passes divided by the total number of passes.

The 5-minute averaged Monin-Obukhov length (L, m) was calculated (Equations 3.1 and 3.2; Flesch et al., 2004; Foken, 2006; Stull, 2012) from the surface friction velocity (u_*, m s^{-1}), the mean absolute air temperature (T, K), the von Kármán's constant ($k_v = 0.41$), the gravitational acceleration (g = 9.81 m s^{-2}), and 3D horizontal/vertical wind vectors (u, v, and w, m s^{-1}). In accordance with previous studies, the sonic temperature, approximately equal to virtual temperature, was used for T in calculating L (Flesch et al., 2004; Foken, 2006). Any resulting error in L from using sonic temperature rather than virtual temperature should be small as the experiments were conducted in dry air conditions (relative humidity: approx. 30%) (Flesch et al., 2004). The Monin-Obukhov length was also converted into Pasquill-Gifford (PG) stability class

as it is more quickly recognized than L by industry practitioners (Ulrich et al., 2019; Riddick et al., 2021), where PG A (extremely unstable) is $-100 \leq L < 0$, PG B/C (unstable) is $-500 \leq L < -100$, PG D (neutral) is $|L| > 500$, PG E/F (stable) is $500 \leq L < 100$, and PG G (extremely stable) is $0 < \mathrm{L} \leq 100$ (Gryning et al., 2007; Breedt et al., 2018).

$$L = -\frac{\mathrm{u}_*^3 \mathrm{T}}{\mathrm{k_v g}\overline{\mathrm{w'T'}}} \tag{3.1}$$

$$\mathrm{u}_* = \left[\left(\overline{\mathrm{u'w'}}\right)^2 + \left(\overline{\mathrm{v'w'}}\right)^2\right]^{1/4} \tag{3.2}$$

The empirical DP data were randomly split into two parts, i.e., 80% as training data for developing the DP model, and 20% as test data for validating the DP model. The DP model was developed by fitting the training data with a multiple logistic function (Equation 3.3), which is similar to previous studies that used a single logistic function to fit the empirical DP and leak rate (Ravikumar et al., 2018; Luetschwager et al., 2021). The variables considered in the DP model include the leak rate, survey distance, survey speed, atmospheric stability (1/L), wind speed, and air temperature. A p-value of less than 0.05 was used to ensure the variables considered in the model are at least 95% statistically significant. The coefficient of determination (R^2) was used as a metric to validate the performance of the DP model by comparing modeled DP with the empirical DP from test data.

$$\mathrm{DP} = \frac{1}{1 + \mathrm{e}^{-(\mathrm{b_0} + \mathrm{b_1 q} + \mathrm{b_2 c} + \mathrm{b_3 s} + \frac{\mathrm{b_4}}{\mathrm{L}} + \mathrm{b_5 U} + \mathrm{b_6 T})}} \tag{3.3}$$

where $\mathrm{b_0}$ is the intercept, $\mathrm{b_1}, \ldots, \mathrm{b_6}$ are the regression coefficients, q is the leak rate (g $\mathrm{min^{-1}}$), c is the survey speed (mph), s is the survey distance (m), L is the Monin-Obukhov length (m), U is the horizontal wind speed (m $\mathrm{s^{-1}}$), and T is the air temperature (°C).

Using the validated DP model and three publicly available NG pipeline emission datasets (Table 3.2), we modeled the weighted DP (Equation 3.4) to quantity detection efficiency of walking and driving survey (Table 3.3) in a range of atmospheric stability and wind speed conditions. The emission datasets (Table 3.2) were directly measured by the surface chamber from NG distribution main and service line leaks across U.S. (Lamb et al., 2015; Hendrick et al., 2016; GTI, 2019). The total sample size is 446, characterized by a right-skewed distribution. Three super large emitters (16, 24, and 38 g min^{-1}) were removed to be consistent with the range of the controlled leak rates. Thus, there are 443 emission rate points used in the DP model. The survey distance was assumed as 5 m downwind of the pipeline, based on general practice during the field pipeline survey. The driving survey speed was assumed as 11, 22, and 34 mph. These speeds are based on low, medium, and high speeds seen in previous field studies of driving surveys (Phillips et al., 2013; Jackson et al., 2014; Gallagher et al., 2015; Zimmerle et al., 2017; Weller et al., 2018).

Table 3.2 General information of three publicly available CH_4 emission rate datasets from NG distribution pipelines. Emission rates in these three datasets were measured directly using surface flux chambers, where all datasets show a right-skewed distribution characteristic. The total sample size used is 443. Three super large emission points were removed to be consistent with the range of controlled NG release rates in the DP model.

Location	Sample size	Leak source	Reference
California	76	NG distribution mains and services	GTI (2019)
Massachusetts	113	NG distribution mains	Hendrick et al. (2016)
U.S. (various)	257	NG distribution mains and services	Lamb et al. (2015)

$$f = \frac{\sum_{i=1}^{n} DP_i q_i}{\sum_{i=1}^{n} q_i} \tag{3.4}$$

where f is the weighted DP, DP_i is the modeled DP for the i^{th} emission rate q_i (unit: g min^{-1}), n is the total number of emission points (n=443).

Table 3.3 Survey distance and speed for walking and driving surveys. The assumed driving survey speed is 11, 22, and 34 mph, which represents the low, medium, and high speeds of the field driving survey, respectively. The survey distance was assumed as 5 m downwind of the pipeline based on general field survey practices.

Survey solution	Survey distance (m)	Survey speed (mph)
Walking survey	5	2
Driving survey	5	11
Driving survey	5	22
Driving survey	5	34

3.4 Results

3.4.1 Empirical Detection Probability with Different Survey Speeds

Figure 3.1 shows the empirical DP as a function of distance with the mobile survey speed ranging from 2 to 34 mph from the five controlled experiments (Table 3.1). The result showed that the empirical DP decreases with the increase in survey speed. The empirical DP increases with the leak rate near the emission point (< 5 m). The empirical DP is between 70% and 100% at a 1 m distance for an emission rate between 0.5 and 8.5 g min^{-1} at a low survey speed (between 2 and 11 mph). DP decreases with the increase in survey distance, especially for the smallest leak (0.5 g min^{-1}), where the detection probability is 25% at a 20 m distance from the leak source (Figure 1a). For the medium to large leak (0.8–8.5 g min^{-1}), the detection probability decreases to between 50% and 80% at a 20 m downwind distance at a low survey speed (2–11 mph). When the survey speed increases (medium survey speed between 11 and 22 mph), the empirical DP is between 25% and 75% at a 1 m downwind distance, and mostly between 25% and 50% at a 20 m distance. Further,

the empirical DP is less than 25% at any distance regardless of leak size when the survey speed is high (22–34 mph). Besides, compared to Exp1-4, the DP in Exp5 mostly showed an increase with the increase in survey distance considered here for a given survey speed. This is probably due to the largest leak rate (8.5 g min^{-1}) in Exp5, which is large enough to produce a broader plume at a farther downwind distance than that at a closer downwind distance to the subsurface leak source. Thus, for a given survey speed, it is more likely to grab a sample within the broader plume at a farther downwind distance than that at a closer distance when the leak rate is large enough (e.g., >8.5 g min^{-1}).

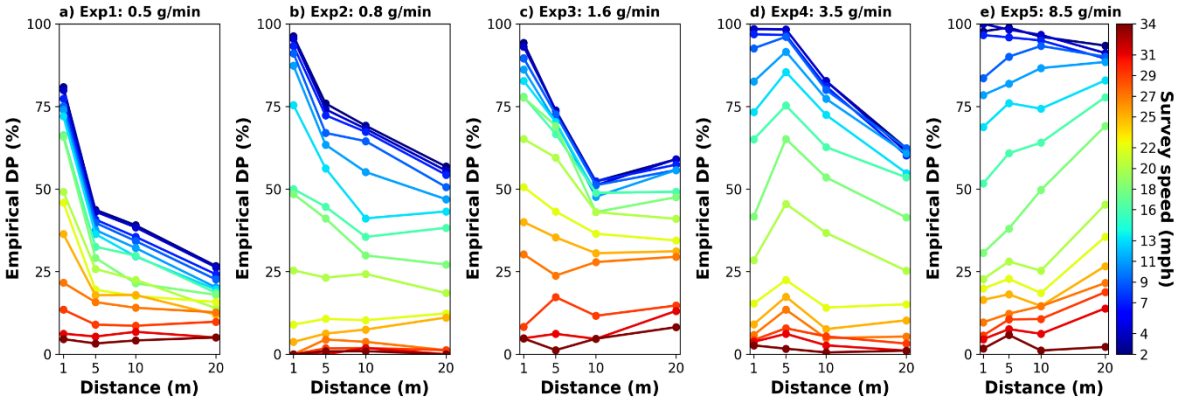

Figure 3.1 Empirical detection probability as a function of distance with the mobile survey speed ranging from 2 to 34 mph for the five controlled experiments (Exp1–5), respectively.

3.4.2 Empirical Detection Probability with Different Atmospheric Stability Conditions

In general, the empirical DP decreases as the atmospheric stability become more stable (PG: A to G) regardless of the survey speed (Figure 3.2). The DP in PG A is between 75% and 100% for the leak rates between 0.5 and 8.5 g min^{-1} with a low survey speed (2–11 mph). With the same low survey speed, the DP decreases to between 45% and 90%, 40% and 85%, 50% and 80%, and 30% and 90% in PG B/C, D, E/F, and G, respectively. When the survey speed increases (medium survey speed between 11 and 22 mph), the empirical DP in PG A is between 50% and 80% for the leak

rates considered here. The DP further reduces to between 25% and 75%, 20% and 70%, 25% and 75%, and 15% and 70% in PG B/C, D, E/F, and G, respectively. When the survey speed increases to high (22–34 mph), the empirical DP is generally less than 25% in PG A, B/C, D, E/F, and G, respectively, for the range of emission rates considered here**.**

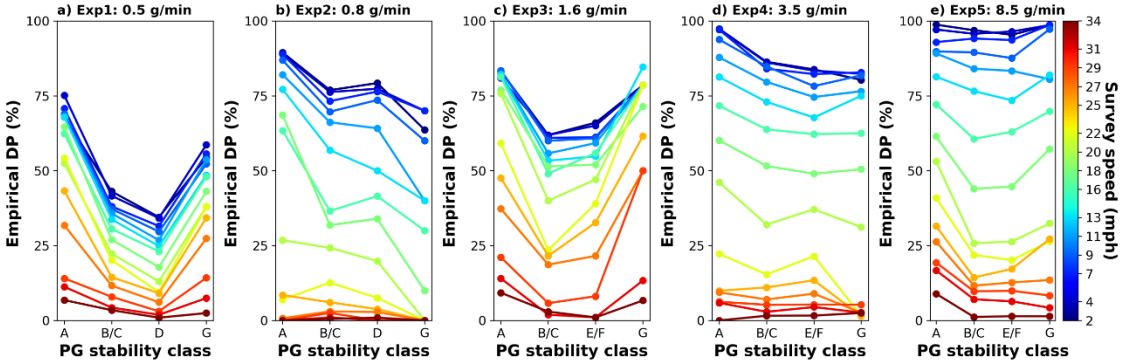

Figure 3.2 Empirical detection probability as a function of the Pasquill-Gifford (PG) stability class with the mobile survey speed of 2–34 mph for the five controlled experiments (Exp1–5), respectively. PG stability class A denotes the extremely unstable condition, PG stability class B/C denotes the unstable condition, PG stability class D denotes the neutral condition, PG stability class E/F denotes the stable condition, and PG stability class G denotes the extremely stable condition. No observation data is available for PG stability class E/F in Exp1–2, and PG stability class D for Exp 3–5.

Generally, each PG stability class can be roughly estimated based on a range of wind speeds (Pasquill, 1961). Calm (0–1 m s^{-1}), small (1–3 m s^{-1}), and medium winds (3–5 m s^{-1}) typically occur during unstable or stable conditions (PG A, B/C, E/F, G). Medium and large winds (5–10 m s^{-1}) generally occur during neutral conditions (PG D). Figure 3.3 further shows the relationship between the empirical DP and the binned wind speed for mobile survey speeds ranging from 2 to 34 mph for the five controlled experiments (Exp1–5). The empirical DP generally decreases with an increase in wind speed. For low survey speeds (2–11 mph), the DP is highest in calm wind conditions (0–1 m s^{-1}), ranging from 70% to 100%. With the same low survey speed, the DP is generally the lowest in large wind conditions (5–10 m s^{-1}), ranging from 30% to 90%. When the survey speed increases to between 11 and 22 mph (medium speeds), the empirical DP reduces to

between 25% and 75%. When the survey speed increases to high speeds (22–34 mph), the empirical DP is generally less than 25%, regardless of wind conditions.

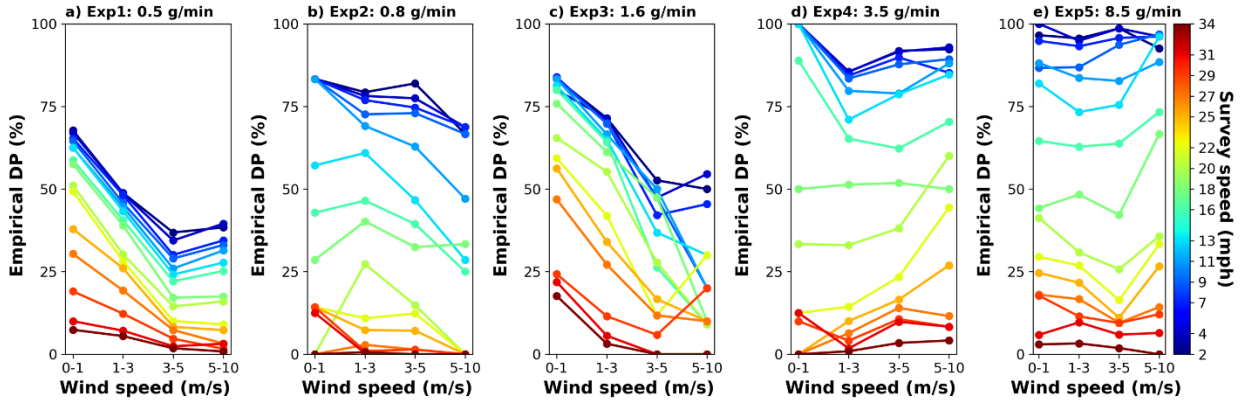

Figure 3.3 Empirical detection probability as a function of the binned wind speed with the mobile survey speed of 2–34 mph for the five controlled experiments (Exp1–5), respectively. The binned wind speed interval is 0–1, 1–3, 3–5, and 5–10 m s^{-1}, representing the the calm, low, medium, and large wind conditions, respectively, according to the measured wind speed range during the experiments.

3.4.3 Validation of the Detection Probability Model

All variables considered here are at least 95% statistically significant, with p values less than 0.05 (Table 3.4). The height variable did not pass the 95% statistically significant test and was therefore removed from the DP model. This is probably due to the small change in plume width for the height range considered in this study (0.05–0.5 m), thereby not having a significant effect on DP. The leak rate is positively related to the DP with the regression coefficient of 0.139$\pm$ 0.0005 (Table 3.4). The regression coefficients for survey speed, survey distance, Monin-Obukhov length, wind speed, and air temperature are all negative, with the largest ones from the Monin-Obukhov length, wind speed, and survey speed, respectively. The regression coefficients from air temperature and survey distance are relatively low, with the values of -0.0807 $\pm$ 0.0006, and -0.057 ± 0.0002. Using the regression coefficients in Table 3.4, the DP model was rewritten as a function of the leak rate, survey distance, survey speed, Monin-Obukhov length, wind speed, and

air temperature (Equation 3.5). When compared with the empirical DP from the test data, the model shows good performance, with a coefficient of determination (R^2) of 0.76 (Figure 3.4).

Table 3.4 Estimated mean regression coefficients and the respective p values in the fitted model. μ is the mean value, σ is the standard error (SE). μ and σ were calculated by bootstrapping the training data 1000 times.

Parameter	**Regression coefficient (μ ± 1σ)**	**p value (μ ± 1σ)**
Intercept (b_o)	5.0221 ± 0.0117	6.14761E-39 ± 3.65743E-39
Leak rate (b_1)	0.139± 0.0005	4.7734E-16 ± 4.34151E-16
Survey speed (b_2)	-0.1498 ± 0.0002	1.0119E-102 ± 9.1455E-103
Survey distance (b_3)	-0.057 ± 0.0002	1.26593E-13 ± 1.3302E-13
Monin-Obukhov length (b_4)	-12.7024 ± 0.0976	1.0586E-04 ± 4.99716E-05
Wind speed (b_5)	-0.4115 ± 0.0021	1.5131E-07 ± 5.2156E-08
Air temperature (b_6)	-0.0807 ± 0.0006	4.279E-06 ± 2.45119E-06

$$\mathrm{DP} = \frac{1}{1 + e^{-(5.0221 + 0.139q - 0.1498c - 0.057s - \frac{12.7024}{L} - -0.4115U - 0.0807T)}} \tag{3.5}$$

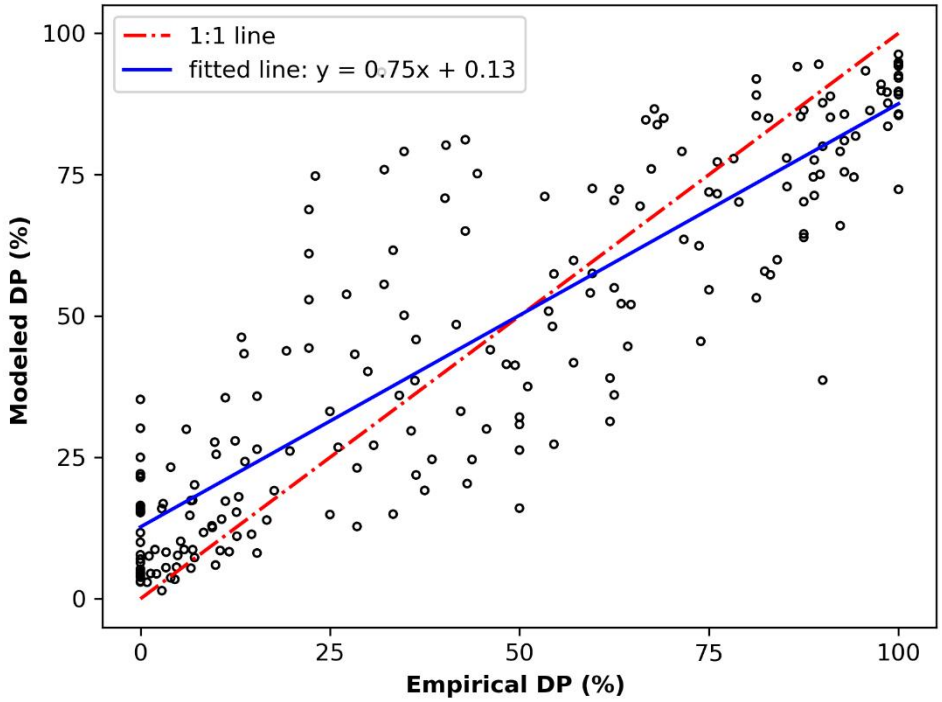

Figure 3.4 Modeled DP vs Empirical DP. The empirical DP is from the test data. The red dashed line is the 1:1 line. The blue line is the fitted equation between Modeled DP and Empirical DP where y is Modeled DP, and x is Empirical DP. The coefficient of determination (R^2) between Modeled DP and Empirical DP is 0.76.

The sensitivity analysis of variables in the DP model showed that survey speed, atmospheric stability (1/L), and wind speed take the most significant effects on the DP (Figure 3.5). DP reduces 20% to 30% when changing survey speed from 2 to 34 mph, atmospheric stability (1/L) from -0.2 to 0.2 m^{-1}, and wind speed from 1 to 10 m s^{-1}, respectively. The change in DP is less than 5% when changing the leak rate from 0.5 to 8.5 g min^{-1}, survey distance from 1 to 20 m, and air temperature from 15 to 30 ℃, respectively. The increase in modeled DP from the sensitivity analysis with an increase in leak rate is smaller than the increase in the empirical DP shown previously (e.g., Figures 3.1a and 3.1e). This is because the empirical DP includes the impacts of other factors, such as atmospheric stability and wind speed. Overall, the modeled DP still reveals the increased trend of DP with the leak rate, which is consistent with observations.

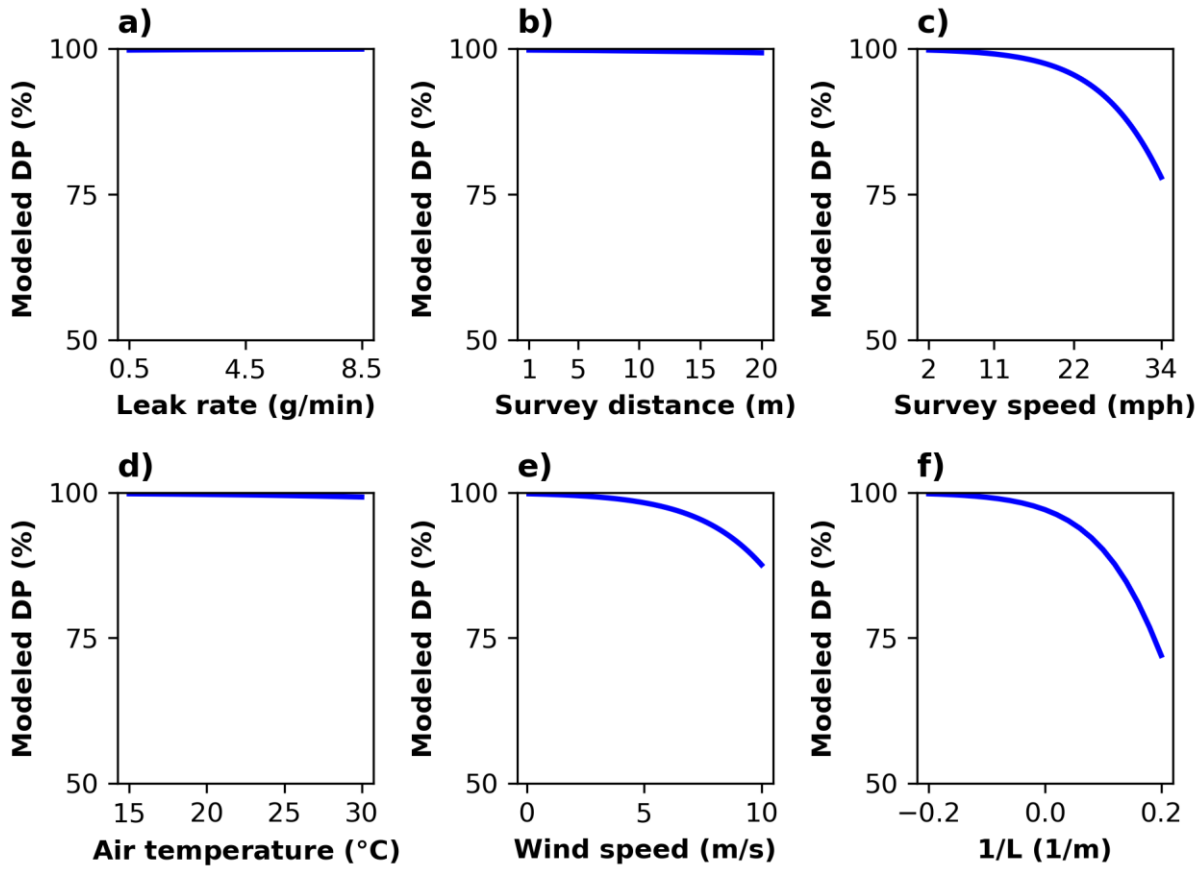

Figure 3.5 Sensitivity analysis of each variable in the model on modeled DP. a)–f) shows the effect of changing leak rate, survey distance, survey speed, air temperature, wind speed, and 1/L input, respectively, while keeping other variables the same as the base case. In the base case, the leak rate is 0.5 g min^{-1}, survey speed is 2 mph, survey distance is 1 m, air temperature is 15 °C, wind speed is 0.1 m s^{-1}, and 1/L is -0.2 m^{-1}. The value of each variable in the base case is the lower limit of the data used for developing the DP model. The maximum value of each variable in a)–f) is the upper limit of the data used for developing the DP model.

3.4.4 Modeled Detection Probability for Walking and Driving Surveys

Given the right-skewed distribution of emissions from the pipeline leaks (Lamb et al., 2015; Hendrick et al., 2016; GTI, 2019), here we modeled the DP for the small and large leaks across different survey speeds, atmospheric stabilities, and wind speed conditions (Figure 3.6). Modeled DP is higher than 90% under the conditions of PG stability class A, low survey speed (2–11 mph),

and calm to medium wind speed (0–5 m s^{-1}), regardless of leak rate. However, when the PG stability class changes to G, modeled DP is less than 50%, and 70% for the small and large leak, respectively, under such a low survey speed and wind speed condition. Modeled average DP reduces about 5% to 25% with the increase in wind speed and survey speed, regardless of PG stability class and leak rate. Generally, as the atmosphere changes from PG stability class A to G, the CH_4 plume becomes more narrow and concentrated, due to the decrease in the gas dispersion (Riddle et al., 2004; Leelőssy et al., 2014; Tian, Smits, et al., 2022). Also, wind speed has been shown to influence the plume shape and size (Carpenter et al., 1971; Thorpe et al., 2016). During high wind speed conditions, the plume has a longer length and narrower width, but it is shorter and wider during low wind conditions (Thorpe et al., 2016). Thus, it is expected that DP is higher in a wider plume than in a narrower plume for each downwind transect survey along the pipeline because one is more likely to collect at least one sample within the plume. That is, for a certain plume width and fixed sample frequency, a higher survey speed results in coarse CH_4 sampling points during each transect. Therefore, DP is lower in high survey speed than in low survey speed.

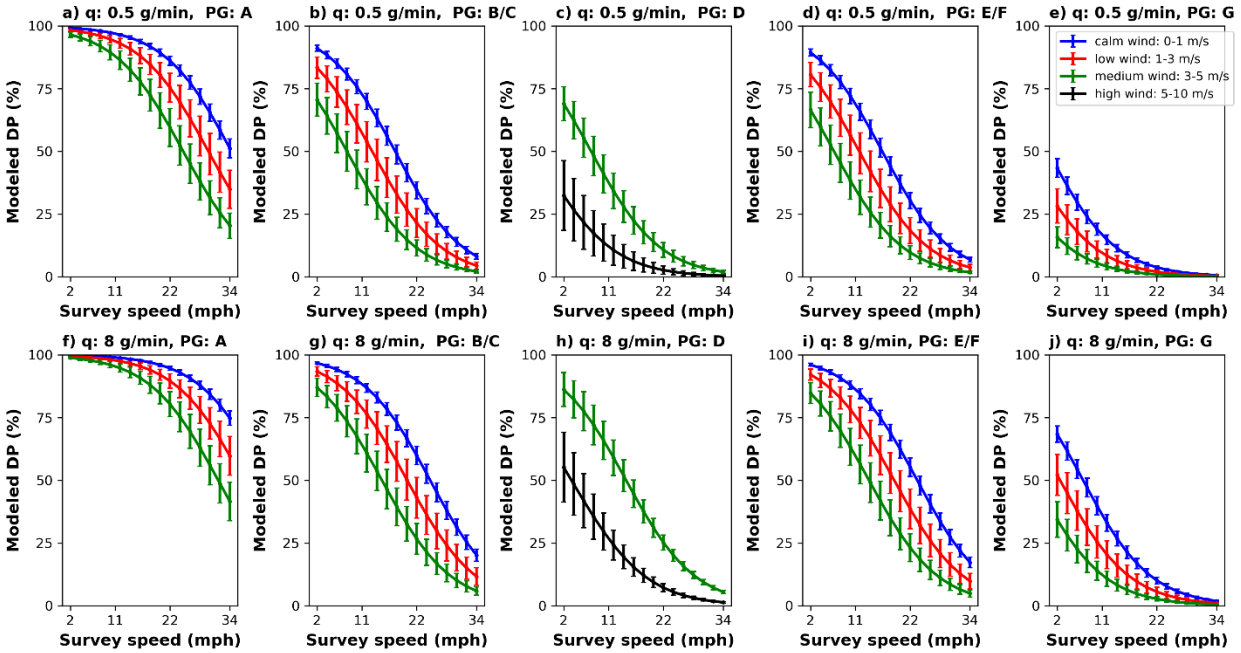

Figure 3.6 Modeled DP as a function of survey speed under different PG stability classes and wind speed conditions. a)–e) is the modeled DP for a small leak (q: 0.5 g min^{-1}). f)–j) is the modeled DP for a large leak (q: 8 g min^{-1}). The survey distance is 5 m, air temperature is 25 $°C$ (average temperature during the experiments). The calm wind is 0–1 m s^{-1}, the low wind is 1–3 m s^{-1}, the medium wind is 3–5 m s^{-1}, and the high wind is 5–10 m s^{-1} according to the measured wind speed range during the experiments. The value of 1/L is -0.2, -0.05, 0.001, 0.05 and 0.2 m^{-1} for PG stability class A, B/C, D, E/F and G, respectively. The error bar is ±1 standard deviation. Note, calm, small, and medium winds typically occur during unstable or stable conditions (PG A, B/C, E/F, G). Medium and large winds generally occur during neutral conditions (PG D) (Pasquill, 1961).

Further, using the publicly available subsurface emission rates measured across the U.S., we modeled the weighed DP to inform the overall detection efficiency of walking and driving surveys on a national scale (Figure 3.7). The weighted average DP in all PG stability class conditions is 83% on average for the walking survey at a calm wind speed (0–1 m s^{-1}). But it reduces to 67%, 42%, and 19% for the driving survey with a low, medium, and high survey speed, respectively. For a high wind speed that typically occurs in PG D (5-10 m s^{-1}), the weighted average DP is less than 37% for all surveys considered here. With the increase of survey speed, the options of favorable weather conditions (i.e., PG stability class and wind speed) are rapidly decreased for

having a high DP. For example, the walking survey has a DP higher than 50% in the PG stability class ranging from A to E/F and calm to medium wind speed conditions (0–5 m s^{-1}). However, this can only be achieved at a calm to low wind speed (0–3 m s^{-1}) for a driving survey at a low speed of 11 mph. When the driving survey speed increases to 34 mph, there is only calm wind in PG A favorable for a DP higher than 50%.

Our results show that DP highly depends on survey speed, atmospheric stability, and wind speed. A higher DP tends to be achieved when surveying at a lower survey speed, atmospheric stability (1/L), and wind speed conditions. The average DP in all weather conditions (PG A to G, calm to large winds) is about 66% for the walking survey, which is close to the assumed 85% detection probability for quantifying the CH_4 emissions from the U.S. NG distribution pipelines (Campbell et al., 1996; Lamb et al., 2015). For a driving survey with low to medium speed (11–22 mph), the average DP in all weather conditions is about 35%, with the highest DP (>80%) under PG A and calm to low wind conditions (0–3 m s^{-1}). Similar to this survey speed range, the field campaign from Weller et al. (2018) showed that their mobile survey method could detect 75% of pipeline leaks, but only 35% were successfully located by local distribution company field crews. As no weather information was provided, it is unknown if their mobile surveys corresponded with the weather conditions tested in this study. Overall, the walking survey has a wide range of favorable weather conditions ranging from PG stability class A to E/F and calm to medium winds (0–5 m s^{-1}) to get a high DP (e.g., at least 50% likely to detect a leak when one is present). The driving survey has limited favorable weather conditions to achieve an equivalent DP. A driving survey with a low speed (11 mph) should survey under the calm to low wind speed (0–3 m s^{-1}) and PG stability class A to E/F conditions to have an equivalent DP to a walking survey. When the survey speed increases to a medium speed (22 mph), the optimum weather condition is limited to the PG

stability class A and calm to medium wind speed conditions (0–3 m s^{-1}). Only calm wind conditions in PG A (0–1 m s^{-1}) are favorable to getting an equivalent DP at a high driving survey speed (34 mph).

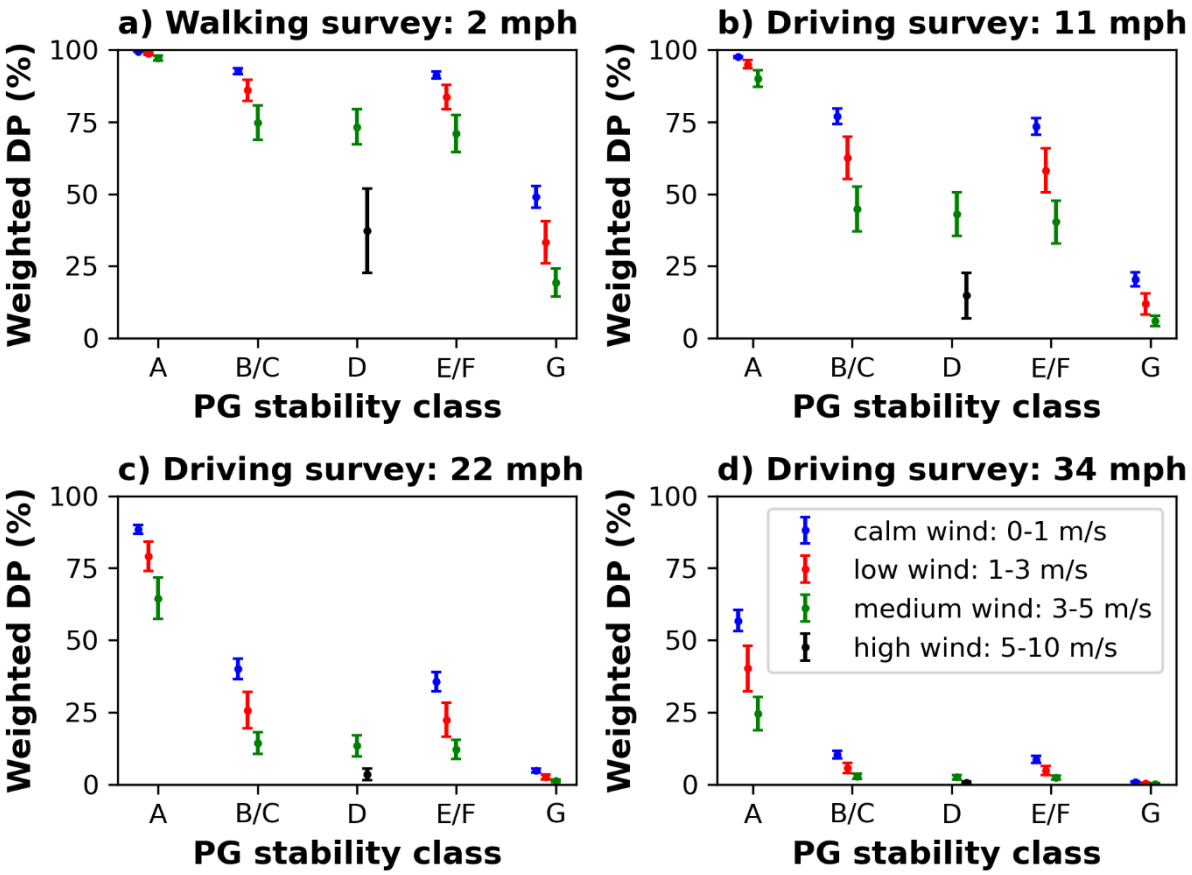

Figure 3.7 Weighed DP for walking and driving surveys under different PG stability and wind speed conditions. The survey distance is 5 m, air temperature is 25 °C (the average temperature during the experiments). The emission rate is from three publicly available emission rate datasets (Table 3.2). The calm wind is 0–1 m s^{-1}, the low wind is 1–3 m s^{-1}, the medium wind is 3–5 m s^{-1}, and the high wind is 5–10 m s^{-1} according to the measured wind speed range during the experiments. The value of 1/L is -0.2, -0.05, 0.001, 0.05, and 0.2 m^{-1} for PG stability class A, B/C, D, E/F, and G, respectively. The assumed driving survey speeds are 11 and 22, 34 mph, representing the field survey's low, medium, and high driving speeds, respectively (Table 3.3). The error bar is ±1 standard deviation. Note, calm, small, and medium winds typically occur during unstable or stable conditions (PG A, B/C, E/F, G). Medium and large winds generally occur during neutral conditions (PG D) (Pasquill, 1961)

3.5 Conclusions

3.5.1 Leak Detection

This work characterizes the probability of mobile survey solutions to detect underground pipeline leaks using a comprehensive approach. Our results showed that the empirical DP decreases with the increase in survey speed, survey distance, atmospheric stability (1/L), wind speed, and air temperature, but is positively proportional to the leak rate. Survey speed, atmospheric stability, and wind speed significantly impact the DP. For subsurface leak rates (0.5–8.5 g min^{-1}) considered here, the average empirical DP in PG A is 85% at a low survey speed (2–11 mph) and 68%, 63%, 65%, and 60% in PG B/C, D, E/F, and G respectively. As the survey speed increases to 22–34 mph, the average DP is generally less than 25%, regardless of PG stability class conditions and leak rates considered here. The sensitivity analysis showed that the average modeled DP has a decrease of 25% with an increase in survey speed from 2 to 34 mph, atmospheric stability (1/L) from -0.2 to 0.2 m^{-1}, and wind speed from 0.1 to 10 m s^{-1}, respectively.

The findings of this study emphasize the importance of the leak rate, survey protocols (i.e., survey distance and speed), and weather conditions (i.e., atmospheric stability, wind speed, and air temperature) in influencing the detection efficiency of leak survey solutions. Our work presents a validated DP model for driving survey solution providers to optimize survey conditions to have an equivalent DP to the traditional walking survey

3.5.2 Implications for Leak Detection Solutions

The driving survey has been increasingly used to detect and /or assess the NG pipeline leaks (Von Fischer et al., 2017; Zimmerle et al., 2017; Li et al., 2020; Weller et al., 2020; Defratyka et al., 2021). The primary advantage of the driving survey is that one can cover more areas more

rapidly than a walking survey. However, there is no robust evidence proving that a driving survey is at least as effective in detecting subsurface leaks as the traditional waking survey. Thus, gaps remain in our understanding of the effectiveness of driving survey efforts in detecting subsurface leaks.

This study analyzed the DP of walking and driving surveys in a comprehensive fashion using data from both a newly developed subsurface leak data set and previous studies available in the literature. Our results showed that with the increase of survey speed, the options of favorable weather conditions (i.e., PG stability class and wind speed) rapidly decrease when trying to achieve a high DP (e.g., >50%). The walking survey has a wider range of weather conditions for high DP, ranging from PG stability class A to E/F and clam to medium winds (0–5 m s^{-1}). The driving survey with a low survey speed of 11 mph can only be conducted under calm to low wind speed conditions (0–3 m s^{-1}) to have an equivalent DP to a walking survey. When driving survey speed increases to 34 mph, only calm wind conditions in PG A (0–1 m s^{-1}) are favorable to get an equivalent DP. The driving survey solution providers need to choose a suitable survey speed under different weather conditions to achieve a DP equivalence to the traditional walking survey.

Chapter 4 Estimating Methane Emissions from Underground Natural Gas Pipelines Using an Atmospheric Dispersion-Based Method

Tian, S., Smits, K.M., Cho, Y., Riddick, S.N., Zimmerle, D.J. and Duggan, A., 2022. Estimating methane emissions from underground natural gas pipelines using an atmospheric dispersion-based method. Elem Sci Anth, 10(1), p.00045. DOI: https://doi.org/10.1525/elementa.2022.00045

4.1 Abstract

Methane (CH_4) leakage from natural gas (NG) pipelines poses an environmental, safety, and economic threat to the public. While previous leak detection and quantification studies focus on above-ground infrastructure, analysis of underground NG pipeline leak scenarios is scarce. Furthermore, no data from controlled release experiments have been published on the accuracy of methods used to 1) quantify emissions from an area source and 2) use these emissions to quantify the size of a subsurface leak. This proof-of-concept work uses CH_4 mole fraction, as measured by a single gas sensor, as an input to a simple dispersion-based model (WindTrax) under ideal conditions (i.e., in a field) and compares the calculated emissions to the known controlled NG release rates. Aboveground and surface CH_4 mole fractions were measured for five days at a field testbed using controlled underground release rates ranging from 0.08 to 0.52 kg hr^{-1}(3.83–24.94 ft^3 hr^{-1}). Results confirmed that the mean normalized CH_4 mole fraction increases as the atmosphere transitions from the Pasquill-Gifford (PG) stability class A (extremely unstable) to G (extremely stable). The estimated surface CH_4 emissions showed large temporal variability, and for the emission rates tested, at least 6 hours of data are needed to have a representative estimate from subsurface pipeline leaks (± 27% of the controlled release rate on average). The probability that the emission estimate is within ± 50% of the controlled release rate ($P_{\pm 50\%}$) is approximately 50% when one hour of data is collected; the probability approaches 100% with 3–4 hours of data. Findings demonstrate the importance of providing enough data over time for accurate estimation of belowground leak scenarios. By adopting the estimation method described in this study, operators can better estimate leakage rates and identify and repair the largest leaks, thereby optimizing annual greenhouse gas (GHG) emissions reductions and improving public safety.

4.2 Introduction

Fugitive methane (CH_4) emissions from natural gas (NG) pipelines pose an ongoing threat to the environment and public safety. Common causes of pipeline leakage include corrosion, incorrect operation due to human error, excavation or similar ground disturbances, natural force damage caused by ground shifts or above-ground loads, and equipment failure (PHMSA, 2018). Pipeline leakage events result in significant safety issues. From 2000 to 2019, the Pipeline and Hazardous Materials Safety Administration (PHMSA) reported pipeline incidents resulting in 202 fatalities, 918 injuries, and an estimated total cost of $2.94 billion (PHMSA, 2022). It is estimated that CH_4 emissions from NG distribution main leaks are 0.69 Tg per year, accounting for 7.6% of the total U.S. CH_4 emissions (Weller et al., 2020). Methane emissions from the NG distribution networks contribute to 56% of the total estimated CH_4 emissions in Paris (Defratyka et al., 2021). Given that the global warming potential of CH_4 is 84 times greater than that of CO_2 over a 20-year horizon (IPCC, 2014), the environmental benefits of NG as a short-term approach for mitigating climate change would be negated if CH_4 emissions in the NG supply chain exceed 3.2% of total NG production (Alvarez et al., 2012; UNFCCC, 2022). Typically, local natural gas distribution companies detect atmospheric CH_4 mole fraction from underground leaks using vehicle and walking surveys (PHMSA, 2017). However, studies showed that NG pipeline leaks are difficult to locate and quantify from above-ground observations due to limited understanding of 1) how CH_4 accumulates or disperses in the atmosphere under different environmental conditions, and 2) the underground CH_4 transport and surface manifestation of such leaks (Okamoto and Gomi, 2011; Mitton, 2018; NARUC, 2019; Cho et al., 2020). Therefore, a better understanding of the influence of atmospheric conditions on above-ground CH_4 plume from underground leaks is required to improve leak detection and quantification, and risk assessment.

NG distribution pipelines are surveyed by distribution companies through routine inspection. Once a leak is discovered, it is classified based on the existing or probable hazard to the person and property (Hendrick et al., 2016; WAC, 2019). Generally, Grade 1 leaks are prioritized for immediate repair. Grade 2 and Grade 3 leaks are classified as non-hazardous based on location, CH_4 magnitude, and potential for migration of the leaked gas. Grade 2 and 3 leaks require repair within 12 to 15 months of detection and then revaluation after 15 months of discovery. Before repair, unresolved Grade 2 and 3 leaks require periodic inspection.

Despite repeated observation, leak classification does not consider the effects of environmental conditions on the magnitude of the measured CH_4 mole fraction. A recent vehicle survey in Durham, North Carolina showed that leak detection density was 50% higher at night (0.33 leaks per mile) compared to daytime conditions (0.22 leaks per mile) when following the same route (Gallagher et al., 2015). Therefore, many underground leaks may go undetected using current survey criteria that fail to incorporate the effects of environmental conditions on leak detection.

Previous studies have used several methods to estimate emissions from underground NG pipeline leaks, including bottom-up, local level methods such as the surface dynamic chamber method (Lamb et al., 2015; Hendrick et al., 2016; Zimmerle et al., 2017), downwind tracer-ratio methods (Lamb et al., 2015; Weller et al., 2018) and vehicle-based statistical methods (Von Fischer et al., 2017; Weller et al., 2018; Weller et al., 2020). Enclosing a surface area to measure the CH_4 enhancement, the surface dynamic chamber method relies on knowledge of the flow of air through a controlled chamber volume (National Academies of Sciences, 2018; Riddick et al., 2020). The surface enclosure area is typically 1 m^2 in size with measurement times in the range of minutes (National Academies of Sciences, 2018) or a series of gridded enclosure placements to overcome the spatial limitations (Lamb et al., 2015). The main shortcoming of this method is that

the surface CH_4 expression from underground pipeline leaks has been documented to migrate 2–6 m from the leak location, depending upon the leak size and environmental conditions, such as soil properties and moisture (Okamoto and Gomi, 2011; Ulrich et al., 2019; Cho et al., 2020; Cho et al., 2022) and the chamber may not capture all emitted gas. In addition, recent work by Riddick et al. (2021) documents the temporal variability in the surface CH_4 expression above an NG pipeline leak. The authors identify variations in wind speed, roughness length, and atmospheric stability as the key environmental variables most significantly affecting the surface CH_4 mole fraction. Cho et al. (2022) measured this change continuously over 4 days for two different known leakage rates, demonstrating how it varies by over 100%, depending on the time of day.

Downwind tracer-ratio methods are often used as a supplementary quality assurance method to evaluate the performance of other methods such as the surface chamber method (Lamb et al., 2015). Such methods require accurate knowledge of the known leak location and are sensitive to environmental conditions such as wind and the accurate co-placement of the tracer release and leak site (Mønster et al., 2019). Vehicle-based methods estimate emissions using a statistically fitted linear model with the maximum CH_4 mole fraction, the total plume peak area, and the ratio of maximum CH_4 mole fraction to peak area (Von Fischer et al., 2017). Although this method shows promise for city or regional studies, it relies on statistical analysis and does not incorporate the impacts of atmospheric conditions on the dispersion of the CH_4 plume. When compared with surface chamber estimates, vehicle-based statistical estimates show larger emission estimates with very few indications of ground truth estimates from known underground leak rates (Weller et al., 2018).

As few of the above approaches have been verified using controlled underground releases, evaluating their accuracy remains an open challenge and therefore CH_4 emissions from pipeline

systems remain poorly characterized. To the authors' knowledge, there have been no studies to date that investigate the effects of time-varied weather conditions on emission estimate accuracy from subsurface pipeline leaks in controlled conditions. Comparing a method's emission estimates to known, controlled underground releases over a range of environmental and operating conditions is the first step towards method validation.

Atmospheric dispersion models have been used to inversely calculate gas emissions across a wide range of scales, spanning from the microscale to the continental scale (Flesch et al., 2004; Jeong, 2011; Bonifacio et al., 2013; Barkley et al., 2017). The application considered here relies on simple downwind measurements and could be readily applied to open field environments free from obstructions such as buildings, parked vehicles, and trees. Such conditions are typically seen in upstream sectors such as gathering and flowlines or in the downstream sector in rural environments or along open extents. For these scenarios which represent short-range dispersion (1 km or less), the inverse dispersion model WindTrax has reported an accuracy of $\pm$ 10% for emission estimates from agricultural sources (i.e., feedlots, pastures, and farms), landfills, and natural sources (Laubach and Kelliher, 2005; Yang et al., 2017; Riddick et al., 2018). As this method is not limited to specific source sizes and shapes, it allows for flexibility in sensor placement and therefore has good potential for use in estimating CH_4 emissions from NG pipeline leakage scenarios (Riddick et al., 2019).

This study explores the effectiveness of using limited surface and above-ground CH_4 mole fraction data as inputs to a near-field dispersion model to calculate CH_4 emissions from subsurface pipeline leaks under realistic conditions. Explicitly, this study aims to 1) link the variations in atmospheric CH_4 mole fraction magnitude to variations in atmospheric stability under a range of controlled NG leak rates; 2) test the accuracy of an inverse modeling approach to estimate

emissions by comparing estimates directly against known, controlled underground leak rates; 3). understand and quantify how much data is needed to estimate emissions within ±50% of controlled leak rates. To our knowledge, this is the first study of its kind to test the emission estimate accuracy against the known rates for belowground pipeline scenarios. Currently, pipeline operators use surface CH_4 measurements to infer the size of a leak and prioritize repair. By adopting the method described in this study to correctly estimate leak rate, operators can estimate emissions and therefore optimize repair and greenhouse gas (GHG) emission reductions.

4.3 Materials and Methods

4.3.1 Experimental Testbed/Setup

Field experiments were conducted at the Methane Emission Technology Evaluation Center (METEC) field site, Colorado State University (CSU), Colorado. The METEC site includes an underground pipeline testbed that simulates the behavior of pipeline leaks using controlled natural gas releases under varied subsurface, surface, and atmospheric conditions. Details of the testbed design can be found in (Mitton, 2018; Ulrich et al., 2019; Cho et al., 2020; Gao et al., 2021) and will be summarized here. For this work, a testbed simulating a rural right of way with grassy surface cover was selected. The testbed consists of stainless-steel tubing (0.635 cm, model SS-T4-S-035-20, Swagelok, USA) installed at 0.9 m below the ground surface along the east-west direction of the site, configured to release compressed NG at specific rates and locations. The tubing runs adjacent to a 10 cm diameter polyvinylchloride (PVC) pipe to simulate a realistic underground pipeline. The pipeline is backfilled with native soil, classified previously as sandy loam, according to the U.S. Department of Agriculture Soil Texture Classification. The trench is slightly less compact than the surrounding undisturbed soil, as discussed in Ulrich et al. (2019).

Natural gas (87 ± 2 vol % CH_4) was injected through the stainless-steel tubing into the testbed from an aboveground 145-liter compressed natural gas (CNG) tank. The gas release rate (reported at kg hr^{-1} of CH_4) was controlled by pressure regulators, solenoid valves, and choked flow orifices, and measured using a thermal mass flow meter (range: 0–0.66 kg hr^{-1}, accuracy: ±1%, Omega FMA1700 series). Gas was released to the soil through a stainless-steel mud dauber (0.635 cm, model SS-MD-4, Swagelok, USA) with a 10 cm wire mesh cube filled with gravel to prevent clogging.

Methane mole fractions were collected at two elevations, 1 m above ground and at the ground surface. The above-ground CH_4 mole fractions were measured at two separate locations, depending on the experiment (Figure 4.1a). For the first three experiments (June 1st 8:00 AM to June 4th 8:00 AM), a trace gas analyzer (Picarro Inc., G2210, precision: < 0.1 ppb) was positioned at location T1 to measure the CH_4 mole fraction at a distance of 10 m from the leak center and 1 m above the ground surface. The measurement interval was approximately 0.8 to 1 Hz. The analyzer was moved to location T2, located 10 m from the leak center, for the last experiment (June 4th 8:00 AM to June 5th 8:00 AM) with the same measurement height as the predominant wind direction changed during this period.

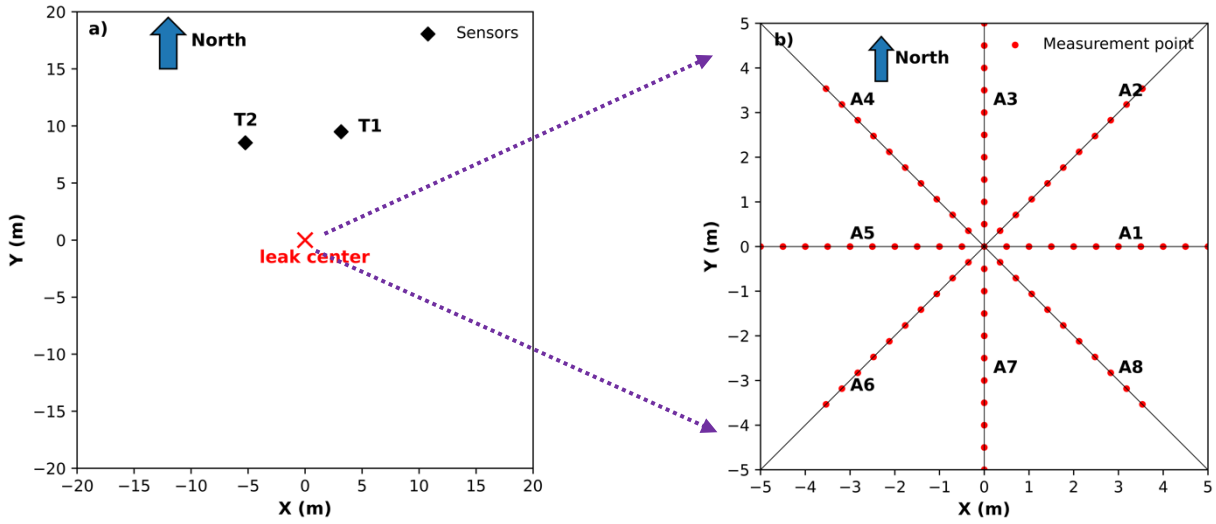

Figure 4.1 Plan views of the above ground and surface measurement locations relative to the NG leak location. a) The above ground sensor to measure the atmospheric CH_4 was located at T1 for the first three experiments and T2 for the fourth experiment, due to a change in the predominant wind direction. b) The gridded layout represents the surface CH_4 measurement locations. In each direction, each point is 0.5 m apart with direction spaced by 45°.

Surface CH_4 was measured at the ground surface at 80 locations (Figure 4.1b) to determine the plume shape and size using a hand-held CH_4 detector (Bascom Turner Instruments Inc., VGI-201 Gas-Rover, resolution: 1.0 ppm, detection limit: approximately 5.0 ppm). The surface CH_4 mole fraction were measured during the last one hour of each experiment following the method used in a previous study (Cho et al., 2022). In accordance with the manufacturer's procedures, at each measurement point (Figure 4.1b), the rubber cup of the detector was lightly pressed onto the ground surface for 30 seconds. Methane mole fraction was averaged over this time. To ensure that most of the surface expression was recorded, measurements were carried out from the leak center in each direction, A1 to A8, until the instrument's detection limit (approximately 5.0 ppm) was reached.

Two meteorological sensors were deployed to continuously measure wind speed, wind direction, solar radiation, and air temperature with a time resolution of 1 min (Figure B.1). The

first meteorological sensor (METER Group Inc., ATMOS41, accuracy: 3% and ±5^{o} for wind speed and direction, respectively; solar radiation: ±5%; air temperature: ± 0.6 ^{o}C; air pressure: ± 0.1 kPa from -10 to 50 ^{o}C, ± 0.5 kPa from -40 to 60 ^{o}C) was co-placed with the trace gas analyzer at T1 (1 m height). The second sensor (YOUNG Model 81000 Ultrasonic Anemometer, accuracy: wind speed: ± 1% ±0.05 m s^{-1} (0 to 30 m/s) and ± 3% (30 to 40 m s^{-1}); wind direction: ± 2^{o} (1 to 30 m s^{-1}) and ±5^{o} (30 to 40 m s^{-1})) was a fixed station installed at 6 m above ground, located 76.2 m northwest of the leak center.

4.3.2 Experiment Procedure

Four 24-hour experiments were conducted with controlled release rates of 0.08, 0.18, 0.27, and 0.52 kg hr^{-1} of CH_4 (3.83, 8.64, 12.94, and 24.94 SCFH (Standard Cubic Feet per Hour)), representing medium to large distribution pipeline leaks (Lamb et al., 2015). Experiments were conducted between the 1st and 5th of June, 2020.

A 0.08 kg hr^{-1} leak was initiated on the first day at approximately 8:00 AM MDT (Mountain Daylight Time), and continuous measurements were conducted over the following 24 hours, at which time the leak rate was increased to 0.18 kg hr^{-1}. This process/timing was repeated for 0.27 and 0.52 kg hr^{-1}. Mitton (2018) showed that NG released in the METEC testbed took approximately 4 hours to migrate to the surface. Therefore, only the last 20 hours of data (12:00 PM to 8:00 AM) were used for each of the four experiments in the analysis to allow equilibration of the subsurface and ensure steady-state conditions. To properly represent atmospheric processes at the microscale, 10-minute averaged data were calculated. For every 10 minutes, atmospheric stability was quantified as the Obukhov length (L, m) to express the relative roles of shear and buoyancy (Foken, 2006). The Obukhov length was calculated from the surface friction velocity

(u_*, m s^{-1}), the mean absolute air temperature (T, K), the von Kármán's constant ($k_v = 0.41$), the gravitational acceleration (g = 9.81 m s^{-2}), and the 3D horizontal and vertical wind vectors (*u*, *v*, *w*, m s^{-1}) (Equations 4.1–4.2) (Flesch et al., 2004; Foken, 2006).

$$L = -\frac{u_*^3 T}{k_v g \overline{w'T'}} \tag{4.1}$$

$$u_* = \left[\left(\overline{u'w'}\right)^2 + \left(\overline{v'w'}\right)^2\right]^{1/4} \tag{4.2}$$

The Obukhov length was converted to the Pasquill-Gifford (PG) stability class to provide practical insight for the industry in situations where on-site 3D sonic anemometer data are not available (Ulrich et al., 2019; Riddick et al., 2021). In this work, $-100 \leq L < 0$, $-500 \leq L < -100$, $|L| > 500$, $50 \leq L < 100$, $0 < L < 50$ are considered as extremely unstable (PG: A), unstable (PG: B-C), neutral (PG: D), stable (PG: E-F), and extremely stable conditions (PG: G), respectively (Gryning et al., 2007).

4.3.3 Model Setup

The surface CH_4 emissions were inversely calculated using WindTrax version 2.0 (Crenna, 2020). WindTrax is a publicly available backward Lagrangian stochastic-based model that can simulate the trajectories of thousands of tracer particles in the atmosphere surface layer (Flesch et al., 1995). The surface CH_4 emissions Q (kg hr^{-1}) were calculated inversely using Equation 4.3 by assuming the simulated normalized CH_4 mole fraction ($(C/Q)_{sim}$) equals the actual normalized CH_4 mole fraction (Flesch et al. 2004).

$$Q = \frac{(C_{obs} - C_b)}{(C/Q)_{sim}} \tag{4.3}$$

where C_{obs} is the measured CH_4 mole fraction (ppm) at the downwind location, C_b is the measured local CH_4 background mole fraction (ppm). Additional details about the calculation of $(C/Q)_{sim}$ in this model can be found in appendix B (Equations B.1–B.7).

Modeling inputs included CH_4 concentration, 10-minute averaged wind speed and direction, air temperature, roughness length, surface expression area, and Obukhov length. The surface roughness length was estimated at 0.02 m, approximated as one-tenth of grass height (Gutmann and Small, 2005). The surface expression area was approximately 7 to 20 m^2 (Table 4.1), which was estimated using the measured surface CH_4 mole fractions (Figure B.2). Atmospheric CH_4 mole fractions were filtered for two criteria, 1) the measurement was downwind of the known leak source (± 90° of leak center); and 2) the CH_4 mole fraction was higher than the background CH_4 mole fraction. The background CH_4 mole fraction ranged from 1.88 to 1.92 ppm (Table 4.1), which was calculated by averaging the mole fraction within 25% of the cumulative distribution frequency (Figure B.3).

Table 4.1 Background CH_4 mole fraction (1 m above ground, 10 m from the leak source) and surface expression area for Exp1–4. Standard deviations from the background CH_4 mole fraction are noted in parentheses.

Exp	Background CH_4 mole fraction at 1 m (ppm)	Surface expression area (m^2)
1	1.89 (±0.004)	7
2	1.90 (±0.006)	13
3	1.92 (±0.042)	20
4	1.88 (±0.002)	20

Sensitivity analysis on seven stability cases (Srun1-7) was used to evaluate the effects of atmospheric stability on the surface CH_4 emission estimate by changing L from -75 to 100% relative to the base case (Baserun) (Table 4.2). The base case was the controlled case in WindTrax

to calculate the surface emission using 10-minute averaged CH_4 mole fraction and associated meteorological variables as the model input parameters.

Table 4.2 General information about the stability sensitivity and base case in WindTrax. L in the base case (Baserun) was calculated using Equations 4.1–4.2. The Obukhov length for the seven sensitivity cases (Srun1–7) were -75 to 100% of L, respectively ($L \neq 0$ in Wind WindTrax (Flesch et al., 2004)), other input model parameters were the same as the Baserun.

Baserun	**Srun1**	**Srun2**	**Srun3**	**Srun4**	**Srun5**	**Srun6**	**Srun7**
L	L *(1-75%)	L *(1-50%)	L *(1-25%)	L *(1+25%)	L *(1+50%)	L *(1 +75%)	L *(1+100%)

4.4 Results

4.4.1 Impact of Atmospheric Stability on CH_4 Mole Fraction

Figure 4.2 shows the mean normalized CH_4 mole fraction as a function of the Pasquill-Gifford (PG) stability class for the four experiments (Exp1–4). The mean normalized CH_4 mole fractions consistently increase with the increase in atmospheric stability, ranging from 12.31 to 23.41 s m^{-3} when the atmosphere transitions from the PG stability class A to G. The large variability in mean normalized CH_4 mole fraction may result from only measuring CH_4 mole fraction at one location within the plume for each measurement interval as well as the variations in CH_4 mole fraction within the plume for the same stability condition. The normalized CH_4 mole fraction at the plume center was larger than that at the plume edge for the same stability condition, and the normalized mole fraction near the plume centerline during the unstable condition (e.g., PG stability class A) was larger than that at the edge of the plume during the stable condition (e.g., PG stability class E–F) (Figure B.4). In all, the results confirmed that the mean normalized CH_4 mole fraction increases as the atmosphere transitions from PG stability A to G. For the conditions tested, our

results show that measured CH_4 mole fraction cannot be used to infer the size of a leak without considering the impacts of atmospheric stability conditions.

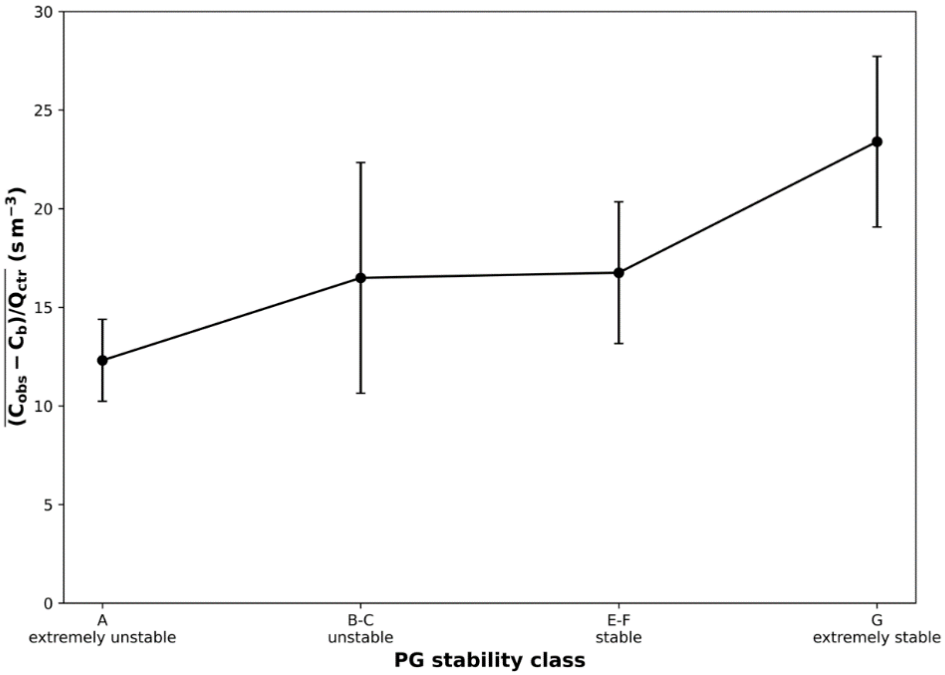

Figure 4.2 Mean normalized CH_4 mole fraction grouped by the Pasquill-Gifford (PG) stability class for the four experiments (Exp1–4). C_b is the background CH_4 mole fraction (ppm), C_{obs} is the measured CH_4 mole fraction (ppm), Q_{ctr} is the release rate (kg hr^{-1}). The error bar represents $\pm 1\sigma$(σ: standard error). The total number of data points is 70, 10, 22, and 47 for PG stability classes A, B-C, E-F, and G. Note, PG stability class D was not included due to limited data points (6). The averaging interval for each data point is 10 minutes.

4.4.2 Methane Emissions Calculated by WindTrax

As seen in Figure 4.3a, the model estimated surface CH_4 emissions showed large temporal variability, with the maximum estimates 3–5 times higher than the observed release rates. The absolute percent difference between the estimated surface CH_4 emissions and the controlled release rate ranged from 1 to 48% for the four experiments (27% on average). The large absolute percent difference in Exp4 may be due to the lower sample size, compared to Exp1–3. While

Exp1–3 had a sample size of 6-9 hours, only 3.5 hours were available for Exp4. It is possible that the shortened time (3.5 hours) is too short to accurately represent the highly temporally variable surface CH_4 emissions from a subsurface leak. Thus, the results demonstrate that for the emission rates tested, the average surface CH_4 emissions from WindTrax can provide promising estimates (within 27% on average) of the leak rate from an underground NG pipeline release based on 6.5 hours of downwind measurements from a single sensor location. The average ratio of the calculated surface CH_4 emissions by WindTrax to the controlled release rate tend to decrease with the increase in atmospheric stability except for PG stability class G, i.e., a larger emission estimate during unstable conditions than in stable conditions (Figure 4.3b). The larger average ratio in PG stability class G than E-F suggests that other factors not considered in the atmospheric model, such as soil conditions, impact the surface CH_4 emissions (Cho et al., 2020; Gao et al., 2021). Previous studies have shown that temporal variability of surface CH_4 emissions is associated with both soil and atmospheric conditions, such as soil moisture and fluctuations in atmospheric pressure (Czepiel et al., 2003; Poulsen and Møldrup, 2006; Forde et al., 2019; Kim et al., 2020).

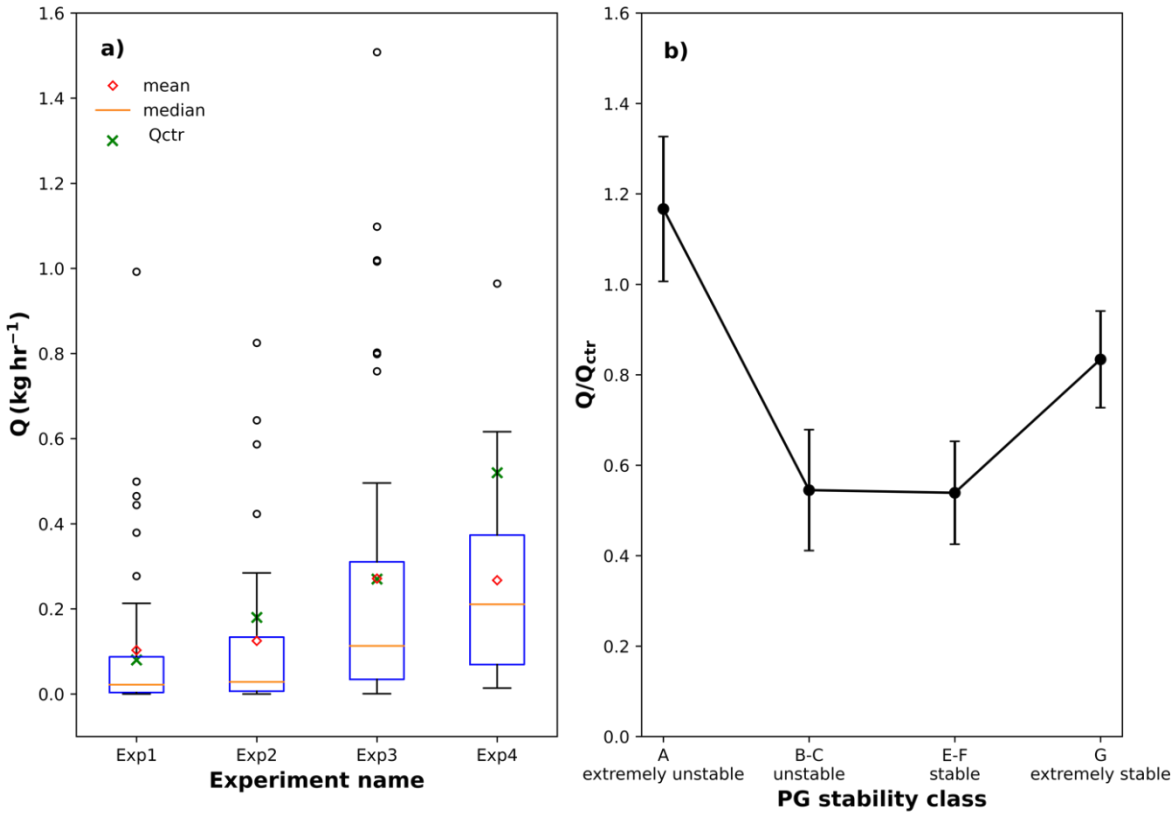

Figure 4.3 a) Box and whisker plots of estimated surface CH_4 emissions (Q, kg hr^{-1}) compared with the controlled release rate (Qctr, kg hr^{-1}) for the four controlled release experiments (Exp1–4); Boxes and whiskers in a) show the median (orange), 25th and 75th percentile (blue), and minimum and maximum values (black). The mean is depicted by the hollow red diamond. The black circles represent the outliers, and the green cross-mark is the controlled release rate (Q_{ctr}). b) The average ratio of estimated surface CH_4 emissions (Q, kg hr^{-1}) to the controlled release rate (Q_{ctr}, kg hr^{-1}) grouped by the Pasquill-Gifford (PG) stability classes. Data are from the experimental base case. The total number of data points in b) is 70, 10, 22, and 47 for PG stability classes A, B-C, E-F, and G. Note, PG stability class D was not included due to limited data points (6).

4.4.3 Effect of Atmospheric Stability on CH_4 Emission Estimates

Seven sensitivity cases were further used to evaluate the effect of atmospheric stability on the calculated emission rate by altering the Obukhov length in the model from -75 to 100% of L (Table 4.2). As shown in Figure 4.4a, the ratio of estimated surface CH_4 emissions to the controlled release rate decreases with the increase in atmospheric stability, where the PG stability class changes from

PG stability class A (extremely unstable) to G (extremely stable). As the atmosphere transitions from A to G, the average dispersion coefficients of the along-wind, crosswind, and vertical direction decrease rapidly (Figure 4.4b). The dispersion coefficient in the 3D direction is about 0.4–0.8 m s^{-1} when the atmosphere is in PG stability class A (extremely unstable), but it reduces to below 0.2 in PG stability class G (extremely stable, a 50–70% decrease). Thus, the strong dispersion during unstable atmospheric conditions results in enhanced vertical and horizontal mixing compared to the inhibited dispersion and hence mixing during stable conditions (Riddle et al., 2004; Leelőssy et al., 2014). This results in broad yet diluted CH_4 plume during unstable conditions (e.g., PG stability class A) and narrow yet concentrated CH_4 plume during stable conditions (e.g., PG stability class E–F) (Figure B.4).

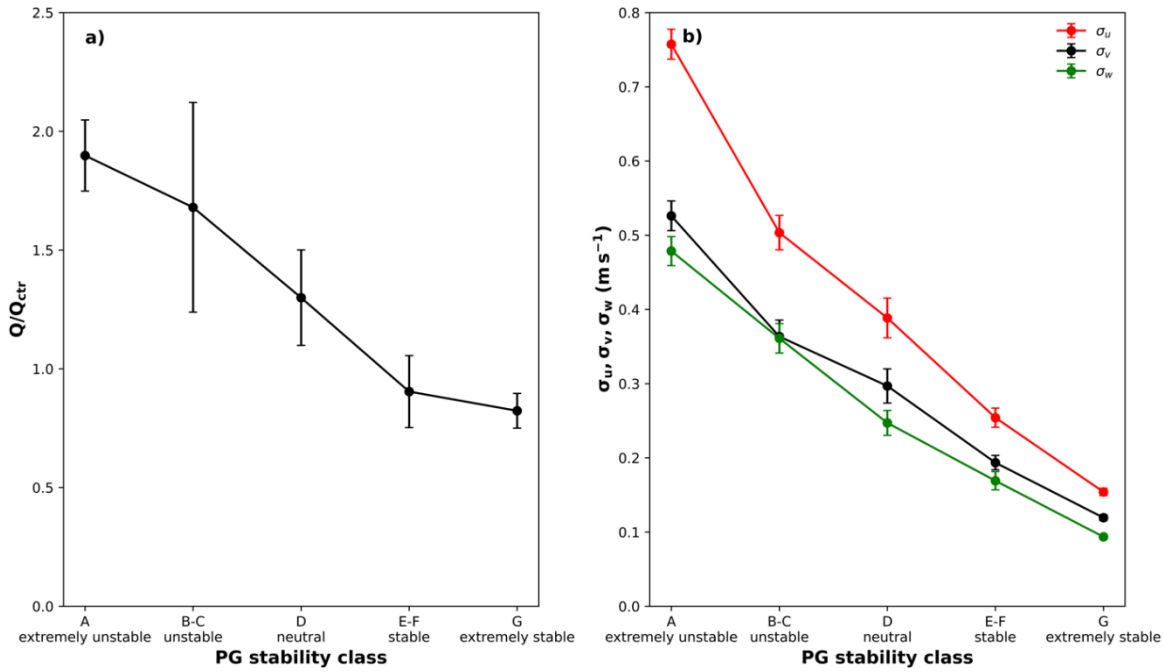

Figure 4.4 a) The average ratio of estimated surface CH_4 emissions (Q, kg hr^{-1}) to the controlled release rate (Qctr, kg hr^{-1}) grouped by the Pasquill-Gifford (PG) stability classes. b) The average dispersion coefficients (σ_u: along-wind direction; σ_v: crosswind direction; σ_w: vertical direction) grouped by the Pasquill-Gifford (PG) stability class. The unit of dispersion coefficient is m s^{-1}. The data in a) and b) are from the sensitivity cases, as shown in Table 4.2. The error bars in a) and b) represent $\pm 1\sigma$(σ: standard error). The total number of data points is 326, 91, 58, 191, and 355 for PG stability class A, B–C, D, E–F, and G, respectively.

4.4.4 Effect of Time Averaging on CH_4 Emission Estimates

Using the estimated emissions from the base case (Baserun), a rolling mean method was used to understand the amount of downwind data needed over time to estimate the emission rate accurately. Although our experiments collected data for 24 hours, in field scenarios, this is often not possible. We therefore wanted to understand the effect of time averaging on the emission estimate. Figure 4.5 shows the probability that the emission estimate is within ± 50% of the controlled release rate ($P_{\pm 50\%}$) for data averaging time of 0.33 to 9.33 hrs. As expected, the probability increases with the increase in the rolling mean time in Exp1 through 3 (Figure 4.5). A probability of 50% is achieved when approximately one hour of data is collected. The probability increases to 80% with about 2 hours of data and reaches 100% with 3–4 hours of data. However, the probability was not observed to increase with an increase in time in Exp4 (Figure 4.5). This may be due to the smaller sample size (3.5 hours of downwind data in Exp4) and its distribution characteristics. As shown in Figure 4.3a, the distribution was normal for Exp4 but was right-skewed for Exp1–3. Despite this, it should be acknowledged that the low sample size for Exp4 may have affected the probability.

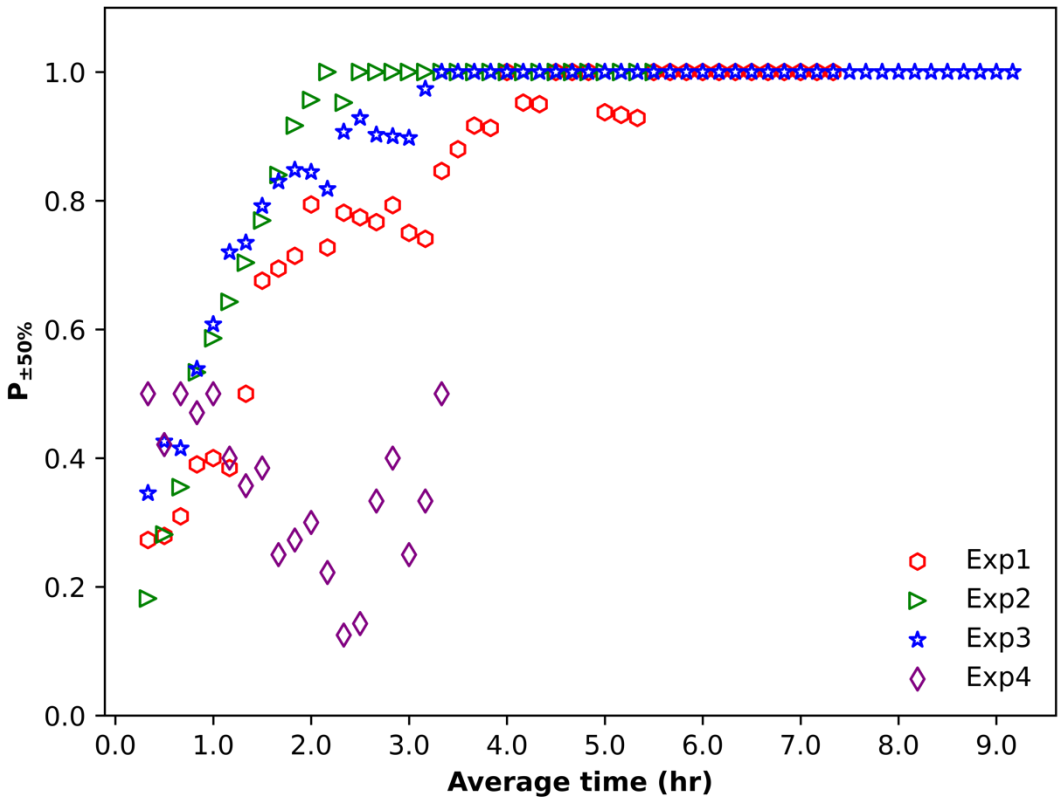

Figure 4.5 Probability ($P_{\pm 50\%}$) that the calculated mean CH_4 emissions (Q, kg hr^{-1}) are within ± 50% of the controlled release rate (Q_{ctr}, kg hr^{-1}) with the rolling mean time ranging from 0.33 to 9.33 hours. The data were individual surface CH_4 emission points from the base case (Baserun). The probability was calculated by dividing the number of emission estimates within ± 50% of the controlled release rate by the total sample size in each rolling time interval.

4.5 Discussion

This work demonstrates the viability of linking a simple publicly available dispersion model with limited aboveground and surface CH_4 mole fraction, and micrometeorological data to estimate CH_4 emissions from underground pipeline leaks. Previous downwind methods used for above-ground NG infrastructure leaks show that emission estimate accuracy is about ± 70% when calculating based on 15–20 minutes of downwind stationary measurements (Heltzel et al., 2020).

For belowground CH_4 leaks, our method shows that downwind measurements measured over four hours can be used to estimate a leak between 0.08 to 0.52 kg h^{-1} to within ±50% in an open field condition. Although the average CH_4 emissions calculated by WindTrax showed good agreement with the controlled release rate, we also recognize that it might not be feasible to directly apply this method to estimate emissions from a large number of pipeline leaks (U.S. Energy Information Administration, 2021). However, this method could be modified to vehicle-based surveys using a gas sensor and associated 3D anemometer data to extend its applicability. The method presented here is similar to the survey protocols outlined in other mobile methods for NG above-ground infrastructure leaks (Brantley et al., 2014; Caulton et al., 2018; Edie et al., 2020), that is, mobile monitoring and downwind stationary CH_4 mole fraction measurements, yet demonstrates the importance of providing enough data over time for proper estimation of belowground leak scenarios. The length of time needed for mobile methods to achieve an equivalent accuracy remains unknown as there are currently no controlled belowground experiments results for mobile methods. The reported large emission estimate uncertainty (between -50 and +350%) of mobile methods on above-ground NG infrastructure leaks suggests more mobile transects are needed to improve the emission estimate (Lan et al., 2015; Rella et al., 2015; Yacovitch et al., 2015). A driving measurement campaign by Caulton et al. (2018) shows that at least 10 repeat transects are needed to reduce uncertainty, where the uncertainty is estimated at 0.05–6.5 times the emission rate for single-transect sites and 0.5–2.7 times the emission rate for sites with more than 10 transects. Therefore, Caulton's emphasis on more transect time may also apply to the mobile methods for improving emission accuracy from pipeline leaks.

There is limited information regarding emissions from both flow and gathering lines (Zimmerle et al., 2017; Li et al., 2020). The emission factors of NG gathering lines in the current US EPA

Greenhouse Gas Inventory (Hockstad and Hanel, 2018) are based on emission estimates from the distribution pipelines (Campbell et al., 1996). With enhanced mobility, the method presented here shows potential for estimating CH_4 emissions from NG flow and gathering lines. Similarly, it is also useful for NG distribution and transmission pipeline operators when an accurate estimate of emission rate is required to inform the priority of leak repairs such as finding and repairing the largest leaks and prioritizing work schedules.

4.6 Conclusions

This work tests an approach to estimate CH_4 emission rates compared to known leak rates from subsurface pipeline leaks under realistic conditions. Our results confirm that the mean normalized CH_4 mole fraction increases as the atmosphere transitions from PG stability class A to G. The measured CH_4 mole fraction cannot be used to infer the size of a leak without considering the impacts of atmospheric stability conditions. The estimated CH_4 surface emissions from a simple publicly available dispersion model showed large temporal variability, and for the emission rates tested, at least 6 hours of data are needed to have a representative estimate from subsurface pipeline leaks (±27% of the controlled release rate on average). The probability that the emission estimate is within ± 50% of the controlled release rate ($P_{\pm 50\%}$) is about 50% when approximately one hour of data is collected. Probability increases to 80% with about 2 hours of data and reaches 100% with 3–4 hours of data. A sensitivity analysis also showed that the estimated surface CH_4 emissions from the underground leaks tend to decrease when the atmosphere transitions from the PG stability class A (extremely unstable) to G (extremely stable) due to the inhibited dispersion and mixing in the atmosphere.

These findings of this study emphasize that a certain amount of data is necessary to have an estimate that can reflect the true subsurface leak rates. Atmospheric stability conditions should be incorporated in pipeline emission estimates based on the atmospheric CH_4 measurements.

Chapter 5 Improving the Efficacy of Leak Detection and Quantification Survey Methods Using 3D Plume Measurements

Tian, S., Riddick, S.N., Mbua, M., Jayarathne, N., Cheponui, F., Cho, Y., Zimmerle, D.J., and Smits, K.M., in review.

5.1 Abstract

Identifying underground pipeline natural gas (NG) leaks using mobile survey methods is a significant challenge. Although survey methods find leaks, the overall effectiveness of such methods is uncertain due, in part, to a lack of understanding of the gas plume behaviors in the vicinity of a leak. In this study, controlled underground subsurface NG releases (0.44 kg hr^{-1} of CH_4) were used to observe the near-field 3D plume evolution behavior (size and shape) under a range of atmospheric conditions and use these findings to inform leak survey parameters. Measurements were made at 7 m downwind of the emissions at heights between 0.5 and 7 m above the ground surface. Results showed that atmospheric stability, wind speed, and air humidity significantly impact the plume width and survey speed. The average plume width reduces by 36% as atmospheric stability changes from Pasquill–Gifford (PG) stability class A (extremely unstable) to PG G (extremely stable), and wind from calm (0–1 m s^{-1}) to medium and high wind speed (5–12 m s^{-1}) conditions. And it increases by 22% with the increase of air humidity from low (0–50%) to very high (80–100%) humidity conditions. The plume is typically the widest at 5 m above the ground, decreasing both above and below this height. The maximum survey speed is about 25 mph in PG A, but it reduces to 16 mph in PG G. Leak survey typically has a larger range of survey speed options at 5 m above the ground under unstable (PG A to B/C), calm to medium speed (0–3 m s^{-1}), and high to very high (50–80%) humidity conditions. Overall, the results suggest that understanding atmospheric CH_4 plume behavior can inform and optimize survey protocols to improve detection performance.

5.2 Introduction

Natural gas (NG), composed of 60–98% methane (CH_4), is currently being used as a bridging fuel from traditional fossil fuels (coal and oil) to sustainable renewable energy sources (Levi, 2013; Zhang et al., 2016; Zhang et al., 2022) as it produces fewer undesirable by-products such as CO_2, NO_x, SO_2, and particulates per unit of energy than coal or oil (Liang et al., 2012; The National Academy of Sciences, 2022). There are over three million miles of NG pipeline throughout the United States, generating ~33% of the US electricity demand (U.S. Energy Information Administration, 2021a; The National Academy of Sciences, 2022). Fugitive CH_4 emissions from NG pipeline leaks have been identified as both environmental and safety risks (Alvarez et al., 2012; UNFCCC, 2022) in addition to financial losses (PHMSA., 2022) as it is highly flammable and has a global warming potential 84 times greater than that of CO_2 over a 20-year horizon (IPCC, 2014). From 2002 to 2021, the Pipeline and Hazardous Materials Safety Administration (PHMSA) reported 2,986 NG pipeline incidents (~150 incidents each year on average), resulting in 227 fatalities, 1,030 injuries, and an estimated total cost of $6.22 billion (PHMSA., 2022). A recent national estimate shows that NG distribution pipeline leaks emit CH_4 0.69 Tg per year and contribute to 7.6% of the total U.S. CH_4 emissions (Weller et al., 2020). The latest basin-wide based emission factor (EF) is 14−52 times higher than the U.S. Environmental Protection Agency's national estimate for natural gas gathering lines (Yu et al., 2022). Given the amount of NG pipelines throughout the U.S., most of which are buried underground (U.S. Energy Information Administration, 2021a; The National Academy of Sciences, 2022), an effective leak detection method is critical to identifying leaks promptly after they have commenced and initiating appropriate responses to repair the pipeline quickly. Fixing the leaks on time can prevent accidents,

reduce risk to public safety and property, lower economic costs, and reduce CH_4 emissions to the environment.

To find CH_4 emissions from NG pipeline leaks, survey methods, such as walking surveys (PHMSA., 2017; GPTC, 2018; Chen et al., 2020; Cho et al., 2020; Riddick et al., 2021; Tian et al., 2022), driving surveys (Phillips et al., 2013; Gallagher et al., 2015; Von Fischer et al., 2017; Zimmerle et al., 2017; Weller et al., 2018; Keyes et al., 2020), unmanned-aerial-vehicle (UAV) surveys (Golston et al., 2018; Yang et al., 2018; Barchyn et al., 2019; Fox et al., 2019; Li et al., 2020), and aircraft surveys (Kligman, 2011; Vaughn et al., 2017; FlyARH, 2021; LASEN, 2021; Heliops, 2022), have been used to detect the leaks. The methods generally consist of an instrument used to measure CH_4 mole fraction, a method of deployment (i.e., patrol platform and survey protocol), and a data analysis method to interpret the collected data. There is currently no universal standard leak survey protocol, and survey protocols are usually dependent on patrol platforms.

In a walking survey, surveyors walk at a distance of up to 30 m from the pipelines to detect enhanced CH_4 mole fractions between 0 and 1 m above the ground, using a hand-held analyzer such as Heath Inc. Remote Methane Leak Detector (RMLD; range: 0–99,999 ppm-m; sensitivity: 5−10 ppm-m, frequency: 3 Hz) or a Bascom-Turner Gas-Rover (GR; range: 5–10,000 ppm; accuracy: 2% ± 10 ppm; frequency: 1–2 Hz) (Zimmerle et al., 2017; Weller et al., 2018; Cho et al., 2020; Riddick et al., 2021). In a driving survey, surveyors drive a vehicle at a speed of 4–15 m s^{-1} (9–34 mph) at a distance of up to 200 m from the source to detect enhanced CH_4 mole fractions between 0.3 and 4.5 m above the ground using a tracer gas analyzer, such as Picarro GasScouter (range: 0–20 ppm; precision: < 0.5 ppb) or an ABB micro-portable greenhouse gas analyzer (MGGA; range: 0.01–100 ppm; precision: < 2 ppb) (Phillips et al., 2013; Jackson et al., 2014; Gallagher et al., 2015; Rella et al., 2015; Von Fischer et al., 2017; Caulton et al., 2018;

Weller et al., 2020). The UAV survey flies at a speed of between 2 and 30 m s^{-1} (4–67 mph) at a distance of up to 1,000 m from the source to detect enhanced CH_4 mole fractions or path-integrated CH_4 mole fractions with a flight height of up to 122 m, equipped with a point gas analyzer such as (e.g., ABB MGGA) or path-integrated gas analyzer (e.g., Heath Inc., RMLD) (Golston et al., 2018; Yang et al., 2018; Barchyn et al., 2019; Fox et al., 2019; Li et al., 2020). The aircraft survey flies at a survey speed of between 11 and 51m s^{-1} (25–114 mph) at a distance of 900–1500 from the source to detect enhanced CH_4 mole fractions or path-integrated CH_4 mole fractions with a flight height of 60–580 m, usually equipped with an infrared imaging spectrometer such as Kairos Aerospace's hyperspectral CH_4 imaging system (resolution: 3 m) (Kligman, 2011; Vaughn et al., 2017; Sherwin et al., 2021; FlyARH, 2021; LASEN, 2021; Heliops, 2022). Even though using these emerging advanced survey methods to improve leak detection efficacy is promising, no controlled subsurface NG release experiments have been conducted to understand the effectiveness of different survey protocols' operational parameters, such as survey speed, height, and survey time, and survey weather conditions, creating a challenge of assessing the advantages or limitations of each survey method's ability to detect the pipeline leaks. Two side-by-side studies by the Pacific Gas & Electric (PG&E) showed that the walking survey and driving survey detected a different subset of leaks, and the percentage of overlapped detection was only 5% and 12%, respectively (Clark et al., 2012; Kerans et al., 2012). The low percentage of overlapped detection in both methods is probably due to the difference in survey protocols' operational parameters, such as survey time and weather conditions, where the driving survey was followed by approximately 5 weeks of the competition of the walking survey. The belowground controlled release experiments from Tian et al. (2022) showed that detection probability (DP) is highly influenced by survey speed, atmospheric stability, and wind speed. The average DP in Pasquill–Gifford stability (PG) class A

is 85% at a low survey speed (2–11 mph), and it reduces to below 25% at a high survey speed (22–34 mph). Therefore, it is clear that understanding different survey protocols' operational parameters is necessary to make useful comparisons of the efficiency between leak survey methods.

The detection of enhanced CH_4 mixing ratios from the aboveground plume is very sensitive to atmospheric conditions and the specification of survey protocols such as survey speed, height, and distance (Nathan et al., 2015; Yacovitch et al., 2015; Albertson et al., 2016; Riddick et al., 2021; Tian et al., 2022). Aboveground emission studies have shown that a gas plume becomes more narrow and concentrated as the atmosphere changes from unstable to stable due to weakened dispersion processes (Riddle et al., 2004; Luketa-Hanlin et al., 2007; Pontiggia et al., 2009; Stull, 2012; Leelőssy et al., 2014; Askariyeh et al., 2017; Seigneur, 2019). A gas plume during high wind speed conditions is longer and narrower than during low wind speed conditions (Carpenter et al., 1971; Thorpe et al., 2016). However, there has been little work to understand 3D gas plume behaviors (i.e., shape and size) from the controlled subsurface NG pipeline leaks under a range of atmospheric conditions, and explicitly link this understanding with the design or use of survey protocols deployed for leak survey methods.

This study investigates variability in the size and shape of a 3D plume above a subsurface NG emission with changing atmospheric conditions and, most importantly, how this can be used to inform and optimize leak survey protocols. Explicitly, the aims are 1) to use controlled release experiments to characterize plume width variability in a range of atmospheric conditions; and 2) to use these findings to provide a physical basis to inform the survey protocols' operational parameters, including survey speed, survey height, survey time, and survey weather conditions, thus increasing the likelihood of detection for a range of survey methods. To our knowledge, this is the first time that the plume shape and size above a subsurface emission have been systematically

investigated using controlled released experiments in a range of atmospheric conditions with the objective of improving the efficacy of leak survey methods.

5.3 Materials and Methods

5.3.1 Experiment and Measurement Approaches

The controlled NG release (0.44 kg hr^{-1} of CH_4) experiments were conducted at a rural testbed, Methane Emission Technology Evaluation Center (METEC), Colorado State University (CSU), Colorado, between March 2nd and April 29th, 2022, under a range of atmospheric conditions, including atmospheric stability, air temperature, air humidity, and wind speed (Table 5.1). The emission point used in this study was buried 0.9 m below the ground surface at the METEC site and backfilled with the native soil (sandy loam, U.S. Department of Agriculture Soil Texture Classification). The surface was covered by short vegetation (average height: 0.05 m). NG was injected through stainless-steel tubing (0.635 cm, model SS-T4-S-035-20, Swagelok, USA) into the testbed from an aboveground 145-Liter compressed natural gas (CNG) tank. The gas flow rate was controlled through the pressure regulators, solenoid valves, and choked flow orifices and measured by a thermal mass flow meter (range: 0–0.66 kg hr^{-1}, accuracy: ±1%, Omega FMA1700 series). This rural testbed can simulate different gas compositions (combinations of methane, ethane, propane, and butane) with a rate of up to 13 kg hr^{-1}. More detailed descriptions of this testbed can be found in Jayarathne et al (2022).

Variables investigated were atmospheric stability, air temperature, air humidity, and wind speed (Table 5.1). The downwind CH_4 mixing ratio measurements were started 20 hours after the release to allow the steady subsurface emission state. The CH_4 mixing ratios were measured sequentially using the ABB's Ultra-Portable Greenhouse Gas Analyzer (Model 915-0011), with 3 ppb

measurement precision at 1 Hz measurement frequency. For each height at each downwind distance, 5 minutes of data were collected by switching the connection of the tubing inlet with the gas analyzer sequentially. The meteorological/micrometeorological data (3D wind fields, air temperature, relative humidity) were measured at 10 Hz using an RM Young 81000 Ultrasonic Anemometer and a meteorological sensor (Met One Instruments Inc., 597A) installed 6 m above the ground at the METEC site.

Table 5.1 General information of the fourteen controlled belowground NG release experiments at the METEC site between March 2nd and April 29th, 2022. The release rate was 0.44 kg hr^{-1} of CH_4. The measurement distance is 7 m downwind of the pipeline, and the height ranges from 0.5 to 7 m. The variables considered here include different Pasquill-Gifford (PG) stability classes ranging from PG A to G, calm to high wind speed, low to very high humidity, and freezing to nonfreezing air temperature. The categorized wind speed interval is 0–1, 1–3, and 3–12 m s^{-1} for the calm, low, and medium to high wind conditions, respectively (Tian et al., 2022). The categorized relative humidity interval is 0–50%, 50–80%, and 80–100% for the low, high, and very high humidity conditions, respectively (Ku-Mahamud and Khor, 2009).

Exp	Q (kg hr^{-1})	Distance (m)	Height (m)	Atmospheric variables investigated
1	0.44	7	0.5, 2, 5, 7	PG A (extremely unstable); PG B/C (unstable); PG D (neutral); PG E/F (stable)
2	0.44	7	0.5, 2, 5, 7	Calm wind (0–1 m s^{-1}); Low wind (1–3 m s^{-1}); Medium to high wind (3–12 m s^{-1})
3	0.44	7	0.5, 2, 5, 7	Freezing temperature (-16 to 0 degC); Nonfreezing temperature (0 to 24 degC)
4	0.44	7	0.5, 2, 5, 7	Low humidity (0–50%); High humidity (50–80%); Very high humidity (80–100%)

5.3.2 Plume Width

For each 5-minute measurement period, CH_4 mixing ratios were first binned by the wind direction in 2-degree increments (Foster-Wittig et al., 2015) and then averaged. The crosswind distance from the plume center (Equation 5.1, Figure 5.1) was calculated for every 5-minute

averaged CH_4 mixing ratio using the plume reconstructed lateral geometry method of Foster-Wittig et al (2015).

$$y = s \cdot sin\,(\theta_m - \theta_c) \tag{5.1}$$

where y is crosswind distance from the plume center (m), s is the measurement distance downwind of leak location (m), θ_m is the wind direction (°), and θ_c is the wind direction of the plume center (°) (Equation 5.1).

The plume width (Figure 5.1) was then calculated using a Gaussian function to fit the crosswind distance and elevated CH_4 mixing ratio ($C - C_0$). The upwind background CH_4 mixing ratio (C_0) is 2.0 ppm at the METEC site. A 100 ppb CH_4 mixing ratio enhancement was used as the detection threshold to calculate the plume width. Previous studies have shown that a leak can be inferred using a 100 ppb CH_4 mixing ratio enhancement threshold (Chen et al., 2020; Riddick et al., 2021). The survey speed is calculated using the plume width divided by the hypothesized 1 Hz frequency CH_4 analyzer. This assumption is based on the fact that most of the mobile leak surveys equip with a 1 Hz frequency CH_4 analyzer such as the ABB's Ultra-Portable Greenhouse Gas Analyzer (Model 915-0011) or Picarro Mobile Gas Concentration Analyzer GasScouter G430.

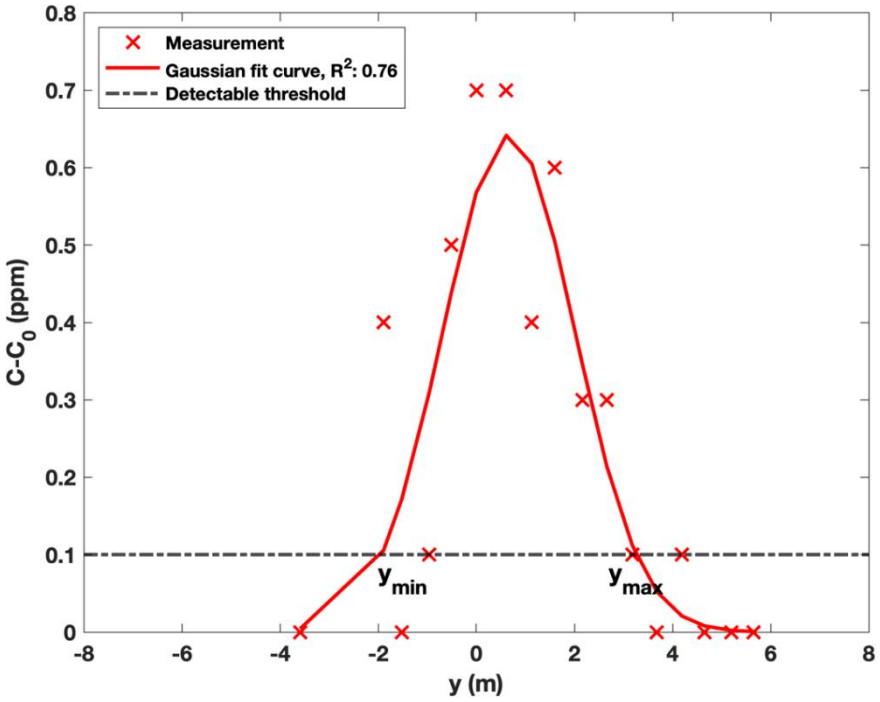

Figure 5.1 Elevated CH_4 mixing ratio (C-C_0) as a function of crosswind distance from the plume center (y=0). The red cross is the measurement point. The red line is the Gaussian fit curve (R^2: 0.76). The black dashed line is the defined detectable threshold (i.e., CH_4 mixing ratio enhancements of 0.1 ppm above the background value) for calculating plume width ($y_{max} - y_{min}$). C is the binned CH_4 mixing ratio. C_0 is the background CH_4 mixing ratio (2.0 ppm). The sample data used here is the binned average of the 5-minute measurements at 5.0 m above the ground from the experiment.

For each 5-minute CH_4 mixing ratio measurement period, the Monin-Obukhov length (L, m) was calculated using Equations 5.2 and 5.3 (Kaimal and Finnigan, 1994; Flesch et al., 2004; Foken, 2006; Stull, 2012) using the surface friction velocity (u_*, m s^{-1}), the mean absolute air temperature (T, K), the von Kármán's constant ($k_v = 0.41$), the gravitational acceleration (g = 9.8 m s^{-2}) and the 3D horizontal/vertical wind vectors (u, v, w, m s^{-1}), respectively. The L was further converted into Pasquill-Gifford (PG) stability class for easy use by industry practitioners (Ulrich et al., 2019; Riddick et al., 2021), where PG A is extremely unstable ($-100 \leq L < 0$), PG B/C is unstable ($-500 \leq L < -100$), PG is D ($|L| > 500$), PG E/F is stable ($500 \leq L < 100$), and PG G is extremely stable ($0 < \mathrm{L} \leq 100$) (Gryning et al., 2007; Breedt et al., 2018). The converted PG

stability class was thus chosen to reveal the impacts of atmospheric stability on plume width and survey speed in this study.

$$L = -\frac{u_*^3 T}{k_v g \overline{w'T'}} \tag{5.2}$$

$$u_* = \left[\left(\overline{u'w'}\right)^2 + \left(\overline{v'w'}\right)^2\right]^{1/4} \tag{5.3}$$

5.4 Results

5.4.1 Diurnal Variability in Plume Width

The plume width shows a diurnal variability between the day and night (Figure 5.2a). The plume width during the day is larger than at night in each measurement height ranging from 0.5 m to 7 m above the ground. The plume during the day is about 10 m wide on average for the four heights, and it reduces to 9 m wide at night (10% decrease). Also, the plume width changes with the change in height, regardless of day and night. The plume is widest at 5 m above the ground with the value of 10 and 9 m during the day and at night, respectively, and it decreases as the height is higher or lower than such a height.

Further, the result demonstrates that survey speed depends on survey time (Figure 5.2b). Survey speed during the day is about 2 mph higher on average than at night for the four heights (range: 1–3 mph). The maximum survey speed is 22 and 20 mph during the day and at night, respectively, for a driving survey with CH_4 sampling height below 2.0 m above the ground. The maximum survey speed is 23 and 21 mph during the day and at night, respectively, for a UAV survey with CH_4 sampling height between 5 and 7 m above the ground.

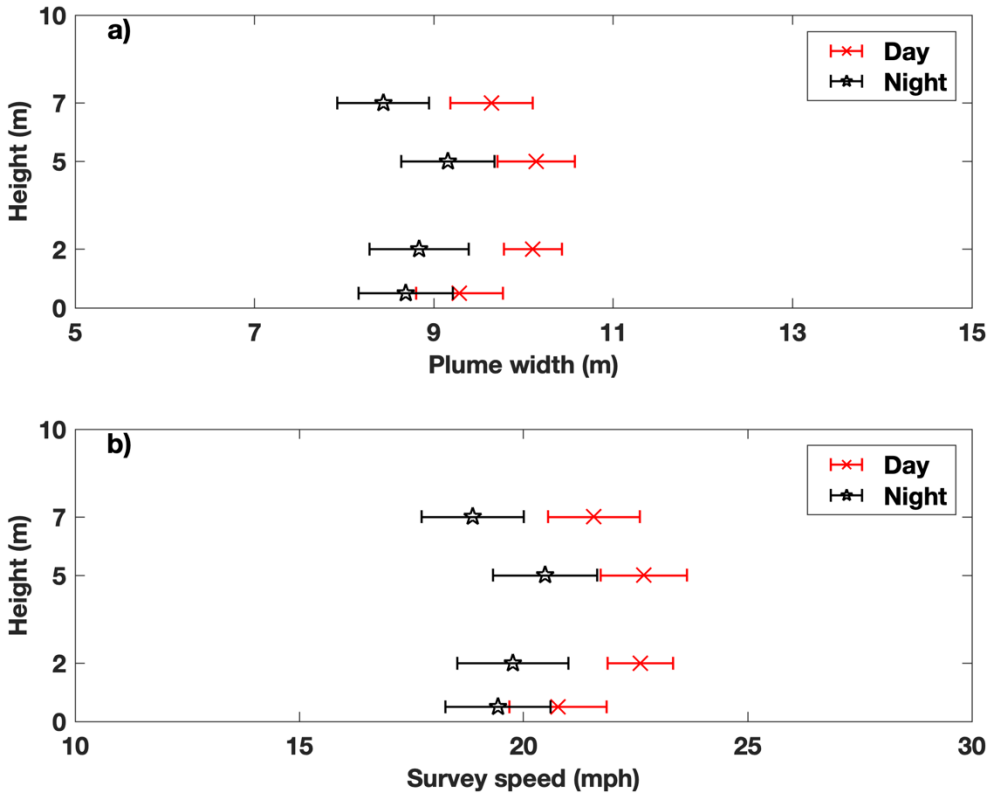

Figure 5.2 The plume width and survey speed at heights between 0.5 and 7 m above the ground during the day (07:00–17:00) and at night (00:00–07:00, 17:00–24:00). The error bar is ±1 standard error.

5.4.2 Variability in Plume Width Due to Different Atmospheric Stability Conditions

The plume width at each height consistently decreases with increased atmospheric stability (PG: A to G) (Figure 5.3a). The plume is about 11 m wide on average during PG A (extremely unstable) condition, but it reduces to 7 m wide as the stability changes to PG G (extremely stable) (36% decrease). The percentage change range of the plume width due to atmospheric stability conditions is 3.6 times that due to diurnal variation, suggesting the large variability in plume width within a sub-day scale (i.e., day and night). The plume is the widest at 5 m above the ground, with values of approximately 11, 10, 9, 9, and 7 m for PG A, B/C, D, E/F, and G, respectively. And it decreases both above and below this height.

The survey speed decreases rapidly as the atmospheric stability transitions from PG A to G (Figure 5.3b). The average survey speed decreases from 25 mph during PG A to 16 mph during PG G (36% decrease). The maximum survey speed is 24, 23, 20, 19, and 16 mph during PG A, B/C, D, E/F, and G, respectively, for a driving survey with CH_4 sampling height below 2.0 m above the ground. The maximum survey speed is 25, 23, 20, 19, and 16 mph during PG A, B/C, D, E/F, and G, respectively, for a UAV survey with CH_4 sampling height between 5 and 7 m above the ground.

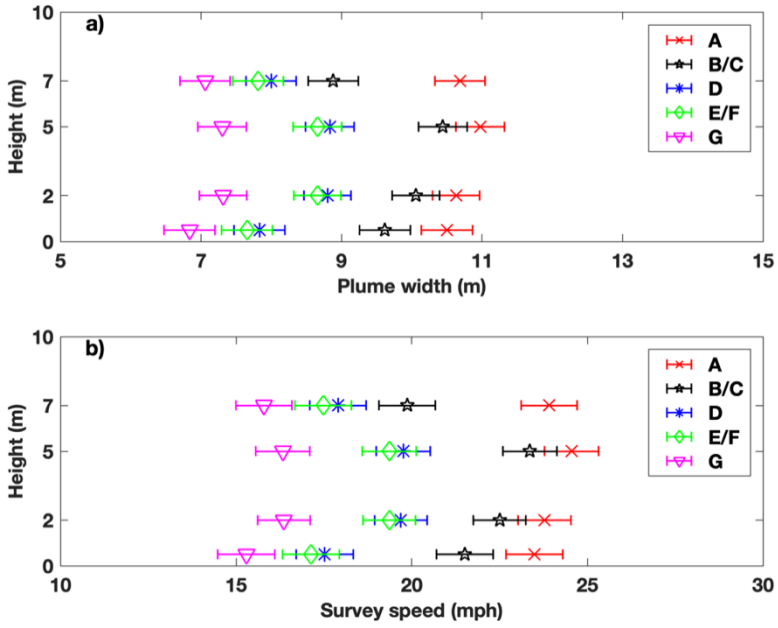

Figure 5.3 The plume width and survey speed at heights between 0.5 and 7 m above the ground under different stability conditions ranging from PG stability class A to G. The error bar is ±1 standard error.

5.4.3 Variability in Plume Width with the Change in Air Humidity, Wind Speed, and Air Temperature

The plume width at each height increases with the increase in air humidity (Figure 5.4a). The plume is about 9 m wide on average in low humidity conditions, and it increases to 11 m wide as the air humidity changes to very high humidity conditions (22% increase). The plume is the widest

at 5 m above the ground, with values of approximately 9, 10, and 11 m in low, high, and very high humidity conditions, decreasing above and below this height. The survey speed also increases, accompanied by the increase in air humidity (Figure 5.4b). The average survey speed increases from 20 mph in low humidity to 24 mph in very high humidity conditions (20% increase). The maximum survey speed is 20, 21, and 25 mph in low, high, and very high humidity conditions, respectively, for a driving survey with CH_4 sampling height below 2.0 m above the ground. The maximum survey speed is 21, 21, and 25 mph in low, high, and very high humidity conditions, respectively, for a UAV survey with CH_4 sampling height between 5 and 7 m above the ground.

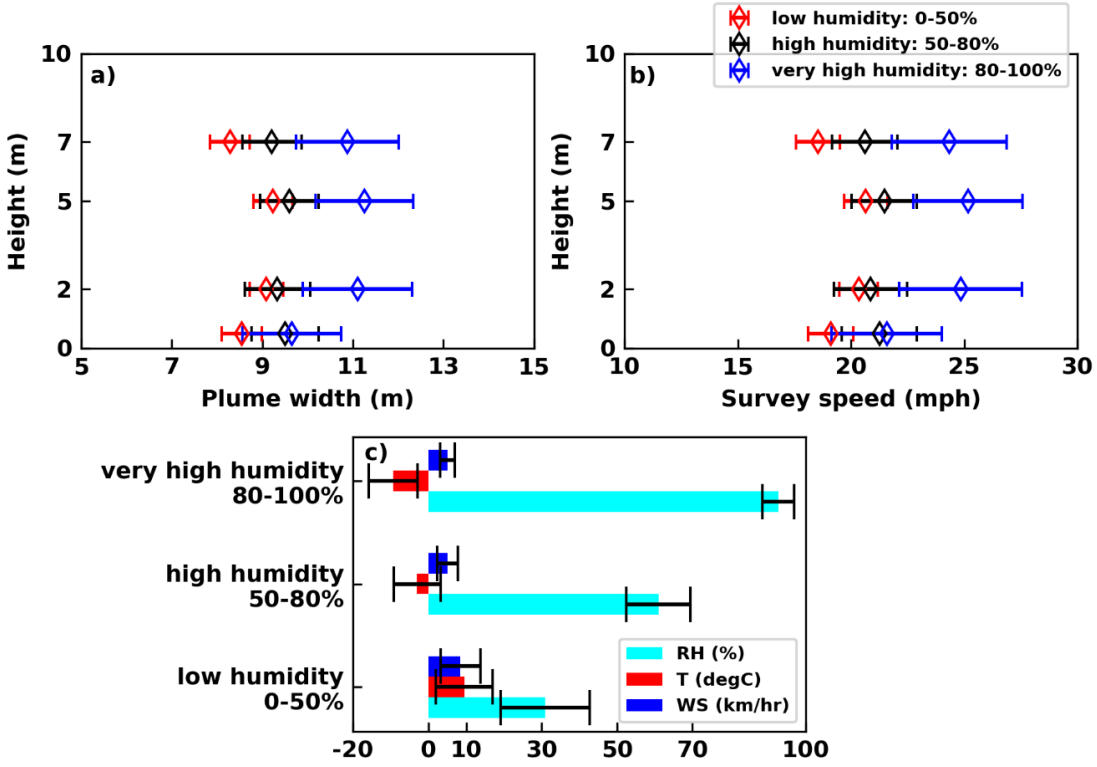

Figure 5.4 a)-b) the plume width and survey speed at heights between 0.5 and 7 m above the ground under different humidity conditions; c) the average relative humidity (RH), temperature (T), and wind speed (WS) in each humidity condition. The categorized relative humidity interval is 0–50%, 50–80%, and 80–100% for the low, high, and very high humidity conditions, respectively (Ku-Mahamud and Khor, 2009). The error bar is ± 1 standard error. The unit of WS is converted to km hr^{-1} for visualization purposes.

The air temperature and wind speed decrease with the increase in air humidity (Figure 5.4c). The Pearson correlation coefficient is -0.83, -0.41, and 0.33 between air temperature and relative humidity, between wind speed and relative humidity, and between air temperature and wind speed, respectively (Table 5.2). All are statistically significant, with p-values of less than 0.05.

Table 5.2 Pearson correlation coefficients (r) and the respective p values between air temperature (T, degC), relative humidity (RH, %), and wind speed (WS, m s^{-1}).

Atmospheric variables	r	p-value
T, RH	-0.83	1.15E-182
T, WS	0.33	3.98E-20
WS, RH	-0.41	9.15E-31

Further analyses show that both plume width and survey speed decrease rapidly with the increase in wind speed and decrease slightly with the increase in air temperature (Figures 5.5a and 5.5c). The plume is about 11 m wide on average in calm wind conditions, and it reduces to 7 m wide as the wind changes to medium to high wind conditions (36% decrease). The average survey speed decreases from 25 mph in calm wind to 16 mph in medium to high wind conditions (36% decrease). The maximum survey speed is 25, 22, and 17 mph in calm, small, and medium to high wind conditions, respectively, for a driving survey with CH_4 sampling height below 2.0 m above the ground. The maximum survey speed is 24, 22, and 16 mph in calm, small, and medium to high wind conditions, respectively, for a UAV survey with CH_4 sampling height between 5 and 7 m above the ground. However, the average plume width decreases by 3% as air temperature changes from freezing temperature (plume width: 9.4 m) to nonfreezing temperature (plume width: 9.1 m). The average survey speed is about 21 and 20 mph in freezing temperature and nonfreezing temperature, respectively. The result suggests the negligible impacts of air temperature on the

plume width and survey speed, relative to the air humidity, wind speed, and atmospheric stability, providing the evidence for a previous study showing the significant effects of wind speed and atmospheric stability on the detection probability of driving surveys (Tian et al., 2022). This is because turbulent diffusion due to buoyancy and shear forces dominates the gas dispersion in the atmosphere, rather than the molecular diffusivity (Csanady, 1973; Ounis and Ahmadi, 1990).

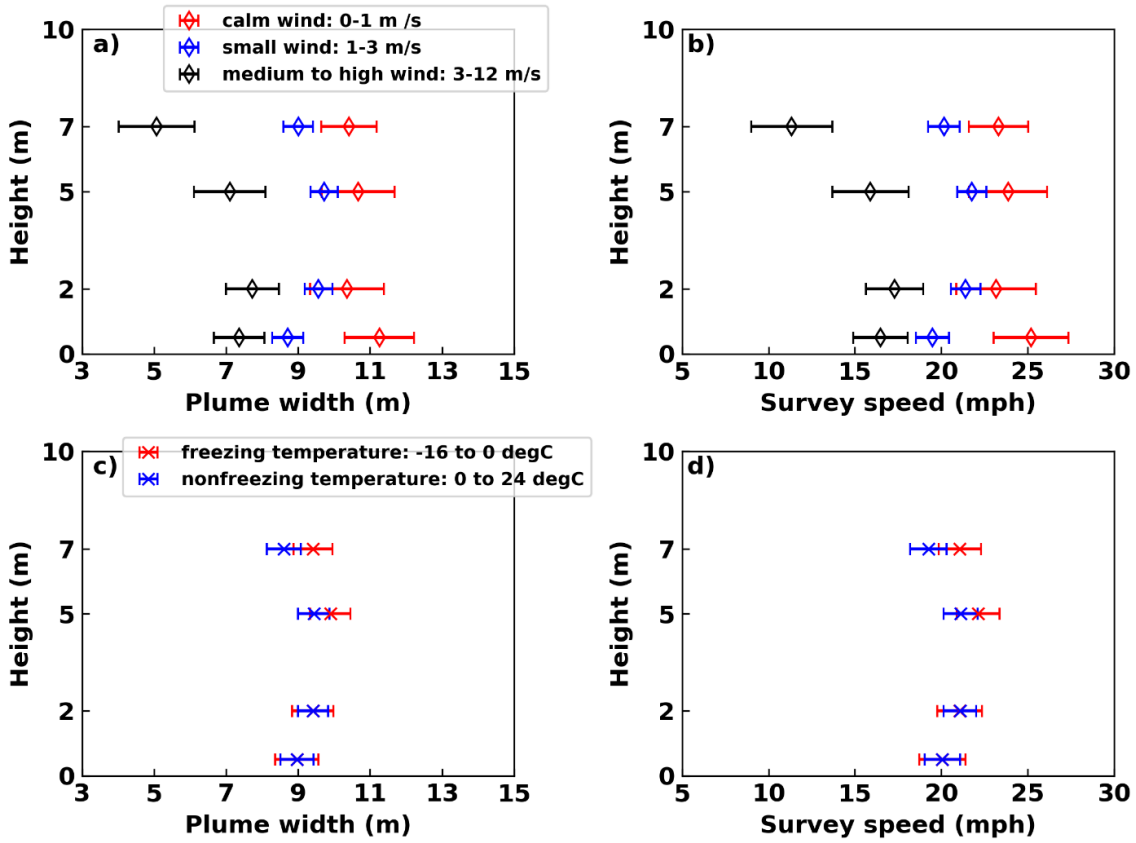

Figure 5.5 Plume width and survey speed at heights between 0.5 and 7 m above the ground under different wind speed, and air temperature conditions. The categorized wind speed interval is 0–1, 1–3, and 3–12 m s^{-1} for the calm, low, medium, and medium to high wind conditions, respectively (Tian et al., 2022). The temperature bin interval is according to the measured temperature range during the experiments. The error bar is $\pm$1 standard error.

5.5 Discussion

The LDAQ survey operators usually transect downwind of the pipelines to detect the methane leaks. This chapter physically reveals the significance of incorporating the transect plume width

into LDAQ survey protocols. However, this chapter did not include the alongwind plume length due to the logistic challenges of measuring CH_4 concentration simultaneously in all three dimensions (i.e., alongwind, crosswind, and vertical direction) with one single gas analyzer. Currently, survey distance depends on the operators ranging from 0 m to more than 1,000 m (Zimmerle et al., 2017; Caulton et al., 2018; Weller et al., 2018; Li et al., 2020; Heliops, 2022). There are no studies providing the justifications for the setting of survey distance by linking with the plume length. Previous studies have demonstrated that gas plume tend to be elongated in high wind condition due to the effective transport processes in these wind conditions (Carpenter et al., 1971; Choi et al., 2014; Thorpe et al., 2016). According to the mass balance, it is consistent the finding of narrow plume width during high wind conditions in this chapter to some extent. But the detection probability generally is expected to be lower when trespassing an elongated and narrowed plume compared to a short and wide one. In order to overcome the limited data, the follow-on work in this chapter will use fully simulated 3D gas plume though CFD modeling to investigate how the evolution of 3D plume impacts on the LDAQ survey efficiency in more comprehensive approach.

5.6 Conclusions

This work characterizes the CH_4 plume variability to inform the design or use of survey speed for underground pipeline leak survey methods under a wide range of weather conditions. Our results showed that atmospheric stability, wind speed, and air humidity significantly impact the plume width and survey speed. The plume width decreases by 36% on average, with atmospheric stability changing from PG A (extremely unstable) to PG G (extremely stable) and wind from calm to medium and high wind speed conditions. But it increases by 22% as the air humidity rises from

low humidity to very high humidity conditions. The widest plume typically occurs 5 m above the ground, decreasing above and below this height, regardless of weather conditions considered here.

When applied to mobile leak survey methods, our results showed that survey speed is mainly affected by survey time, survey height, and atmospheric conditions (i.e., atmospheric stability, wind speed, and air humidity). The average survey speed is 22 mph during the day and 20 mph at night (~10% decrease). The survey speed changes by up to 34% due to the change in survey height, with the highest value of 25 mph, usually occurring 5 m above the ground, decreasing both and below this height. The average survey speed decreases by 36%, from 25 mph to 16 mph, with increased atmospheric stability from PG A to G and wind speed from calm to medium and high winds, respectively. But the average survey speed increases by 20%, from 20 mph to 24 mph, accompanied by the increase in air humidity from low to very high humidity conditions. Our results show that the leak survey has a wider range of survey speed options (0–25 mph) to detect subsurface pipeline leaks at a middle height of approximately 5 m during the day when the atmosphere is unstable (PG A to B/C), the wind is calm to medium speed (0–3 m s^{-1}), and air humidity is high to very high (50–80%).

Overall, the findings of this study emphasize the importance of incorporating plume variability into the survey protocols (e.g., survey speed, height, time, and weather conditions) to improve the detection efficiency of leak survey methods.

Chapter 6 Conclusions, Discussions and Future Research

This section summarizes the main conclusions from chapters 3–5, followed by discussions, and suggestions for future research.

6.1 Conclusions

NG has been widely accepted around the world as a bridge fuel to a carbon-free or renewable future. Although it is regarded as a "clean burning" fuel, methane leakages from the underground NG pipelines threaten the global efforts to mitigate greenhouse emissions. Leak detection and quantification (LDAQ) surveys have been recognized as an effective approach to finding and ultimately fixing leaks, aiding methane mitigation efforts. Recently, the applications of many emerging LDAQ survey methods have improved the understanding of CH_4 emissions from NG infrastructure. However, the efficiency of the methods remains unclear, creating a knowledge gap in understanding the disparity in reported leak densities and emission rates based on different survey methods. Therefore, it is imperative to adopt better science into these engineering methods to advance understanding of the knowledge gap between them and improve the robustness of LDAQ survey methods on the mitigation efforts. This doctoral research explores the understanding of the impacts of atmospheric variability on subsurface NG pipeline emissions using controlled experiments, mathematical modeling, and statistical analysis. This work addresses the following three aspects: 1) developing a detection probability model to assess the detection efficacy of mobile survey methods under different atmospheric conditions, 2) investigating the impacts of atmospheric variability on subsurface CH_4 emission estimate accuracy, and 3) characterizing the plume variability due to atmospheric conditions to inform the survey parameters of LDAQ methods.

To this end, chapter 3 presents a comprehensive analysis of how leak rate sizes, survey protocols, and atmospheric conditions affect the DP of subsurface NG emissions. A validated DP model (R^2: 0.76) was developed to model the detection efficiency for walking and driving surveys using three publicly available emission rate datasets from NG distribution pipeline leaks. The results show that the DP is negatively proportional to survey speed, survey distance, atmospheric stability (1/L), wind speed, and air temperature but is positively proportional to the leak rate. The average DP in Pasquill–Gifford stability (PG) class A is 85% at a low survey speed (2–11 mph) and decreases to 68%, 63%, 65%, and 60% in PGSC B/C, D, E/F, and G respectively. It is generally less than 25% at a high survey speed (22–34 mph), regardless of stability conditions and leak rates. Survey speed, atmospheric stability, and wind speed significantly impact the DP. The average modeled DP decreases by 25% with an increase in survey speed from 2 to 34 mph, atmospheric stability (1/L) from −0.2 to 0.2 m^{-1}, and wind speed from 0.1 to 10 m s^{-1}, respectively. The average DP in all weather conditions (PG A to G, calm to large winds) is about 66% for the walking survey, but it reduces to 35% for a driving survey with low to medium speed (11–22 mph). The options of modeled favorable weather conditions (i.e., PG stability class and wind speed) to have a high DP (e.g., >50%) are rapidly decreased with the increase in survey speed. A walking survey is applicable over a wider range of weather conditions, including PG stability class A to E/F and calm to medium winds (0–5 m s^{-1}). A driving survey at a low speed (11 mph) can only be conducted under calm to low wind speed conditions (0–3 m s^{-1}) to have an equivalent DP to a walking survey. Only calm wind conditions in PG A (0–1 m s^{-1}) are appropriate for a high driving speed (34 mph). These findings in this chapter highlight the importance of atmospheric stability, wind speed, and survey parameter in influencing the detection efficiency of leak survey methods,

as well as optimization of the driving survey schemes to achieve a DP equivalence to the traditional walking survey.

Chapter 4 explores the effectiveness of an atmospheric dispersion-based inverse modeling method in quantifying CH_4 emissions from subsurface pipeline leaks under realistic conditions and analyzes the impacts of atmospheric variability on the below-ground emission estimate accuracy. Results show the large temporal variability of surface CH_4 emissions from the subsurface pipeline leaks. It typically decreases with the increase in atmospheric stability when the PG stability class changes from A (extremely unstable) to G (extremely stable) due to the inhibited dispersion and mixing in the atmosphere. The average surface CH_4 emissions over 6.5 h downwind measurements can provide a representative estimate from subsurface pipeline leaks (±27% of the controlled release rate on average). The probability that the emission estimate is within ±50% of the controlled release rate ($P_{\pm 50\%}$) is about 50% using approximately 1 h downwind data. And it increases to 80% and 100% with about 2 h and 3–4 h of data, respectively. The findings of this study emphasize the importance of a certain amount of data covering surface emission variability due to atmospheric conditions to have an estimate that can reflect the actual subsurface leak rates.

Chapter 5 investigates the plume 3D gas plume behaviors (i.e., shape and size) from the controlled subsurface NG pipeline leaks over a wide range of atmospheric conditions and explicitly use these physical understandings of plume variability to inform leak survey parameters. Results show that the plume width decreases with the increase in atmospheric stability and wind speed but increases with the increase in air humidity. Air temperature has a negligible influence on the plume width. The plume width decreases by 36% on average when the atmospheric stability transitions from PG A (extremely unstable) to PG G (extremely stable). But it increases by 22% when the air humidity changes from low humidity (0–50%) to very high humidity (80–100%) conditions. The

plume is typically the widest at 5 m above the ground, decreasing above and below this height. In addition, when applied to mobile leak survey methods, it is found that survey speed is mainly impacted by survey time, survey height, and survey weather conditions, including atmospheric stability, wind speed, and air humidity. The percentage change in survey speed is 10–36%, depending on the survey parameters considered here. The average survey speed decreases from 25 mph to 16 mph as atmospheric stability changes from PG A to G and wind speed from calm to medium and high winds, respectively. Leak survey has a wider range of survey speed options (0–25 mph) to detect subsurface pipeline leaks at a middle height of approximately 5 m during the day when the atmosphere is unstable (PG A to B/C), the wind is calm to medium speed (0–3 m s^{-1}), and air humidity is high to very high (50–80%).

Overall, the findings of this study highlight the importance of adopting the understanding of plume variability into the survey protocols (e.g., survey speed, survey height, survey time, and survey weather conditions) to optimize leak survey methods for underground pipeline leaks.

6.2 Discussions

The findings of this research can be extended into other fields such as hydrogen leakage and landfills methane emissions to improve the detection and quantification efficiency. With zero greenhouse gas (GHG) emissions such as CO_2 and CH_4, hydrogen has been recognized as a promising renewable energy to reduce and or replace the use of fossil fuel such as gasoline, and natural gas to achieve a carbon-neutral future (Crowl and Jo, 2007; Elaoud et al., 2010; Molnarne and Schroeder, 2019; Abohamzeh et al., 2021; Kovač et al., 2021). The wide distribution of underground pipeline network will serve as a critical infrastructure for the large-scale implementation of hydrogen energy (Abohamzeh et al., 2021). Compared to methane, hydrogen

has a lower ignition energy (hydrogen: 0.019 mJ; methane: 0.28 mJ), and a higher deflagration index (hydrogen: 550; methane:55) (Crowl and Jo, 2007; Elaoud et al., 2010; Molnarne and Schroeder, 2019). Hydrogen leakage from underground pipelines has a higher probability of a fire or explosion risk than methane leakage (Crowl and Jo, 2007; Elaoud et al., 2010; Molnarne and Schroeder, 2019). Periodic LDAQ surveys along the hydrogen pipeline would expect to be of particular importance for preventing hydrogen leakage resulted in explosion and fire accidents.

Methane emission from the landfill is a significant global sources of greenhouse gases, taking about 20% among all global anthropogenic methane emission sources (UNEP&CCAC, 2021). Previous studies (Czepiel et al., 2003; Gasbarra et al., 2019; Mønster et al., 2019) have demonstrated landfill methane emissions have temporal variability due to the change in environmental conditions, and longer time periods measurements are required to have a representative estimate for the actual emissions. The emission estimate method in this work for underground NG pipeline leaks provide a benchmark for improving the landfill methane emission accuracies.

6.3 Recommendations for Future Research

This doctoral research provides a baseline framework for underground pipeline LDAQ survey methods by incorporating the plume behaviors under different atmospheric conditions in realistic controlled conditions. There are three recommendations for future work to extend this dissertation's research into a broader science and engineering scope.

(1) Development of the plume parameterization scheme by numerical modeling

The efficiency of LDAQ survey methods depends on the representation of the plume behaviors. In this research, we used a series of observations, but still limited, to reveal the significance of environmental conditions impacting the plume. But it remains a key question of how to parameterize the plume to apply to the LDAQ survey methods robustly. Once validated, the numerical models can be used as a valuable tool to understand the gas plume behaviors fully and further parameterize the plume. The increasingly affordable computation resources and availability of various dispersion modeling frameworks across a wide range of scales, such as Gaussian, Lagrangian, and CFD (computational fluid dynamics) models, provide a promising tool to fully understand leaked plume behaviors under different leak scenarios (e.g., leaks in open and urban environments) and environmental conditions not achievable in the field.

(2) Development of the national CH_4 emission baseline dataset from underground natural gas pipeline leaks by integrating multiple dataset sources

The accuracy of CH_4 emission serves as a foundation across a wide range of communities with their objectives, such as industry operators for leak repair, policymakers for mitigation regulations, and scientists for assessing CH_4 emissions resulting in climate impacts. Currently, the national CH_4 emission inventory from underground pipeline sectors is poorly characterized compared to the upstream sectors of the NG supply chain (e.g., production). NG pipelines are distributed across the U.S., and most of them are buried below ground. Thus, relying on one data source to characterize the national CH_4 emission is not feasible. Instead, it is necessary to establish a baseline CH_4 emission dataset by integrating multiple source datasets and following the transparent data analytic methods. The DP model developed in this research can be extended into the framework of the data analytic approach in the future.

(3) Investigating the relative contribution of air humidity on methane plume shape and size in a range of atmospheric conditions

In this study, it was observed that air humidity significantly impacts methane plume width, in addition to atmospheric stability and wind speed. Some CFD dispersion modeling studies on LNG (liquified natural gas) and liquid hydrogen spills have shown that the phase change of water vapor in the atmosphere such as water condensation, affects impacts the hydrogen and methane gas plume (Giannissi et al., 2014; Giannissi and Venetsanos, 2018; Liu et al., 2019; Sun et al., 2020). The high air humidity means a high-water vapor mixing ratio, resulting in a decrease in gas density (e.g., hydrogen, methane). This decreased gas density will in turn increase the buoyancy force when mixing with the ambient air. The increased buoyancy forces enhance the atmospheric turbulence by influencing the energy balance of turbulent motions, promoting the expansion of gas plume along the 3D directions (Csanady, 1973; Hanna, 1986; Assou and Saadeddine, 2018). Given the significant relationship between air humidity, air temperature, and wind speed (Chapter 5), further research is needed to investigate the relative contribution of air humidity on the plume shape and size through the CFD dispersion modeling.

Appendix A Field Experiments*

All experiments in this doctoral research were conducted at the Methane Emission Technology Evaluation Center (METEC) site, at Colorado State University (CSU) (Figure A.1). The testbed can simulate different underground pipeline leaks, including gathering line, flowline, and distribution pipeline, and allowing for continuously monitoring of the subsurface, surface, and atmospheric conditions. Both the environmental sensors (soil moisture, soil temperature, and matric potential) and INIR (Integrated Infrared) sensors have been permanently installed at multiple locations (0-30 m away from the leak point) and depths (0.3-0.9 m belowground) to measure the migration behavior of leaked CH_4 and corresponding soil conditions (Figure A.2). The atmospheric measurements include the downwind CH_4 measurements and the micrometeorological measurements (Figure A.3 to 4).

Figure A.1 Methane Emission Technology Evaluation Center (METEC) site at Colorado State University (CSU).

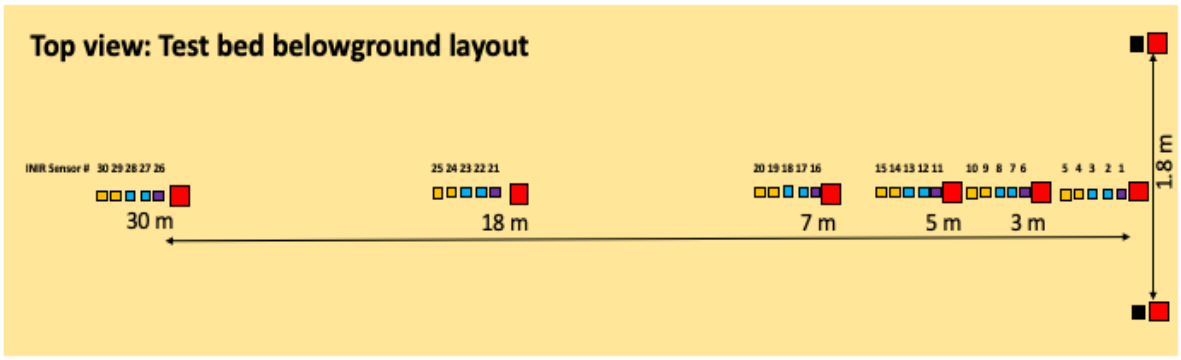

Environmental sensors (0.3 m, 0.6m, 1.8 m)	
INIR sensor (0.3 m)	
INIR sensor (0.9 m)	
INIR sensor (1.8 m)	
Leak point (0.9 m , 1.8 m)	

Sensor name	Description
Environmental sensors	Soil moisture-TEROS 10 Metric potential-TEROS11 Soil temperature-TEROS21
INIR sensor	SGX Integrated Infrared (INIR) Sensor

Figure A.2 Top view of sensor layout in the METEC pipeline testbed.

Figure A.3 Left: installments of the 3D sonic anemometer and weather sensors; Right: walking survey CH_4 measurements.

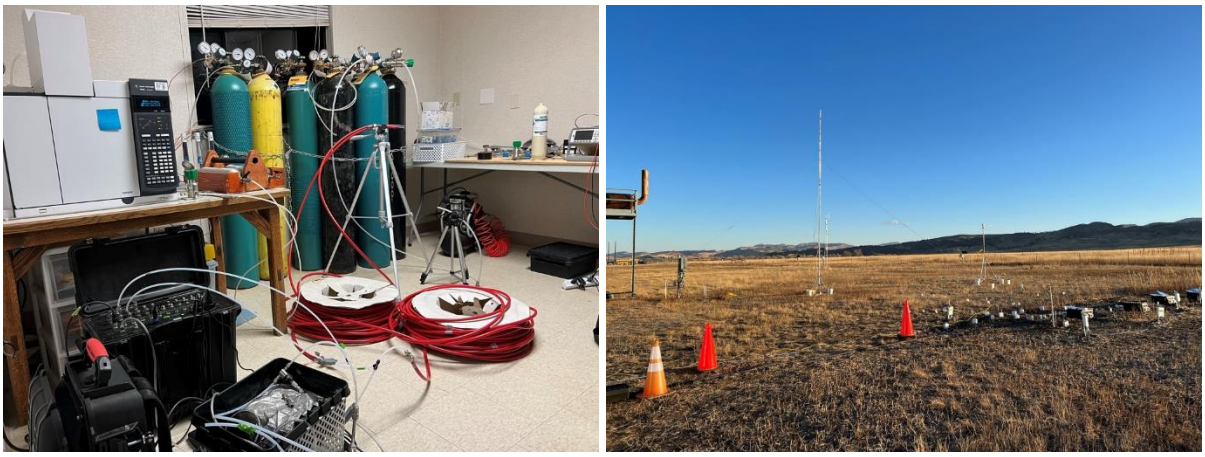

Figure A.4 Left: laboratory experiments to test the multiplexer system; Right: field 3D plume experiments using the multiplexer system.

*Data availability

Tian, S., Smits, K.M., Cho, Y., Riddick, S.N., Zimmerle, D.J. and Duggan, A., 2022. Replication Data for estimating methane emissions from underground natural gas pipelines using an atmospheric dispersion-based method. https://doi.org/10.18738/T8/UAO5XX, Texas Data Repository.

Tian, S., Riddick, S.N., Cho, Y., Bell, C.S., Zimmerle, D.J. and Smits, K.M., 2022. Replication Data for investigating detection probability of mobile survey solutions for natural gas pipeline leaks under different atmospheric condition. https://doi.org/10.18738/T8/DYIIJY, Texas Data Repository.

Appendix B Supplemental Materials for Chapter 4

B.1 Equations in Windtrax

The particle trajectories are modeled in WindTrax based on Langevin equations, which assume that position and velocity of a single particle evolve jointly as a Markov process (Flesch et al. 2004).

$$u_i = a_i \Delta t + b_i R_i \tag{B.1}$$

$$\Delta x_i = u_i \Delta t \tag{B.2}$$

where the coefficients a_i and b_i are functions of position and velocity, and R_i is a Gaussian random number, u_i represents the u, v, w (along-wind, cross-wind, and vertical velocities, unit: m/s), x_i represents the x, y, z (along-wind, cross-wind, vertical coordinates, unit: m) for $i = 1,2,3$. Δt is the model timestep (unit: s).

The coefficients a_i, b_i are solved according to the simplified Thomson's solution (Flesch et al. 2004; Hatfield et al. 2005; Thomson 1987).

$$a_u(u,v,w,z) = -\frac{b_u^2}{2(\sigma_u^2\sigma_w^2 - u_*^4)}[\sigma_w^2(u-U) + u_*^2 w] + w\frac{\partial U}{\partial z} \tag{B.3}$$

$$a_v(u,v,w,z) = -\frac{b_v^2}{2\sigma_v^2} v \tag{B.4}$$

$$a_w(u,v,w,z) = -\frac{b_w^2}{2(\sigma_u^2\sigma_w^2 - u_*^4)}[u_*^2(u-U) + \sigma_u^2 w] + \frac{1}{2}\frac{\partial \sigma_w^2}{\partial z} + \frac{1}{2(\sigma_u^2\sigma_w^2 - u_*^4)}\left[u_*^2\frac{\partial \sigma_w^2}{\partial z}(u-U)w + \sigma_u^2\frac{\partial \sigma_w^2}{\partial z}w^2\right] \tag{B.5}$$

$$b_u = b_v = b_w = b = (2\sigma_w^2/T_L)^{1/2} \tag{B.6}$$

where $\sigma_u^2,\sigma_v^2,\sigma_w^2$ is the variance of 3D velocity fluctuation (m^2/s^2) along-wind, crosswind, and vertical directions, respectively, U is the average wind velocity (m/s), u_* is the surface friction velocity (m/s), T_L is a Lagrangian time scale (s). Velocity variances ($\sigma_u^2,\sigma_v^2,\sigma_w^2$), surface friction velocity (u_*), and Lagrangian time scale (T_L) are derived by the wind flow parameterization equations (Flesch et al. 1995) with known average wind speed U, surface roughness length, and atmospheric stability.

After the "vertical touchdown velocity", w_0, the vertical velocity where particle hits the ground at the location (x_0, y_0) within the source boundary is solved by discretization of the Langevin trajectory equations (Eqs.B.1-B.2), the ratio of concentration over the background at a downwind location to the source emission rate $(C/Q)_{sim}$ within the source boundary is predicted as:

$$(C/Q)_{sim} = \frac{1}{N}\sum\left|\frac{2}{w_0}\right| \quad \text{(B.7)}$$

where N is the total number of particles released from the downwind point, $N = 500{,}000$.

B.2 Supplemental Figures

Figure B.1 shows the time series of solar radiation, air temperature, wind direction, and wind speed at 1 m (blue line) and 6m (red line) above the ground and Obukhov length during the experiments. In general, these meteorological variables showed a diurnal cycle. The solar radiation changed from as high as 1,000 W m^{-2} at mid-noon to 0 W m^{-2} at night. During the day (e.g., 10:00 AM-5:00 PM), air temperature at 1 m height was usually higher than at 6 m height, but it was usually lower at night (e.g., 7:00 PM-5:00 AM). Wind speed was higher during the day than at night, with a maximum wind speed of approximately 10 and 9 m s^{-1} at 1 m and 6 m height,

respectively. The wind direction usually changed from northerly at night to southerly during the day. The Obukhov length was about -500 m to 500 m for most of the time.

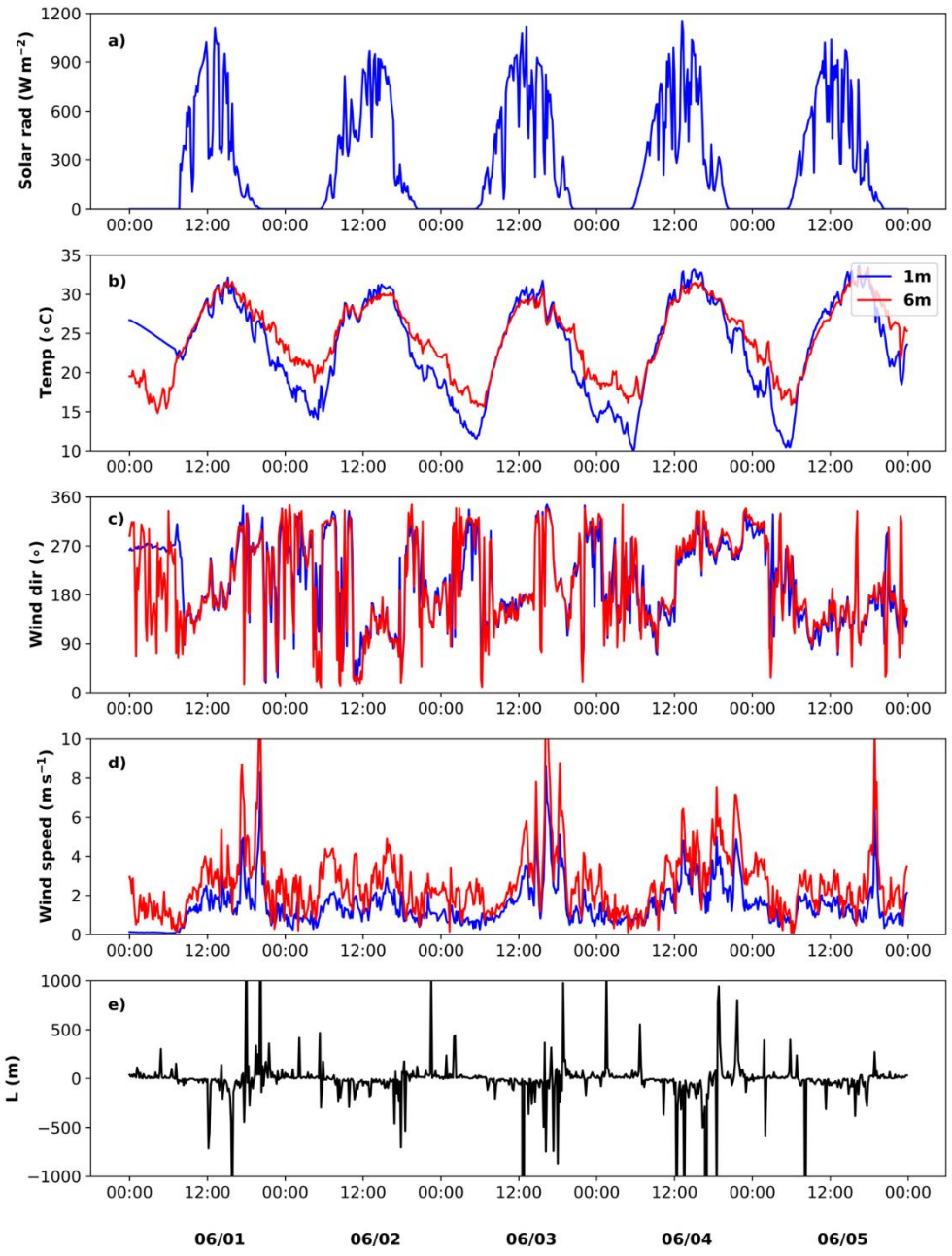

Figure B.1 Time series of solar radiation, air temperature, wind direction, and wind speed at 1 m (blue line) and 6 m (red line) above the ground, and Obukhov length (L) from June 1st to June 5th, 2020. The Obukhov length was calculated using 1 min 3D sonic data (YOUNG Model 81000 Ultrasonic Anemometer) at 6 m height. Data were averaged every 10 minutes. The time is MDT (Mountain Daylight Time). The meteorological sensor ATMOS 41 was in an adjustment period before June 1st, 9:00 AM, 2020. Thus, meteorological data from ATMOS 41 showed abnormal values before this time.

Figure B.2 shows the surface CH_4 mole fraction plots for the four experiments (Exp1–4). The area surrounded by a 100-ppm contour was used to calculate the area of surface expression. We assumed that the surface mole fraction is at least one time larger than the observed maximum atmospheric CH_4 mole fraction (65 ppm at 0.5 m height) to represent the average conditions of the belowground release source for the four experiments. We also used 50 ppm and 200 ppm contours as the mapped surface area in the WindTrax model and found that the absolute percentage difference between the average surface CH_4 emissions and the controlled release rate was about 26% and 29%, respectively. It was 27% using the mapped surface area surrounded by 100 ppm contour. Thus, the sensitivity was about 1–3% for the surface area using 50–200 ppm.

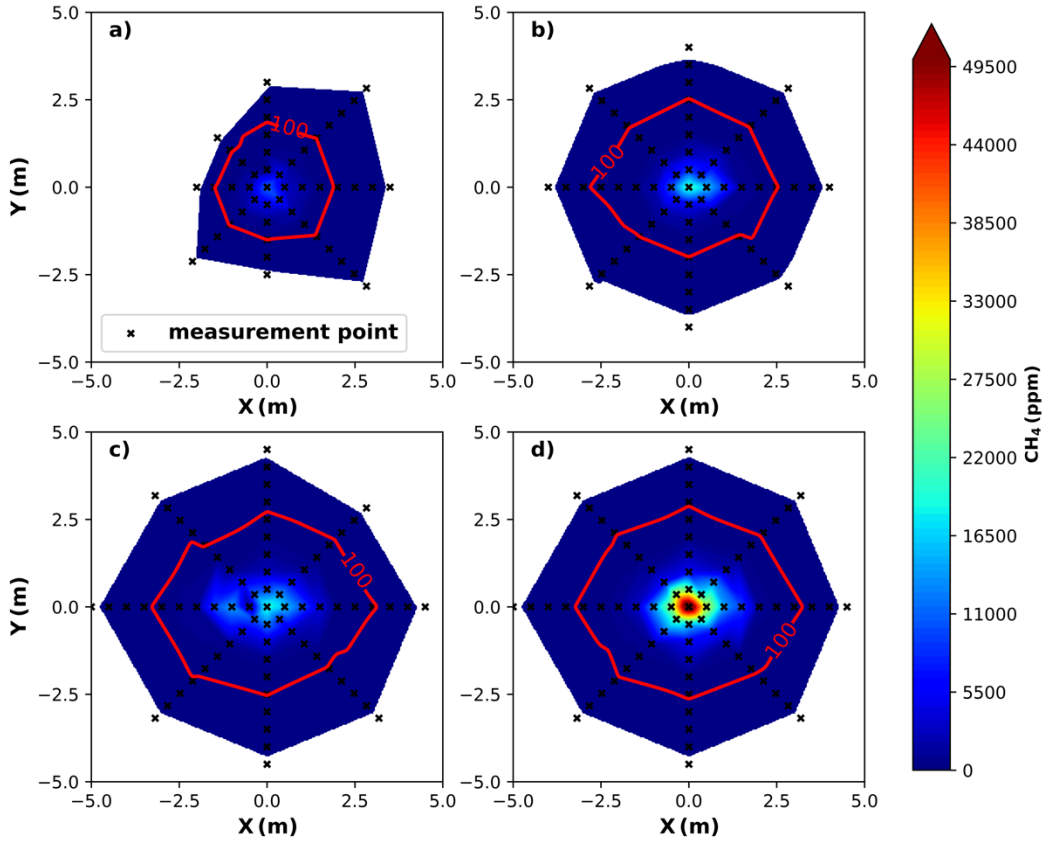

Figure B.2 The surface CH_4 mole fraction plots for the four experiments (Exp1–4). The red contour is 100 ppm CH_4 mole fraction. The release rate is 0.08, 0.18, 0.27, 0.52 kg hr-1 of CH_4 for Exp1-4 (Figure B.2a to 2d), respectively.

Figure B.3 shows the cumulative distribution frequency (CDF) of 10-min averaged CH_4 mole fraction at 1 m above ground for the four experiments, respectively. The CH_4 mole fraction within the lowest 25% quantile was approximately constant, which was used to calculate the local background CH_4 mole fraction for each experiment (Exp1–4) at the experimental site.

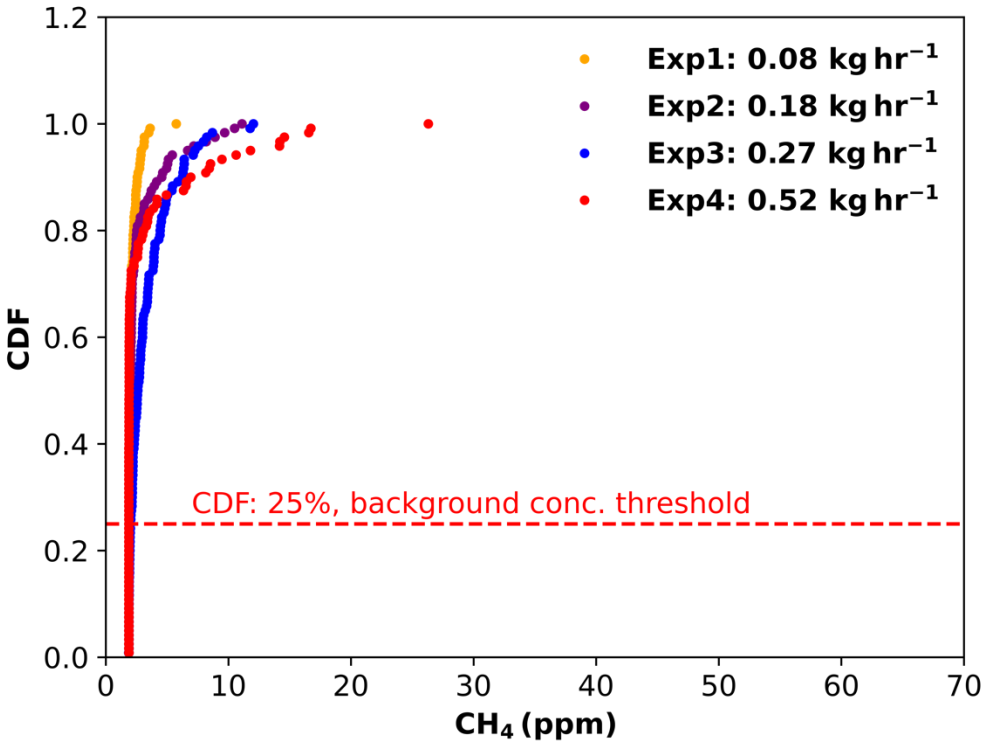

Figure B.3 Cumulative distribution frequency (CDF) of 10-min averaged CH4 mole fraction at 1 m above ground for all experiments (Exp1–4).

Figure B.4 shows the normalized mole fraction with the crosswind distance in the Pasquill-Gifford (PG) stability class A (extremely unstable) and E–F (stable), respectively. Two periods of approximately two hours of constant wind direction (June 1st 1: 00 PM-3:20 PM, June 5th 6: 40 AM-8:00 AM, 2020) were chosen here to illustrate the characteristics of the plume (width and magnitude) under extremely unstable, and stable conditions. The data time interval was 1 min. We first calculated the average CH_4 mole fraction binned by four-degree interval of wind direction for each period. Then, the crosswind distance Y (Foster-Wittig et al., 2015) was calculated by

$$y = s \cdot sin\,(\theta_m - \theta_c) \tag{B.8}$$

where s is the measured distance from the leak center to the downwind measurement location, θ_m is the wind direction at the actual measurement time, θ_c is the wind direction at the plume centerline. The effective downwind region is within $\pm 90^{\circ}$of θ_c ($|\theta_m - \theta_c| \leq 90^{\circ}$).

The results showed a narrow plume with a larger maximum of normalized CH_4 mole fraction in PG stability class E–F (stable) but a broader one with a lower maximum of normalized CH_4 mole fraction in PG stability class A (very unstable). The maximum CH_4 mole fraction was about 65 s m^{-3}, and the plume width was 12 m PG stability class E–F. However, it was about 27 s m^{-3} and 16 m wide in unstable conditions in PG stability class A.

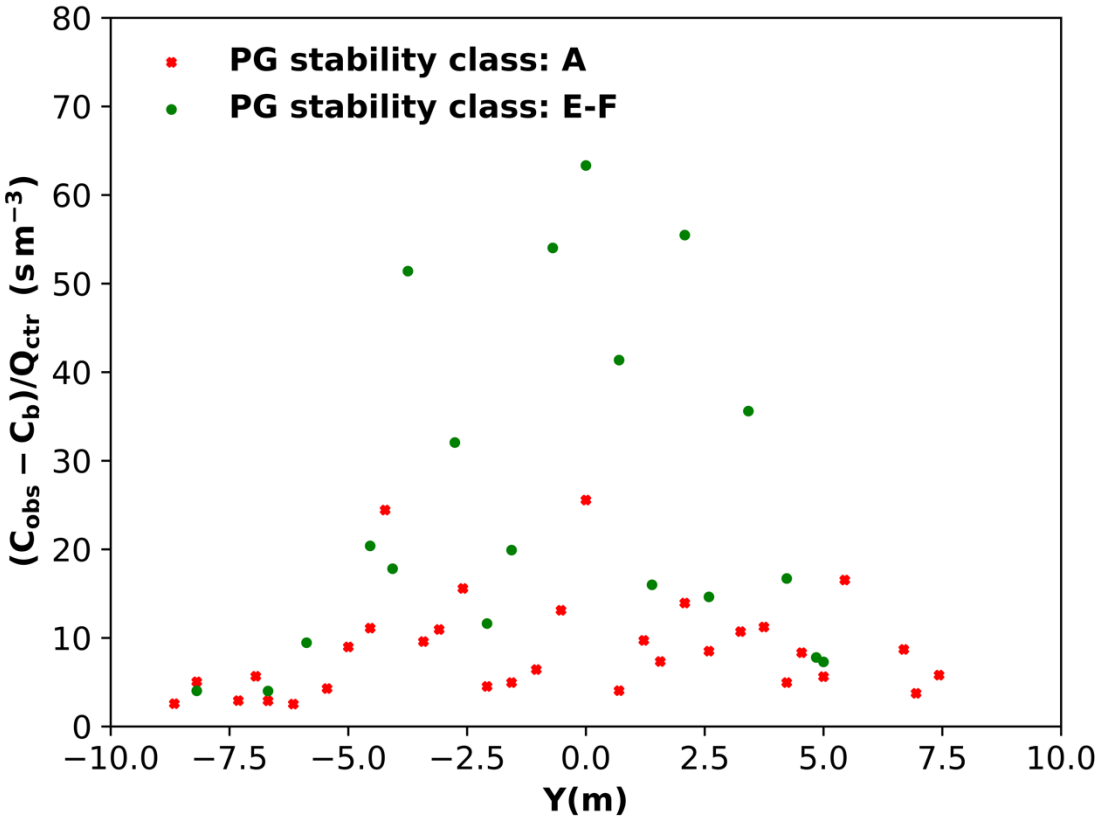

Figure B.4 The normalized CH_4 mole fraction ($(C_{obs}-C_b)/Q_{ctr}$) and crosswind distance (Y) in the Pasquill-Gifford (PG) stability class A (extremely unstable) and E–F (stable), respectively. C_b is the background CH_4 mole fraction (ppm), C_{obs} is the measured CH_4 mole fraction (ppm), Q_{ctr} is the release rate (kg hr^{-1}).

Appendix C Numerical Modeling of Atmospheric Methane Plume

C.1 Equations solved in the CFD Dispersion Model

The CFD dispersion model used here is OpenFOAM v2006, a free and open-source CFD software package. This model has been applied to simulate the dispersions of various gases such as SF_6, CO_2, CH_4, and LNG (liquefied natural gas) vapor in the near surface of the atmosphere (Fiates et al. 2016; Fiates and Vianna 2016; Mack and Spruijt 2013, 2014; Tran et al., 2020; Wang et al., 2016b). The standard solver buoyantBoussinesqSimpleFoam in this model was modified to include the passive scalar (CH_4) turbulent transport in the atmosphere. This newly modified solver was then used to solve the incompressible Reynolds-averaged Navier-Stokes (RANS) equations with the standard $k-\epsilon$ turbulence model (Launder and Spalding 1974) using the SIMPLE algorithm (Ferziger et al., 2002). The equations therein include the continuity equation, momentum equation, temperature equation, the passive scalar transport equation, and turbulent closure equations (Eqs.C.1-C.8).

The continuity equation

$$\frac{\partial u_j}{\partial x_j} = 0 \tag{C.1}$$

The momentum equation

$$\frac{\partial u_j}{\partial t} + \frac{\partial}{\partial x_j}(u_j u_i) - \frac{\partial}{\partial x_j}\left[\nu_{eff}\left(\frac{\partial u_i}{\partial x_j} + \frac{\partial u_j}{\partial x_i}\right)\right] = -\frac{\partial p^*}{\partial x_i} + g_i[1-\beta(T-T_0)] \tag{C.2}$$

The temperature equation

$$\frac{\partial T}{\partial t} + \frac{\partial}{\partial x_j}(u_j T) - \frac{\partial}{\partial x_k}\left(K_{eff}\frac{\partial T}{\partial x_k}\right) = 0 \tag{C.3}$$

The passive scalar transport equation

$$\frac{\partial C}{\partial t} + \frac{\partial}{\partial x_j}(u_j C) - \nu_t \frac{\partial^2 C}{\partial x_k^2} = S \quad \text{(C.4)}$$

where u_i is the ith velocity component (m s^{-1}), T is the temperature (K), C is the concentration of CH_4 (kg m^{-3}), S is the surface emission source (kg $m^{-3}s^{-1}$), ν_{eff} is the effective kinematic viscosity (m^2 s^{-1}), p^* is a modified mean kinematic pressure (Pa), T_0 is the reference temperature (K), β is the coefficient of expansion with temperature of the fluid (K^{-1}), K_{eff} is the heat transfer coefficient (m^2 $K^{-1}s^{-1}$).

$$\nu_{eff} = \nu_0 + \nu_t \quad \text{(C.5)}$$

where ν_0 is the molecular viscosity (m^2 s^{-1}), ν_t is the turbulent viscosity (m^2 s^{-1}).

The standard $k - \epsilon$ model is given by

$$\frac{\partial k}{\partial t} + \frac{\partial k u_j}{\partial x_j} = \frac{\partial}{\partial x_j}\left[\left(\nu + \frac{\nu_t}{\sigma_k}\right)\frac{\partial k}{\partial x_j}\right] + G - \epsilon \quad \text{(C.6)}$$

$$\frac{\partial \epsilon}{\partial t} + \frac{\partial \epsilon u_j}{\partial x_j} = \frac{\partial}{\partial x_j}\left[\left(\nu + \frac{\nu_t}{\sigma_\epsilon}\right)\frac{\partial \epsilon}{\partial x_j}\right] + \frac{c_1 \epsilon}{k} G - c_2 \frac{\epsilon^2}{k} \quad \text{(C.7)}$$

where k is the turbulent kinematic energy (m^2 s^{-2}), ϵ is the turbulent dissipation energy (m^2 s^{-3}), σ_k, σ_ϵ, c_1, c_2 are empirical constants. G is the production of kinematic energy (m^2 s^{-3}), expressed as

$$G = \nu_t \left(\frac{\partial u_i}{\partial x_j} + \frac{\partial u_j}{\partial x_i}\right)\frac{\partial u_i}{\partial x_j} \quad \text{(C.8)}$$

C.2 Preliminary Numerical Modeling Results

The uncoupled modeling was used to test if the OpenFOAM can simulate the impacts of atmospheric stability on the observed gas plume behaviors using a constant surface area emission rate (Table C.1). The numerical experiments consist of 6 stability classes, and the model domain is 100*50* 50 (unit: m), with a grid resolution of 0.5 m, the time step is 1 second, and the total

simulation length is 27.78 hr (Figure C.1). Taking the model results from two stability classes (unstable, slightly unstable) as an example, it shows that the CH_4 mole fraction is higher in the slightly unstable condition than that in unstable conditions under the condition of the same surface emission rate (Figure C.2). Therefore, it initially demonstrates that OpenFOAM can simulate the gas transport and dispersion processes in the atmosphere.

Table C.1 The design schemes for uncoupled numerical dispersion experiments. It includes the modeling under different atmospheric stabilities from the most unstable (PG A) to the most stable (PG F) with constant surface CH_4 emission conditions.

Ref	**CFD dispersion model**	**Subsurface model**	**PG stability**	**Source conditions of CH_4 emission**
Uncoupled modeling	✓	×	A-F	Surface release with a constant rate

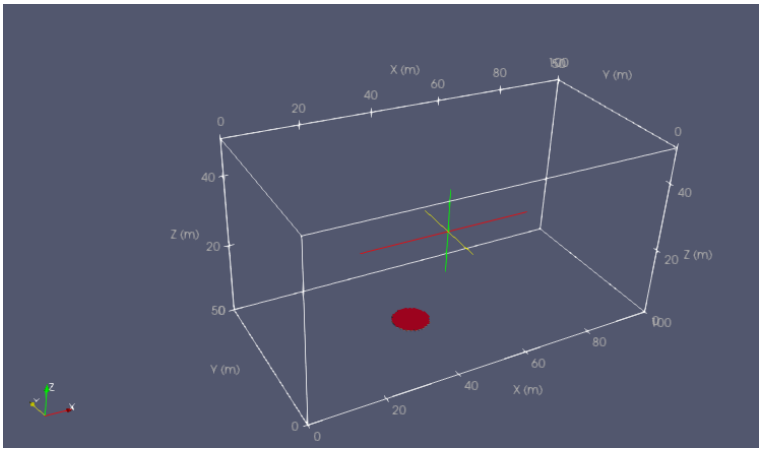

Figure C.1 Model domain (L: 100 m, W: 50 m, H: 50 m) for the CFD modeling. The red shaded circle at the bottom is the leak surface area. The crossline (red, green) shows the center of the model domain.

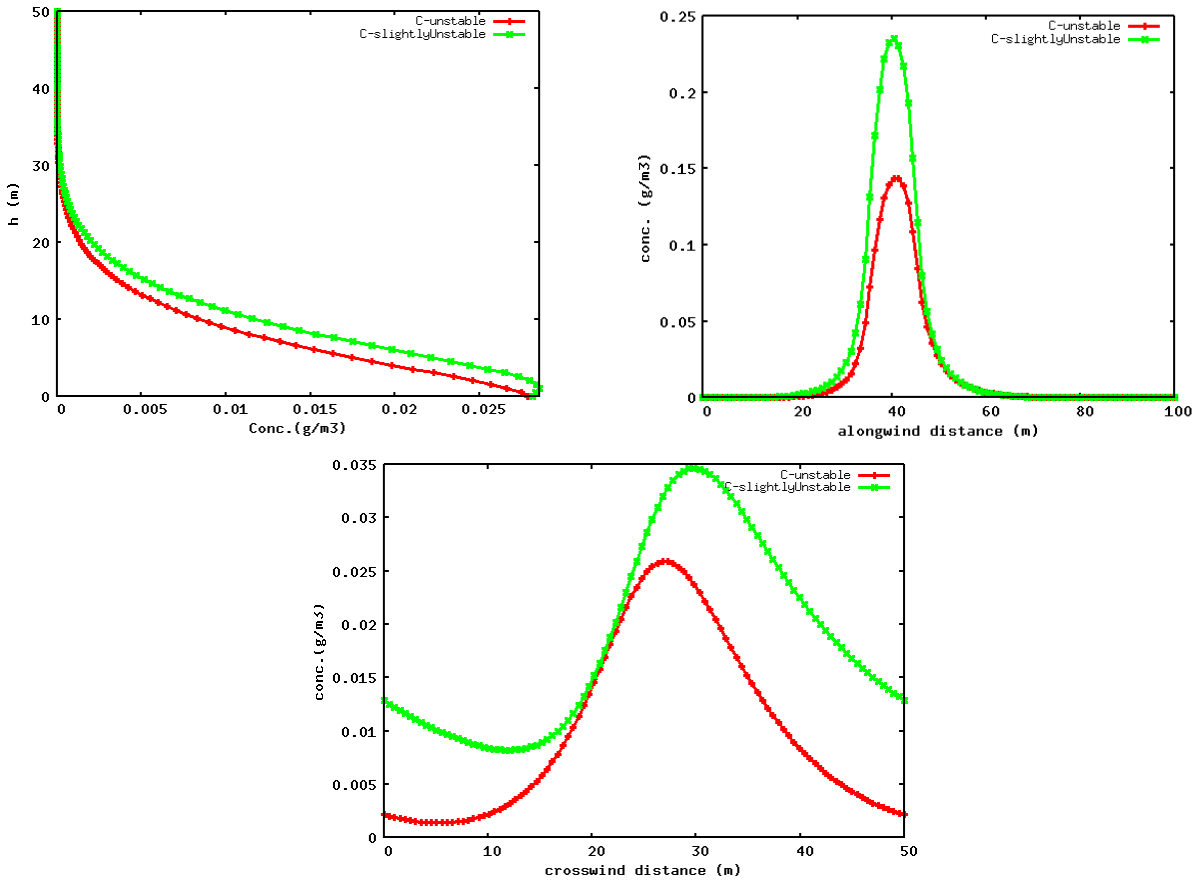

Figure C.2 The modeled CH_4 mole fraction profiles at two stability conditions (unstable: red dot; slightly unstable: green dot) with the same surface emission rate. Top left: vertical profile at the center of the model domain. Top right: along with the distance at the height of 2 m. Bottom center: along with the crosswind distance at the height of 2 m.

Appendix D Copyright Permission

Copyright permission for chapter three:

"Use and share their works for scholarly purposes (with full acknowledgment of the original article): Include in a thesis or dissertation (provided this is not published commercially)"

Elsevier, the publisher of Environmental Pollution, 2022

Copyright permission for chapter four:

"This is an open-access article distributed under the terms of the Creative Commons Attribution 4.0 International License (CC-BY 4.0), which permits unrestricted use, distribution, and reproduction in any medium, provided the original author and source are credited."

University of California Press, the publisher of Elementa: Science of the Anthropocene, 2022

Appendix E Coauthor Release Forms

Multiple Author Release for Master's Thesis or Doctoral Dissertation

Thesis / Dissertation Writer Name: Shanru Tian

Co-Author Name: Kathleen M. Smits

Title(s) of Co-Authored Work(s):

Investigating Detection Probability of Mobile Survey Solutions for Natural Gas Pipeline Leaks Under Different Atmospheric Conditions

Estimating Methane Emissions from Underground Natural Gas Pipelines Using an Atmospheric Dispersion-Based Method

Improving The Efficacy of Leak Detection and Quantification Survey Methods Using 3D Plume Measurements

Co-Author Statement of Consent:

As the co-author of the above named work(s), I acknowledge the above-named thesis / dissertation writer as the primary author of the work(s) listed above. I authorize the thesis / dissertation writer named above to use the listed work(s) in their thesis / dissertation. I further agree that the thesis / dissertation writer may use this work to comply with requirements for graduation.

Co-Author Signature: Kathleen Smits Digitally signed by Kathleen Smits Date: 2022.10.25 13:11:55 -05'00'

Date: 10/25/2022

Please maintain a copy of this completed form for your records.

You may be entitled to know what information The University of Texas at Arlington (UT Arlington) collects concerning you. You may review and have UT Arlington correct this information according to procedures set forth in UTS 139. The law is found in sections 552.021, 552.023 and 559.004 of the Texas Government Code.

UNIVERSITY OF TEXAS ARLINGTON | OFFICE OF GRADUATE STUDIES

Multiple Author Release for Master's Thesis or Doctoral Dissertation

Thesis / Dissertation Writer Name: Shanru Tian

Co-Author Name: Stuart N. Riddick

Title(s) of Co-Authored Work(s):

Investigating Detection Probability of Mobile Su

Estimating Methane Emissions from Undergrou

Improving The Efficacy of Leak Detection and

Co-Author Statement of Consent:

As the co-author of the above named work(s), I acknowledge the above-named thesis / dissertation writer as the primary author of the work(s) listed above. I authorize the thesis / dissertation writer named above to use the listed work(s) in their thesis / dissertation. I further agree that the thesis / dissertation writer may use this work to comply with requirements for graduation.

Co-Author Signature: 

Date: 24th October 2022

Please maintain a copy of this completed form for your records.

You may be entitled to know what information The University of Texas at Arlington (UT Arlington) collects concerning you. You may review and have UT Arlington correct this information according to procedures set forth in UTS 139. The law is found in sections 552.021, 552.023 and 559.004 of the Texas Government Code.

UNIVERSITY OF TEXAS ARLINGTON | OFFICE OF GRADUATE STUDIES

Multiple Author Release for Master's Thesis or Doctoral Dissertation

Thesis / Dissertation Writer Name: Shanru Tian

Co-Author Name: Younki Cho

Title(s) of Co-Authored Work(s):

Investigating Detection Probability of Mobile Survey Solutions for Natural Gas Pipeline Leaks Under Different Atmospheric Conditions

Estimating Methane Emissions from Underground Natural Gas Pipelines Using an Atmospheric Dispersion-Based Method

Improving The Efficacy of Leak Detection and Quantification Survey Methods Using 3D Plume Measurements

Co-Author Statement of Consent:

As the co-author of the above named work(s), I acknowledge the above-named thesis / dissertation writer as the primary author of the work(s) listed above. I authorize the thesis / dissertation writer named above to use the listed work(s) in their thesis / dissertation. I furth agree that the thesis / dissertation writer may use this work to comply with requirements for graduation.

Co-Author Signature: Younki Cho

Date: 10/24/2022

Please maintain a copy of this completed form for your records.

You may be entitled to know what information The University of Texas at Arlington (UT Arlington) collects concerning you. You may review and have UT Arlington correct this information according to procedures set forth in UTS 139. The law is found in sections 552.021, 552.023 and 559.004 of the Texas Government Code.

UNIVERSITY OF TEXAS ARLINGTON | OFFICE OF GRADUATE STUDIES

Multiple Author Release for Master's Thesis or Doctoral Dissertation

Thesis / Dissertation Writer Name: Shanru Tian

Co-Author Name: Daniel J. Zimmerle

Title(s) of Co-Authored Work(s):

Investigating Detection Probability of Mobile Survey Solutions for Natural Gas Pipeline Leaks Under Different Atmospheric Conditions

Estimating Methane Emissions from Underground Natural Gas Pipelines Using an Atmospheric Dispersion-Based Method

Improving The Efficacy of Leak Detection and Quantification Survey Methods Using 3D Plume Measurements

Co-Author Statement of Consent:

As the co-author of the above named work(s), I acknowledge the above-named thesis / dissertation writer as the primary author of the work(s) listed above. I authorize the thesis / dissertation writer named above to use the listed work(s) in their thesis / dissertation. I further agree that the thesis / dissertation writer may use this work to comply with requirements for graduation.

Co-Author Signature: Daniel Zimmerle Digitally signed by Daniel Zimmerle Date: 2022.11.01 07:54:39 -06'00'

Date:

Please maintain a copy of this completed form for your records.

You may be entitled to know what information The University of Texas at Arlington (UT Arlington) collects concerning you. You may review and have UT Arlington correct this information according to procedures set forth in UTS 139. The law is found in sections 552.021, 552.023 and 559.004 of the Texas Government Code.

UNIVERSITY OF TEXAS ARLINGTON | OFFICE OF GRADUATE STUDIES

Multiple Author Release for Master's Thesis or Doctoral Dissertation

Thesis / Dissertation Writer Name: Shanru Tian

Co-Author Name: Aiddan Duggan

Title(s) of Co-Authored Work(s):

Estimating Methane Emissions from Underground Natural Gas Pipelines Using an Atmospheric Dispersion-Based Method

Co-Author Statement of Consent:

As the co-author of the above named work(s), I acknowledge the above-named thesis / dissertation writer as the primary author of the work(s) listed above. I authorize the thesis / dissertation writer named above to use the listed work(s) in their thesis / dissertation. I further agree that the thesis / dissertation writer may use this work to comply with requirements for graduation.

Co-Author Signature: Aidan Duggan Digitally signed by Aidan Duggan Date: 2022.11.02 11:19:08 -06'00'

Date: 11/2/2022

Please maintain a copy of this completed form for your records.

You may be entitled to know what information The University of Texas at Arlington (UT Arlington) collects concerning you. You may review and have UT Arlington correct this information according to procedures set forth in UTS 139. The law is found in sections 552.021, 552.023 and 559.004 of the Texas Government Code.

UNIVERSITY OF TEXAS ARLINGTON | OFFICE OF GRADUATE STUDIES

Multiple Author Release for Master's Thesis or Doctoral Dissertation

Thesis / Dissertation Writer Name: Shanru Tian

Co-Author Name: Clay S. Bell

Title(s) of Co-Authored Work(s):

Investigating Detection Probability of Mobile Survey Solutions for Natural Gas Pipeline Leaks Under Different Atmospheric Conditions

Co-Author Statement of Consent:

As the co-author of the above named work(s), I acknowledge the above-named thesis / dissertation writer as the primary author of the work(s) listed above. I authorize the thesis / dissertation writer named above to use the listed work(s) in their thesis / dissertation. I further agree that the thesis / dissertation writer may use this work to comply with requirements for graduation.

Co-Author Signature: Clay Bell

Date: 11/1/2022

Please maintain a copy of this completed form for your records.

You may be entitled to know what information The University of Texas at Arlington (UT Arlington) collects concerning you. You may review and have UT Arlington correct this information according to procedures set forth in UTS 139. The law is found in sections 552.021, 552.023 and 559.004 of the Texas Government Code.

UNIVERSITY OF TEXAS ARLINGTON | OFFICE OF GRADUATE STUDIES

Multiple Author Release for Master's Thesis or Doctoral Dissertation

Thesis / Dissertation Writer Name: Shanru Tian

Co-Author Name: Mercy Mbua

Title(s) of Co-Authored Work(s):

Improving The Efficacy of Leak Detection and Quantification Survey Methods Using 3D Plume Measurements

Co-Author Statement of Consent:

As the co-author of the above named work(s), I acknowledge the above-named thesis / dissertation writer as the primary author of the work(s) listed above. I authorize the thesis / dissertation writer named above to use the listed work(s) in their thesis / dissertation. I further agree that the thesis / dissertation writer may use this work to comply with requirements for graduation.

Co-Author Signature: Mercy Mbua Digitally signed by Mercy Mbua Date: 2022.10.24 08:38:17 -06'00'

Date: 10/24/2022

Please maintain a copy of this completed form for your records.

You may be entitled to know what information The University of Texas at Arlington (UT Arlington) collects concerning you. You may review and have UT Arlington correct this information according to procedures set forth in UTS 139. The law is found in sections 552.021, 552.023 and 559.004 of the Texas Government Code.

UNIVERSITY OF TEXAS ARLINGTON | OFFICE OF GRADUATE STUDIES

Multiple Author Release for Master's Thesis or Doctoral Dissertation

Thesis / Dissertation Writer Name: Shanru Tian

Co-Author Name: Fancy Cheptonui

Title(s) of Co-Authored Work(s):

Improving The Efficacy of Leak Detection and Quantification Survey Methods Using 3D Plume Measurements

Co-Author Statement of Consent:

As the co-author of the above named work(s), I acknowledge the above-named thesis / dissertation writer as the primary author of the work(s) listed above. I authorize the thesis / dissertation writer named above to use the listed work(s) in their thesis / dissertation. I further agree that the thesis / dissertation writer may use this work to comply with requirements for graduation.

Co-Author Signature: 

Date: 10/30/2022

Please maintain a copy of this completed form for your records.

You may be entitled to know what information The University of Texas at Arlington (UT Arlington) collects concerning you. You may review and have UT Arlington correct this information according to procedures set forth in UTS 139. The law is found in sections 552.021, 552.023 and 559.004 of the Texas Government Code.

UNIVERSITY OF TEXAS ARLINGTON | OFFICE OF GRADUATE STUDIES

Multiple Author Release for Master's Thesis or Doctoral Dissertation

Thesis / Dissertation Writer Name: Shanru Tian

Co-Author Name: Navodi Jayarathne J R R

Title(s) of Co-Authored Work(s):

Improving The Efficacy of Leak Detection and Quantification Survey Methods Using 3D Plume Measurements

Co-Author Statement of Consent:

As the co-author of the above named work(s), I acknowledge the above-named thesis / dissertation writer as the primary author of the work(s) listed above. I authorize the thesis / dissertation writer named above to use the listed work(s) in their thesis / dissertation. I further agree that the thesis / dissertation writer may use this work to comply with requirements for graduation.

Co-Author Signature: 

Date: 24 - October - 2022

Please maintain a copy of this completed form for your records.

You may be entitled to know what information The University of Texas at Arlington (UT Arlington) collects concerning you. You may review and have UT Arlington correct this information according to procedures set forth in UTS 139. The law is found in sections 552.021, 552.023 and 559.004 of the Texas Government Code.

References

Abohamzeh, E, Salehi, F, Sheikholeslami, M, Abbassi, R, Khan, F. 2021. Review of hydrogen safety during storage, transmission, and applications processes. *J Loss Prev Process Ind* **72**(May): 104569. doi: 10.1016/j.jlp.2021.104569

Albertson, JD, Harvey, T, Foderaro, G, Zhu, P, Zhou, X, Ferrari, S, Amin, MS, Modrak, M, Brantley, H, Thoma, ED. 2016. A mobile sensing approach for regional surveillance of fugitive methane emissions in oil and gas production. *Environ Sci Technol* **50**(5): 2487–2497. doi: 10.1021/acs.est.5b05059

Alvarez, RA, Pacala, SW, Winebrake, JJ, Chameides, WL, Hamburg, SP. 2012. Greater focus needed on methane leakage from natural gas infrastructure. *Proc Natl Acad Sci U S A* **109**(17): 6435–6440. doi: 10.1073/pnas.1202407109

Alvarez, RA, Zavala-Araiza, D, Lyon, DR, Allen, DT, Barkley, ZR, Brandt, AR, Davis, KJ, Herndon, SC, Jacob, DJ, Karion, A, Kort, EA, Lamb, BK, Lauvaux, T, Maasakkers, JD, Marchese, AJ, Omara, M, Pacala, SW, Peischl, J, Robinson, AL, et al. 2018. Assessment of methane emissions from the U.S. oil and gas supply chain. *Science* **361**(6398): 186–188. doi: 10.1126/science.aar7204

Arya, PS. 2001. Introduction to Micrometeorology. Elsevier.

Askariyeh, MH, Kota, SH, Vallamsundar, S, Zietsman, J, Ying, Q. 2017. AERMOD for near-road pollutant dispersion: Evaluation of model performance with different emission source representations and low wind options. *Transp Res Part D Transp Environ* **57**(October): 392–402. doi: 10.1016/j.trd.2017.10.008

Assou, M, Saadeddine, S. 2018. Effect of the relative humidity on an industrial plume behavior. *Glob NEST J* **8**(3): 297–305. doi: 10.30955/gnj.000294

Barchyn, TE, Hugenholtz, CH, Fox, TA. 2019. Plume detection modeling of a drone-based natural gas leak detection system. *Elem Sci Anthr* **7**. doi: 10.1525/elementa.379

Bardal, LM, Onstad, AE, Sætran, LR, Lund, JA. 2018. Evaluation of methods for estimating atmospheric stability at two coastal sites. *Wind Eng* **42**(6): 561–575. doi: 10.1177/0309524X18780378

Barkley, ZR, Lauvaux, T, Davis, KJ, Deng, A, Miles, NL, Richardson, SJ, Cao, Y, Sweeney, C, Karion, A, Smith, M, Kort, EA, Schwietzke, S, Murphy, T, Cervone, G, Martins, D, Maasakkers, JD. 2017. Quantifying methane emissions from natural gas production in north-eastern Pennsylvania. *Atmos Chem Phys* **17**(22): 13941–13966. doi: 10.5194/acp-17-13941-2017

Bell, CS, Vaughn, T, Zimmerle, DJ. 2020. Evaluation of next generation emission measurement technologies under repeatable test protocols. *Elem Sci Anthr* **8**. doi: 10.1525/elementa.426

Bonifacio, HF, Maghirang, RG, Razote, EB, Trabue, SL, Prueger, JH. 2013. Comparison of AERMOD and WindTrax dispersion models in determining PM10 emission rates from a beef cattle feedlot. *J Air Waste Manag Assoc* **63**(5): 545–556. doi: 10.1080/10962247.2013.768311

Bosveld, FC, Beljaars, ACM. 2001. The impact of sampling rate on eddy-covariance flux estimates. *Agric For Meteorol* **109**(1): 39–45. doi: 10.1016/S0168-1923(01)00257-X

Brandt, AR, Heath, GA, Cooley, D. 2016. Methane leaks from natural gas systems follow extreme distributions. *Environ Sci Technol* **50**(22): 12512–12520. doi: 10.1021/acs.est.6b04303

Brandt, AR, Heath, GA, Kort, EA, O'Sullivan, F, Pétron, G, Jordaan, SM, Tans, P, Wilcox, J, Gopstein, AM, Arent, D, Wofsy, S, Brown, NJ, Bradley, R, Stucky, GD, Eardley, D,

Harriss, R. 2014. Methane leaks from North American natural gas systems. *Science* **343**(6172): 733–735. doi: 10.1126/science.1247045

Brantley, HL, Thoma, ED, Squier, WC, Guven, BB, Lyon, D. 2014. Assessment of methane emissions from oil and gas production pads using mobile measurements. *Environ Sci Technol* **48**(24): 14508–14515. doi: 10.1021/es503070q

Breedt, HJ, Craig, KJ, Jothiprakasam, VD. 2018. Monin-Obukhov similarity theory and its application to wind flow modelling over complex terrain. *J Wind Eng Ind Aerodyn* **182**: 308–321. doi: 10.1016/j.jweia.2018.09.026

Campbell, LM, Campbell, MV, Epperson, D. 1996. Methane emissions from the natural gas industry volume 9: underground pipelines. U.S. Environmental Protection Agency, Washington, D.C., EPA/600/R-96/080i (NTIS PB97-143002). Available at https://cfpub.epa.gov/si/si_public_record_report.cfm?Lab=NRMRL&dirEntryId=115618. Accessed 2022 Feb 5.

Carpenter, SB, Montgomery, TL, Leavitt, JM, Colbaugh, WC, Thomas, FW. 1971. Principal plume dispersion models: TVA power plants. *J Air Pollut Control Assoc* **21**(8): 491–495. doi: 10.1080/00022470.1971.10469560

Caulton, DR, Li, Q, Bou-Zeid, E, Fitts, JP, Golston, LM, Pan, D, Lu, J, Lane, HM, Buchholz, B, Guo, X, McSpiritt, J, Wendt, L, Zondlo, MA. 2018. Quantifying uncertainties from mobile-laboratory-derived emissions of well pads using inverse Gaussian methods. *Atmos Chem Phys* **18**(20): 15145–15168. doi: 10.5194/acp-18-15145-2018

Chamindu Deepagoda, TKK, Smits, KM, Oldenburg, CM. 2016. Effect of subsurface soil moisture variability and atmospheric conditions on methane gas migration in shallow subsurface. *Int J Greenh Gas Control* **55**: 105–117. doi: 10.1016/j.ijggc.2016.10.016

Chen, J, Dietrich, F, Maazallahi, H, Forstmaier, A, Winkler, D, Hofmann, MEG, Van Der Gon, HD, Röckmann, T. 2020. Methane emissions from the Munich Oktoberfest. *Atmos Chem Phys* **20**(6): 3683–3696. doi: 10.5194/acp-20-3683-2020

Cho, Y, Smits, KM, Riddick, SN, Zimmerle, DJ. 2022. Calibration and field deployment of low-cost sensor network to monitor underground pipeline leakage. *Sensors Actuators B Chem* **355**: 131276. doi: 10.1016/j.snb.2021.131276

Cho, Y, Ulrich, BA, Zimmerle, DJ, Smits, KM. 2020. Estimating natural gas emissions from underground pipelines using surface concentration measurements☆. *Environ Pollut* **267**: 115514. doi: 10.1016/j.envpol.2020.115514

Choi, W, Winer, AM, Paulson, SE. 2014. Factors controlling pollutant plume length downwind of major roadways in nocturnal surface inversions. *Atmos Chem Phys* **14**(13): 6925–6940. doi: 10.5194/acp-14-6925-2014

Clark, T, Conley, E, Kerans, M, Piazza, M. 2012. Picarro surveyor leak detection study: Diablo side-by-side study; Internal Study Report, Pacific Gas and Electric.

Crenna, B. 2020. An introduction to WindTrax. Available at http://www.thunderbeachscientific.com. Accessed 2022 May 2.

Crowl, DA, Jo, Y Do. 2007. The hazards and risks of hydrogen. *J Loss Prev Process Ind* **20**(2): 158–164. doi: 10.1016/j.jlp.2007.02.002

Csanady, GT. 1973. Effects of density differences on environmental diffusion. In turbulent diffusion in the environment. Springer, Dordrecht.

Czepiel, PM, Shorter, JH, Mosher, B, Allwine, E, McManus, JB, Harriss, RC, Kolb, CE, Lamb, BK. 2003. The influence of atmospheric pressure on landfill methane emissions. *Waste Manag* **23**(7): 593–598. doi: 10.1016/S0956-053X(03)00103-X

Defratyka, SM, Paris, JD, Yver-Kwok, C, Fernandez, JM, Korben, P, Bousquet, P. 2021. Mapping urban methane sources in Paris, France. *Environ Sci Technol* **55**(13): 8583–8591. doi: 10.1021/acs.est.1c00859

Edie, R, Robertson, AM, Field, RA, Soltis, J, Snare, DA, Zimmerle, D, Bell, CS, Vaughn, TL, Murphy, SM. 2020. Constraining the accuracy of flux estimates using OTM 33A. *Atmos Meas Tech* **13**(1): 341–353. doi: 10.5194/amt-13-341-2020

Elaoud, S, Hadj-Taïeb, L, Hadj-Taïeb, E. 2010. Leak detection of hydrogen-natural gas mixtures in pipes using the characteristics method of specified time intervals. *J Loss Prev Process Ind* **23**(5): 637–645. Elsevier Ltd. doi: 10.1016/j.jlp.2010.06.015

Fiore, AM, West, JJ, Horowitz, LW, Naik, V, Schwarzkopf, MD. 2008. Characterizing the tropospheric ozone response to methane emission controls and the benefits to climate and air quality. *J Geophys Res Atmos* **113**(8): 1–16. doi: 10.1029/2007JD009162

Von Fischer, JC, Cooley, D, Chamberlain, S, Gaylord, A, Griebenow, CJ, Hamburg, SP, Salo, J, Schumacher, R, Theobald, D, Ham, J. 2017. Rapid, vehicle-based identification of location and magnitude of urban natural gas pipeline leaks. *Environ Sci Technol* **51**(7): 4091–4099. doi: 10.1021/acs.est.6b06095

Flesch, TK, Wilson, JD, Yee, E. 1995. Backward-time lagrangian stochastic dispersion models and their application to estimate gaseous emissions. *J Appl Meteorol Climatol* **34**(6): 1320–1332. doi: 10.1175/1520-0450(1995)034<1320:BTLSDM>2.0.CO;2

Flesch, TK, Wilson, JD, Harper, LA, Crenna, BP, Sharpe, RR. 2004. Deducing ground-to-air emissions from observed trace gas concentrations: A field trial. *J Appl Meteorol* **43**(3): 487–502. doi: 10.1175/1520-0450(2004)043<0487:DGEFOT>2.0.CO;2

FlyARH. 2021. Airborne pipeline patrol & inspection services. Available at

https://www.flyarh.com/airborne-pipeline-inspection-services.html. Accessed 2021 Nov 17.

Foken, T. 2006. 50 years of the Monin-Obukhov similarity theory. *Boundary-Layer Meteorol* **119**(3): 431–447. doi: 10.1007/s10546-006-9048-6

Forde, ON, Cahill, AG, Beckie, RD, Mayer, KU. 2019. Barometric-pumping controls fugitive gas emissions from a vadose zone natural gas release. *Sci Rep* **9**(1): 1–9. doi: 10.1038/s41598-019-50426-3

Foster-Wittig, TA, Thoma, ED, Albertson, JD. 2015. Estimation of point source fugitive emission rates from a single sensor time series: A conditionally-sampled Gaussian plume reconstruction. *Atmos Environ* **115**: 101–109. doi: 10.1016/j.atmosenv.2015.05.042

Fox, TA, Barchyn, TE, Risk, D, Ravikumar, AP, Hugenholtz, CH. 2019. Erratum: A review of close-range and screening technologies for mitigating fugitive methane emissions in upstream oil and gas. *Environ Res Lett* **14**(6). doi: 10.1088/1748-9326/ab20f1

Gallagher, ME, Down, A, Ackley, RC, Zhao, K, Phillips, N, Jackson, RB. 2015. Natural gas pipeline replacement programs reduce methane leaks and improve consumer safety. *Environ Sci Technol Lett* **2**(10): 286–291. doi: 10.1021/acs.estlett.5b00213

Gao, B, Mitton, MK, Bell, C, Zimmerle, D, Deepagoda, TKKC, Hecobian, A, Smits, KM. 2021. Study of methane migration in the shallow subsurface from a gas pipe leak. *Elem Sci Anth* **9**: 1. doi: 10.1525/elementa.2021.00008

Gasbarra, D, Toscano, P, Famulari, D, Finardi, S, Di Tommasi, P, Zaldei, A, Carlucci, P, Magliulo, E, Gioli, B. 2019. Locating and quantifying multiple landfills methane emissions using aircraft data. *Environ Pollut* **254**: 112987. doi: 10.1016/j.envpol.2019.112987

Giannissi, SG, Venetsanos, AG. 2018. Study of key parameters in modeling liquid hydrogen release and dispersion in open environment. *Int J Hydrogen Energy* **43**(1): 455–467. doi:

10.1016/j.ijhydene.2017.10.128

Giannissi, SG, Venetsanos, AG, Markatos, N, Bartzis, JG. 2014. CFD modeling of hydrogen dispersion under cryogenic release conditions. *Int J Hydrogen Energy* **39**(28): 15851–15863. doi: 10.1016/j.ijhydene.2014.07.042

Global Energy Monitor. 2022. Pipe dreams.

Golston, LM, Aubut, NF, Frish, MB, Yang, S, Talbot, RW, Gretencord, C, McSpiritt, J, Zondlo, MA. 2018. Natural gas fugitive leak detection using an unmanned aerial vehicle: Localization and quantification of emission rate. *Atmosphere* **9**(9). doi: 10.3390/atmos9090333

GPTC. 2018. *Guide for gas transmission, distribution, and gathering piping systems*.

Gryning, SE, Batchvarova, E, Brümmer, B, Jørgensen, H, Larsen, S. 2007. On the extension of the wind profile over homogeneous terrain beyond the surface boundary layer. *Boundary-Layer Meteorol* **124**(2): 251–268. doi: 10.1007/s10546-007-9166-9

GTI. 2019. Quantifying methane emissions from distribution pipelines in california. Available at https://ww2.arb.ca.gov/resources/documents/quantifying-methane-emissions-distribution-pipelines-california. Accessed 2022 May 29.

Gutmann, ED, Small, EE. 2005. The effect of soil hydraulic properties vs. soil texture in land surface models. *Geophys Res Lett* **32**(2): 1–4. doi: 10.1029/2004GL021843

Hanna, S. 1986. Lateral dispersion from tall stacks. *J Clim Appl Meteorol*: 1426–1433. doi: 10.1175/1520-0450(1986)025<1426:LDFTS>2.0.CO;2

Hatfield, JL, Baker, JM, Flesch, TK, Wilson, JD. 2005. Estimating tracer emissions with a backward lagrangian stochastic technique. *Micrometeorology in Agricultural Systems* **47**: 513–531. doi: 10.2134/agronmonogr47.c22

Hausamann, D, Zirnig, W, Schreier, G, Strobl, P. 2005. Monitoring of gas pipelines – a civil UAV application. *Aircr Eng Aerosp Technol* **77**(5): 352–360. doi: 10.1108/00022660510617077

Heath Consultants. 2009. RMLD user's mannual. Available at https://heathus.com/products/remote-methane-leak-detector/. Accessed 2022 Apr 23.

Heath, G, Warner, E, Warner, E, Brandt, A. 2015. Estimating U.S. methane emissions from the natural gas supply chain: Approaches, uncertainties, current estimates, and future studies (No. NREL/TP-6A50-62820). National Renewable Energy Lab (NREL), Golden, CO. doi: 10.2172/1226158

Heliops, C. 2022. Boreal laser pipeline surveys. Available at http://www.coloradoheliops.com/helicopter-hire/borealpipelinesurvey/.

Heltzel, RS, Zaki, MT, Gebreslase, AK, Abdul-Aziz, OI, Johnson, DR. 2020. Continuous OTM 33A analysis of controlled releases of methane with various time periods, data rates and wind filters. *Environments* **7**(9): 65. doi: 10.3390/environments7090065

Hendrick, MF, Ackley, R, Sanaie-Movahed, B, Tang, X, Phillips, NG. 2016. Fugitive methane emissions from leak-prone natural gas distribution infrastructure in urban environments. *Environ Pollut* **213**: 710–716. Elsevier Ltd. doi: 10.1016/j.envpol.2016.01.094

Ho, CK, and Webb, SW. 2006. *Gas transport in porous media*. Springer, Dordrecht.

Hockstad, L, Hanel, L. 2018. Inventory of U.S. Greenhouse Gas Emissions and Sinks (No. cdiac: EPA-EMISSIONS). Environmental System Science Data Infrastructure for a Virtual Ecosystem. doi: 10.15485/1464240

Howarth, RW. 2014. A bridge to nowhere: Methane emissions and the greenhouse gas footprint of natural gas. *Energy Sci Eng* **2**(2): 47–60. doi: 10.1002/ese3.35

IPCC. 2014. Anthropogenic and natural radiative forcing. In climate change 2013 – The physical science basis: working group I contribution to the fifth assessment report of the intergovernmental panel on climate change. *Cambridge University Press: 659-740*. doi: 10.1017/CBO9781107415324.018

Jackson, RB, Abernethy, S, Canadell, JG, Cargnello, M, Davis, SJ, Féron, S, Fuss, S, Heyer, AJ, Hong, C, Jones, CD, Damon Matthews, H, O'Connor, FM, Pisciotta, M, Rhoda, HM, De Richter, R, Solomon, EI, Wilcox, JL, Zickfeld, K. 2021. Atmospheric methane removal: A research agenda. *Philos Trans R Soc A Math Phys Eng Sci* **379**(2210). doi: 10.1098/rsta.2020.0454

Jackson, RB, Down, A, Phillips, NG, Ackley, RC, Cook, CW, Plata, DL, Zhao, K. 2014. Natural gas pipeline leaks across Washington, DC. *Environ Sci Technol* **48**(3): 2051–2058. doi: 10.1021/es404474x

Jayarathne, Navodi J.R.R.; Smits, Kathleen M; Riddick, Stuart N.; Zimmerle, Daniel J.; Cho, Younki; Schwartz, Michelle; Cheptonui, Fancy; Cameron, Kevan; Ronney, P. 2022. Understanding mid-to large underground leaks from buried pipelines as affected by soil and atmospheric conditions – Field scale experimental study. Proceedings from the pipeline research council international (PRCI) REX2022 Meeting. Orlando, FL. doi: https://doi.org/10.18738/T8/MRX54H

Jeong, SJ. 2011. CALPUFF and AERMOD dispersion models for estimating odor emissions from industrial complex area sources. *Asian J Atmos Environ* **5**(1): 1–7. doi: 10.5572/ajae.2011.5.1.001

Kaimal, J. C., and JJF. 1994. Atmospheric boundary layer flows: Their structure and measurement. Oxford University Press.

Kerans, M, Clark, T, Conley, E, Crosson, E, Piazza, M. 2012. Picarro surveyor leak detection study: sacramento side-by-side study; Internal Study Report, Pacific Gas and Electric.

Keyes, T, Ridge, G, Klein, M, Phillips, N, Ackley, R, Yang, Y. 2020. An enhanced procedure for urban mobile methane leak detection. *Heliyon* **6**(10): e04876. Elsevier Ltd. doi: 10.1016/j.heliyon.2020.e04876

Kim, H, Yun, S, Han, SH, Son, Y, Kim, S, Ko, D. 2020. Real-time monitoring of carbon dioxide emissions from a shallow carbon dioxide release experiment. *Vadose Zo Journal*, **19**: e20051. doi: 10.1002/vzj2.20051

Kligman, D. 2011. PG&E tests helicopters as tool to detect pipeline gas leaks. Available at https://www.pgecurrents.com/2011/08/12/pge-tests-helicopters-as-tool-to-detect-pipeline-gas-leaks/. Accessed 2021 Nov 14.

Kovač, A, Paranos, M, Marciuš, D. 2021. Hydrogen in energy transition: A review. *Int J Hydrogen Energy* **46**(16): 10016–10035. doi: 10.1016/j.ijhydene.2020.11.256

Ku-Mahamud, KR, Khor, JY. 2009. Pattern extraction and rule generation of forest fire using sliding window technique. *Comput Inf Sci* **2**(3). doi: 10.5539/cis.v2n3p113

Auer, LH, Rosenburg, ND, Birdsell, KH, Whitney, EM. 1996. The effects of barometric pumping on contaminant transport. *Journal of Contaminant Hydrology* **24** (2). doi: 10.1016/S0169-7722(96)00010-1

Lamb, BK, Edburg, SL, Ferrara, TW, Howard, T, Harrison, MR, Kolb, CE, Townsend-Small, A, Dyck, W, Possolo, A, Whetstone, JR. 2015. Direct measurements show decreasing methane emissions from natural gas local distribution systems in the United States. *Environ Sci Technol* **49**(8): 5161–5169. doi: 10.1021/es505116p

Lan, X, Talbot, R, Laine, P, Torres, A. 2015. Characterizing fugitive methane emissions in the

Barnett Shale area using a mobile laboratory. *Environ Sci Technol* **49**(13): 8139–8146. doi: 10.1021/es5063055

LASEN. 2021. Airborne LiDAR pipeline inspection service.

Laubach, J, Kelliher, FM. 2005. Methane emissions from dairy cows: Comparing open-path laser measurements to profile-based techniques. *Agric For Meteorol* **135**(1–4): 340–345. doi: 10.1016/j.agrformet.2005.11.014

Leelőssy, Á, Molnár, F, Izsák, F, Havasi, Á, Lagzi, I, Mészáros, R. 2014. Dispersion modeling of air pollutants in the atmosphere: a review. *Cent Eur J Geosci* **6**(3): 257–278. doi: 10.2478/s13533-012-0188-6

Levi, M. 2013. Climate consequences of natural gas as a bridge fuel. *Clim Change* **118**(3–4): 609–623. doi: 10.1007/s10584-012-0658-3

Li, HZ, Mundia-Howe, M, Reeder, MD, Pekney, NJ. 2020. Gathering pipeline methane emissions in utica shale using an unmanned aerial vehicle and ground-based mobile sampling. *Atmos* **11**(7): 1–13. doi: 10.3390/atmos11070716

Liang, F-Y, Ryvak, M, Sayeed, S, Zhao, N. 2012. The role of natural gas as a primary fuel in the near future, including comparisons of acquisition, transmission and waste handling costs of as with competitive alternatives. *Chem Cent J* **6**(S1): 1–24. doi: 10.1186/1752-153x-6-s1-s4

Liu, Y, Wei, J, Lei, G, Wang, T, Lan, Y, Chen, H, Jin, T. 2019. Modeling the development of hydrogen vapor cloud considering the presence of air humidity. *Int J Hydrogen Energy* **44**(3): 2059–2068. doi: 10.1016/j.ijhydene.2018.11.123

Luetschwager, E, von Fischer, JC, Weller, ZD. 2021. Characterizing detection probabilities of advanced mobile leak surveys: Implications for sampling effort and leak size estimation in natural gas distribution systems. *Elementa* **9**(1): 1–13. doi: 10.1525/elementa.2020.00143

Luketa-Hanlin, A, Koopman, RP, Ermak, DL. 2007. On the application of computational fluid dynamics codes for liquefied natural gas dispersion. *J Hazard Mater* **140**(3): 504–517. doi: 10.1016/j.jhazmat.2006.10.023

Malley, CS, Henze, DK, Kuylenstierna, JCI, Vallack, HW, Davila, Y, Anenberg, SC, Turner, MC, Ashmore, MR. 2017. Updated global estimates of respiratory mortality in adults ≥ 30 years of age attributable to long-term ozone exposure. *Environ Health Perspect* **125**(8): 1–9. doi: 10.1289/EHP1390

Mitton, M. 2018. Subsurface methane migration from natural gas distribution [M.S. thesis]. Golden, CO: Colorado School of Mines, Dept. of Civil and Environmental Engineering. Available at https://repository.mines.edu/bitstream/handle/11124/172530/Mitton_mines_0052N_11576.pdf?sequence=1&isAllowed=y. Accessed 2022 May 2.

Molnarne, M, Schroeder, V. 2019. Hazardous properties of hydrogen and hydrogen containing fuel gases. *Process Saf Environ Prot* **130**: 1–5. doi: 10.1016/j.psep.2019.07.012

Mønster, J, Kjeldsen, P, Scheutz, C. 2019. Methodologies for measuring fugitive methane emissions from landfills – A review. *Waste Manag* **87**: 835–859. doi: 10.1016/j.wasman.2018.12.047

NARUC. 2019. Sampling of methane emissions detection technologies and practices for natural gas distribution infrastructure. Available at https://pubs.naruc.org/pub/0CA39FB4-A38C-C3BF-5B0A-FCD60A7B3098. Accessed 2022 May 2.

Nathan, BJ, Golston, LM, O'Brien, AS, Ross, K, Harrison, WA, Tao, L, Lary, DJ, Johnson, DR, Covington, AN, Clark, NN, Zondlo, MA. 2015. Near-field characterization of methane emission variability from a compressor station using a model aircraft. *Environ Sci Technol*

49(13): 7896–7903. doi: 10.1021/acs.est.5b00705

National Academies of Sciences, EM. 2018. Improving characterization of anthropogenic methane emissions in the United States. The National Academies Press. doi: 10.17226/24987

National Academies of Sciences, EM. 2022. Natural gas. Available at http://needtoknow.nas.edu/energy/energy-sources/fossil-fuels/natural-gas/. Accessed 2022 May 14.

National Development and Reform Commission of China. 2016. Energy production and consumption revolution strategy (2016–2030).

Nisbet, EG, Fisher, RE, Lowry, D, France, JL, Allen, G, Bakkaloglu, S, Broderick, TJ, Cain, M, Coleman, M, Fernandez, J, Forster, G, Griffiths, PT, Iverach, CP, Kelly, BFJ, Manning, MR, Nisbet-Jones, PBR, Pyle, JA, Townsend-Small, A, al-Shalaan, A, et al. 2020. Methane Mitigation: Methods to Reduce Emissions, on the Path to the Paris Agreement. *Rev Geophys* **58**(1): 1–51. doi: 10.1029/2019RG000675

Okamoto, H, Gomi, Y. 2011. Empirical research on diffusion behavior of leaked gas in the ground. *J Loss Prev Process Ind* **24**(5): 531–540. doi: 10.1016/j.jlp.2011.01.007

Ounis, H, Ahmadi, G. 1990. A comparison of brownian and turbulent diffusion. *Aerosol Sci Technol* **13**(1): 47–53. doi: 10.1080/02786829008959423

Pasquill, F. 1961. The estimation of the dispersion of windborne material. *Meteorol Mag* **Vol. 90**: 33–49.

Phillips, NG, Ackley, R, Crosson, ER, Down, A, Hutyra, LR, Brondfield, M, Karr, JD, Zhao, K, Jackson, RB. 2013. Mapping urban pipeline leaks: Methane leaks across Boston. *Environ Pollut* **173**: 1–4. doi: 10.1016/j.envpol.2012.11.003

PHMSA. 2017. Guidance Manual for Operators of Small Natural Gas Systems. Available at

https://www.phmsa.dot.gov/training/pipeline/small-natural-gas-operator-guide-january-2017-pdf. Accessed 2022 May 2.

PHMSA. 2022. Significant incident 20 year trend. Available at https://www.phmsa.dot.gov/data-and-statistics/pipeline/pipeline-incident-20-year-trends. Accessed 2022 Apr 24.

PHMSA. 2018. Pipeline failure causes. Available at https://www.phmsa.dot.gov/incident-reporting/accident-investigation-division/pipeline-failure-causes. Accessed 2022 May 2.

Plant, G, Kort, EA, Floerchinger, C, Gvakharia, A, Vimont, I, Sweeney, C. 2019. Large fugitive methane emissions from urban centers along the U.S. East Coast. *Geophys Res Lett* **46**(14): 8500–8507. doi: 10.1029/2019GL082635

Pontiggia, M, Derudi, M, Busini, V, Rota, R. 2009. Hazardous gas dispersion: A CFD model accounting for atmospheric stability classes. *J Hazard Mater* **171**(1–3): 739–747. doi: 10.1016/j.jhazmat.2009.06.064

Poulsen, TG, Møldrup, P. 2006. Evaluating effects of wind-induced pressure fluctuations on soil-atmosphere gas exchange at a landfill using stochastic modelling. *Waste Manag Res* **24**(5): 473–481. doi: 10.1177/0734242X06066363

Poulsen Tjalfe G., G, Christophersen, M, Moldrup, P, Kjeldsen, P. 2003. Relating landfill gas emissions to atmospheric pressure using numerical modelling and state-space analysis. *Waste Manag Res* **21**(4): 356–366. doi: 10.1177/0734242x0302100408

Ravikumar, AP, Sreedhara, S, Wang, J, Englander, J, Roda-Stuart, D, Bell, C, Zimmerle, D, Lyon, D, Mogstad, I, Ratner, B, Brandt, AR. 2019. Single-blind inter-comparison of methane detection technologies – results from the Stanford/EDF mobile monitoring challenge. *Elem Sci Anthr* **7**. doi: 10.1525/elementa.373

Ravikumar, AP, Wang, J, McGuire, M, Bell, CS, Zimmerle, D, Brandt, AR. 2018. "Good

versus Good Enough?" Empirical tests of methane leak detection sensitivity of a commercial infrared camera. *Environ Sci Technol* **52**(4): 2368–2374. doi: 10.1021/acs.est.7b04945

Rella, CW, Tsai, TR, Botkin, CG, Crosson, ER, Steele, D. 2015. Measuring emissions from oil and natural gas well pads using the mobile flux plane technique. *Environ Sci Technol* **49**(7): 4742–4748. doi: 10.1021/acs.est.5b00099

Riddick, SN, Bell, CS, Duggan, A, Vaughn, TL, Smits, KM, Cho, Y, Bennett, KE, Zimmerle, DJ. 2021. Modeling temporal variability in the surface expression above a methane leak: The ESCAPE model. *J Nat Gas Sci Eng* **96**: 104275. doi: 10.1016/j.jngse.2021.104275

Riddick, SN, Hancock, BR, Robinson, AD, Connors, S, Davies, S, Allen, G, Pitt, J, Harris, NRP. 2018. Development of a low-maintenance measurement approach to continuously estimate methane emissions: A case study. *Waste Manag* **73**: 210–219. doi: 10.1016/j.wasman.2016.12.006

Riddick, SN, Mauzerall, DL, Celia, M, Harris, NRP, Allen, G, Pitt, J, Staunton-Sykes, J, Forster, GL, Kang, M, Lowry, D, Nisbet, EG, Manning, AJ. 2019. Measuring methane emissions from oil and gas platforms in the North Sea. *Atmos Chem Phys Discuss* **19**(15): 9787–9796. doi: 10.5194/acp-2019-90

Riddick, SN, Mauzerall, DL, Celia, MA, Kang, M, Bandilla, K. 2020. Variability observed over time in methane emissions from abandoned oil and gas wells. *Int J Greenh Gas Control* **100**: 103116. doi: 10.1016/j.ijggc.2020.103116

Riddle, A, Carruthers, D, Sharpe, A, McHugh, C, Stocker, J. 2004. Comparisons between FLUENT and ADMS for atmospheric dispersion modelling. *Atmos Environ* **38**(7): 1029–1038. doi: 10.1016/j.atmosenv.2003.10.052

Schivley, G, Azevedo, I, Samaras, C. 2018. Assessing the evolution of power sector carbon

intensity in the United States. *Environ Res Lett* **13**(6). doi: 10.1088/1748-9326/aabe9d

Seigneur, C. 2019. Atmospheric dispersion. In air pollution: Concepts, theory, and applications. Cambridge University Press. doi: 10.1017/9781108674614.006

Shah, A, Allen, G, Pitt, JR, Ricketts, H, Williams, PI, Helmore, J, Finlayson, A, Robinson, R, Kabbabe, K, Hollingsworth, P, Rees-White, TC, Beaven, R, Scheutz, C, Bourn, M. 2019. A near-field Gaussian plume inversion flux quantification method, applied to unmanned aerial vehicle sampling. *Atmosphere* **10**(7). doi: 10.3390/atmos10070396

Shah, A, Pitt, J, Ricketts, H, Leen, JB, Williams, P, Kabbabe, K, Gallagher, M, Allen, G. 2019. Testing the near-field Gaussian plume inversion flux quantification technique using unmanned aerial vehicle sampling. *Atmos Meas Tech Discuss*: 1–23. doi: 10.5194/amt-2019-289

Sherwin, ED, Chen, Y, Ravikumar, AP, Brandt, AR. 2021. Single-blind test of airplane-based hyperspectral methane detection via controlled releases. *Elementa* **9**(1): 1–10. doi: 10.1525/elementa.2021.00063

Shindell, D, Kuylenstierna, JCI, Vignati, E, Van Dingenen, R, Amann, M, Klimont, Z, Anenberg, SC, Muller, N, Janssens-Maenhout, G, Raes, F, Schwartz, J, Faluvegi, G, Pozzoli, L, Kupiainen, K, Höglund-Isaksson, L, Emberson, L, Streets, D, Ramanathan, V, Hicks, K, et al. 2012. Simultaneously mitigating near-term climate change and improving human health and food security. *Science* **335**(6065): 183–189. doi: 10.1126/science.1210026

Smith, KA, Ball, T, Conen, F, Dobbie, KE, Massheder, J, Rey, A. 2018. Exchange of greenhouse gases between soil and atmosphere: interactions of soil physical factors and biological processes. *Eur J Soil Sci* **69**(1): 10–20. doi: 10.1111/ejss.12539

Stull, RB. 2012. An introduction to boundary layer meteorology. Springer Science & Business

Media.

Sun, B, Wong, J, Wadnerkar, D, Utikar, RP, Pareek, VK, Guo, K. 2020. Multiphase simulation of LNG vapour dispersion with effect of fog formation. *Appl Therm Eng* **166**: 114671. doi: 10.1016/j.applthermaleng.2019.114671

The National Academy of Sciences. 2022. Natural Gas.

Thoma, E. and Squier, B. 2014. OTM 33 geospatial measurement of air pollution, remote emissions quantification (GMAP-REQ) and OTM33A geospatial measurement of air pollution-remote emissions quantification-direct assessment (GMAP-REQ-DA). US Environmental Protection Agency, Cincinnati.

Thomas E. Barchyn, Chris H. Hugenholtz, Stephen Myshak, JB. 2017. A UAV-based system for detecting natural gas leaks. *Journal of Unmanned Vehicle Systems* **6** (1). doi: 10.1139/juvs-2017-0018

Thorpe, AK, Frankenberg, C, Aubrey, AD, Roberts, DA, Nottrott, AA, Rahn, TA, Sauer, JA, Dubey, MK, Costigan, KR, Arata, C, Steffke, AM, Hills, S, Haselwimmer, C, Charlesworth, D, Funk, CC, Green, RO, Lundeen, SR, Boardman, JW, Eastwood, ML, et al. 2016. Mapping methane concentrations from a controlled release experiment using the next generation airborne visible/infrared imaging spectrometer (AVIRIS-NG). *Remote Sens Environ* **179**: 104–115. doi: 10.1016/j.rse.2016.03.032

Tian, S, Riddick, SN, Cho, Y, Bell, CS, Zimmerle, DJ, Smits, KM. 2022. Investigating detection probability of mobile survey solutions for natural gas pipeline leaks under different atmospheric conditions ☆. *Environ Pollut* **312**: 120027. doi: 10.1016/j.envpol.2022.120027

Tian, S, Smits, KM, Cho, Y, Riddick, S, Zimmerle, D, Duggan, A. 2022. Estimating methane emissions from underground natural gas pipelines using an atmospheric dispersion-based

method. *Elementa* **10**(1). doi: https://doi.org/10.1525/elementa.2022.00045

U.S. Energy Information Administration. 2020. EIA projects nearly 50% increase in world energy usage by 2050, led by growth in Asia.

U.S. Energy Information Administration. 2021a. Natural gas explained: Natural gas pipelines. Available at https://www.eia.gov/energyexplained/natural-gas/natural-gas-pipelines.php. Accessed 2022 May 2.

U.S. Energy Information Administration. 2021b. The International Energy Outlook.

U.S. Energy Information Administration. 2022. Annual U.S. natural gas production (1940-2020). Available at https://www.eia.gov/todayinenergy/detail.php?id=46956#. Accessed 2022 May 27.

U.S. EPA. 2022. Inventory of U.S. greenhouse gas emissions and sinks: 1990-2020. Available at https://www.epa.gov/ghgemissions/inventory-us-greenhouse-gas-emissions-and-sinks-1990-2020. Accessed 2022 May 27.

Ulrich, BA, Mitton, M, Lachenmeyer, E, Hecobian, A, Zimmerle, D, Smits, KM. 2019. Natural gas emissions from underground pipelines and implications for leak detection. *Environ Sci Technol Lett* **6**(7): 401–406. doi: 10.1021/acs.estlett.9b00291

UNEP&CCAC. 2021. Global methane assessment: Benefits and costs of mitigating methane emissions.

UNFCCC. 2022. The Paris Agreement. Available at https://unfccc.int/process-and-meetings/the-paris-agreement/the-paris-agreement. Accessed 2022 May 2.

Vaughn, TL, Bell, CS, Yacovitch, TI, Roscioli, JR, Herndon, SC, Conley, S, Schwietzke, S, Heath, GA, Pétron, G, Zimmerle, D. 2017. Comparing facility-level methane emission rate estimates at natural gas gathering and boosting stations. *Elementa* **5**. doi:

10.1525/elementa.257

Villa, T, Gonzalez, F, Miljevic, B, Ristovski, ZD, Morawska, L. 2016. An overview of small unmanned aerial vehicles for air quality measurements: Present applications and future prospectives. *Sensors* **16**(7): 12–20. doi: 10.3390/s16071072

WAC. 2019. Leak classification and action criteria. Available at https://apps.leg.wa.gov/WAC/default.aspx?cite=480-93-18601. Accessed 2022 May 2.

Weller, ZD, Hamburg, SP, Von Fischer, JC. 2020. A national estimate of methane leakage from pipeline mains in natural gas local distribution systems. *Environ Sci Technol* **54**(14): 8958–8967. doi: 10.1021/acs.est.0c00437

Weller, ZD, Roscioli, JR, Daube, WC, Lamb, BK, Ferrara, TW, Brewer, PE, Von Fischer, JC. 2018. Vehicle-based methane surveys for finding natural gas leaks and estimating their size: Validation and uncertainty. *Environ Sci Technol* **52**(20): 11922–11930. doi: 10.1021/acs.est.8b03135

Weller, ZD, Yang, DK, Von Fischer, JC. 2019. An open source algorithm to detect natural gas leaks from mobile methane survey data. *PLoS One* **14**(2): 1–18. doi: 10.1371/journal.pone.0212287

Yacovitch, TI, Herndon, SC, Pétron, G, Kofler, J, Lyon, D, Zahniser, MS, Kolb, CE. 2015. Mobile laboratory observations of methane emissions in the barnett shale region. *Environ Sci Technol* **49**(13): 7889–7895. doi: 10.1021/es506352j

Yang, S, Talbot, RW, Frish, MB, Golston, LM, Aubut, NF, Zondlo, MA, Gretencord, C, McSpiritt, J. 2018. Natural gas fugitive leak detection using an unmanned aerial vehicle: Measurement system description and mass balance approach. *Atmosphere* **9**(10). doi: 10.3390/atmos9100383

Yang, W, Zhu, A, Zhang, J, Xin, X, Zhang, X. 2017. Evaluation of a backward Lagrangian stochastic model for determining surface ammonia emissions. *Agric For Meteorol* **234**: 196–202. doi: 10.1016/j.agrformet.2017.01.001

Yu, J, Hmiel, B, Lyon, DR, Warren, J, Cusworth, DH, Duren, RM, Chen, Y, Murphy, EC, Brandt, AR. 2022. Methane emissions from natural gas gathering pipelines in the Permian basin. in press. doi: 10.1021/acs.estlett.2c00380

Zhang, J, Meerman, H, Benders, R, Faaij, A. 2022. Potential role of natural gas infrastructure in China to supply low-carbon gases during 2020–2050. *Appl Energy* **306**. doi: 10.1016/j.apenergy.2021.117989

Zhang, X, Myhrvold, NP, Hausfather, Z, Caldeira, K. 2016. Climate benefits of natural gas as a bridge fuel and potential delay of near-zero energy systems. *Appl Energy* **167**: 317–322. doi: 10.1016/j.apenergy.2015.10.016

Zimmerle, D, Vaughn, T, Bell, C, Bennett, K, Deshmukh, P, Thoma, E. 2020. Detection limits of optical gas imaging for natural gas leak detection in realistic controlled conditions. *Environ Sci Technol* **54**(18): 11506–11514. doi: 10.1021/acs.est.0c01285

Zimmerle, DJ, Pickering, CK, Bell, CS, Heath, GA, Nummedal, D, Pétron, G, Vaughn, TL. 2017. Gathering pipeline methane emissions in Fayetteville shale pipelines and scoping guidelines for future pipeline measurement campaigns. *Elem Sci Anth* **5**: 70. doi: 10.1525/elementa.258

Zou, C, Zhao, Q, Chen, J, Li, J, Yang, Z, Sun, Q, Lu, J, Zhang, G. 2018. Natural gas in China: Development trend and strategic forecast. *Nat Gas Ind B* **5**(4): 380–390. doi: 10.1016/j.ngib.2018.04.010